

A Framework for Scalable Ambient Air Pollution Concentration Estimation

Liam J. Berrisford^{1,2,3,*}

`l.berrisford@exeter.ac.uk`

Lucy S. Neal⁴

`lucy.neal@metoffice.gov.uk`

Helen J. Buttery⁴

`helen.buttery@metoffice.gov.uk`

Benjamin R. Evans⁴

`benjamin.evans@metoffice.gov.uk`

Ronaldo Menezes^{1,5}

`r.menezes@exeter.ac.uk`
`rmenezes@biocomplexlab.org`

¹ BioComplex Laboratory, Department of Computer Science, University of Exeter, England

² Department of Mathematics, University of Exeter, England

³ UKRI Centre for Doctoral Training in Environmental Intelligence, University of Exeter, England

⁴ Met Office, FitzRoy Road, Exeter, EX1 3PB, U.K.

⁵ Department of Computer Science, Federal University of Ceará, Fortaleza, Brazil

* Corresponding Author

January 18, 2024

Abstract

Ambient air pollution remains a critical issue in the United Kingdom, where data on air pollution concentrations form the foundation for interventions aimed at improving air quality. However, the current air pollution monitoring station network in the UK is characterized by spatial sparsity, heterogeneous placement, and frequent temporal data gaps, often due to issues such as power outages. We introduce a scalable data-driven supervised machine learning model framework designed to address temporal and spatial data gaps by filling missing measurements. This approach provides a comprehensive dataset for England throughout 2018 at a 1km² hourly resolution. Leveraging machine learning techniques and real-world data from the sparsely distributed monitoring stations, we generate 355,827 synthetic monitoring stations across the study area, yielding data valued at approximately £70 billion. Validation was conducted to assess the model's performance in forecasting, estimating missing locations, and capturing peak concentrations. The resulting dataset is of particular interest to a diverse range of stakeholders engaged in downstream assessments supported by outdoor air pollution concentration data for NO₂, O₃, PM₁₀, PM_{2.5}, and SO₂. This resource empowers stakeholders to conduct studies at a higher resolution than was previously possible.

Impact Statement: The current high-quality air pollution monitoring station network in the UK is spatially sparse with heterogeneous placement and commonly suffers from missing data temporally from issues such as power outages. We present a scalable data-driven supervised machine learning model framework to fill missing measurements temporally and spatially, providing a complete dataset for England during 2018 at a 1kmx1km hourly resolution. The approach leverages machine learning and data from the sparse real-world monitoring stations to create 355,827 synthetic monitoring stations across the study area to acquire data worth approximately £70 billion. Validation was conducted regarding the model's performance in forecasting, estimating missing locations and capturing peak concentrations. The dataset provided is of interest to a range of stakeholders conducting downstream assessments underpinned by outdoor air pollution concentration data for NO₂, O₃, PM₁₀, PM₂₅, and SO₂, empowering stakeholders to perform studies at a higher resolution than previously possible.

1 Introduction

Air pollution presents a significant health risk to individuals, with 28-36 thousand deaths per year in the UK associated with air pollution exposure [1]. Estimating ambient air pollution concentration levels is an essential step in tackling the health burden of air pollution due to the high cost of individual monitoring stations. The potential cost for a single multi-pollutant monitoring station could be as high as £198,000 [2]. Even for a country such as the United Kingdom that has highlighted tackling ambient air pollution as a key priority [3], there are only 171 monitoring stations across the UK for all pollutants currently being monitored¹. Therefore, areas without a dedicated monitoring station need to have their ambient air pollution concentrations estimated through models, which go on to inform policy for interventions into air pollution, making the models used for this process of pivotal importance.

Existing national-level datasets produce estimations at the annual temporal scale and 1 km² spatial resolution [4]. However, it is imperative to note that health advisories, as articulated by organizations like the World Health Organisation, delineate constraints not solely on the annual mean of air pollution concentrations within a specified region but also on the daily mean. To illustrate, for NO₂, the stipulated limits include a 10 µg/m³ annual mean and a 25 µg/m³ 24-hour limit [5], with the absence of an explicitly defined hourly limit [6]. The regulatory landscape in the United Kingdom, as governed by the Air Quality Standard Regulations 2010 [7], delineates both limit values—legally binding parameters not to be surpassed—and target values, akin to limit values but lacking legal bindings. Notably, this legislation addresses hourly level means for pollutants like NO₂, with a meticulous limit of 200 µg/m³, not to be exceeded more than 18 times in a year.

The prevailing methodology, limited to generating mean annual estimates at the national scale, introduces a challenge. This stems from the fact that only specific locales, equipped with monitoring stations, possess hourly data on air pollution. Consequently, areas devoid of such monitoring infrastructure are excluded from any analysis of air pollution levels at a more granular temporal resolution. This discrepancy in data availability raises concerns regarding health inequalities, underscoring the imperative need for a more equitable and comprehensive approach.

The utilization of annual pollution levels provides a broad overview of the pollution within a designated study area. However, a notable challenge arises concerning information loss when transitioning from an hourly to a daily or annual temporal scale. This issue has manifested in the United Kingdom, where instances of divergent narratives emerge between the annual and daily means of specific locations. Take, for instance, Leominster² on 03/12/2014 at 08:00, which recorded a peak pollution value for NO₂ of 80.2 µg/m³. The 24-hour mean in the vicinity of this peak, spanning 12 hours on either side (from 02/12/2014 2000 to 03/12/2014 2000), stands at 31.5 µg/m³, as illustrated in Figure 1a. This exceeds the WHO’s daily mean guideline of 25 µg/m³. The complexity deepens when examining Leominster’s annual mean for 2014, registering a value of 9.5 µg/m³, deemed safe by WHO guidelines and depicted in Figure 1b. Similar disparities are observable in other monitoring stations. For instance, London North Kensington exhibits unsafe levels at both the annual and daily scales, with a peak value of 209 µg/m³, a daily mean of 122 µg/m³, and an annual mean of 33 µg/m³ for the pollutant NO₂. Table S1 details the peak values for the five most polluted stations for NO₂ within the study, encompassing the Peak Value, Daily Mean surrounding the peak, and the annual mean for the year of the peak occurrence.

While there is evident importance in hourly air pollution concentration data for compliance and legislation purposes, the data serves a spectrum of other critical purposes. Researchers, policymakers, and public health officials routinely conduct human health assessments [8], enabling informed decisions concerning interventions to protect vulnerable populations [9]. Further, epidemiological studies assessments are routinely conducted [10] and are of crucial importance when significant changes in air pollution are being observed, such as during the COVID-19 pandemic [11]. Beyond human health, ecosystem health can be significantly impacted by air pollution, leading to damage to plants, manifested as leaf injury and stunted growth [12]. This has critical implications for concerns related to crop yields and food security [13].

As such, this work introduces a data-driven machine learning model designed to estimate the hourly concentration of air pollutants at the same spatial resolution (1 km²) as the existing annual dataset available for the UK³. We argue that this work leads to a dataset of substantial value to various stakeholders.

2 Related Work

2.1 Measuring Air Pollution

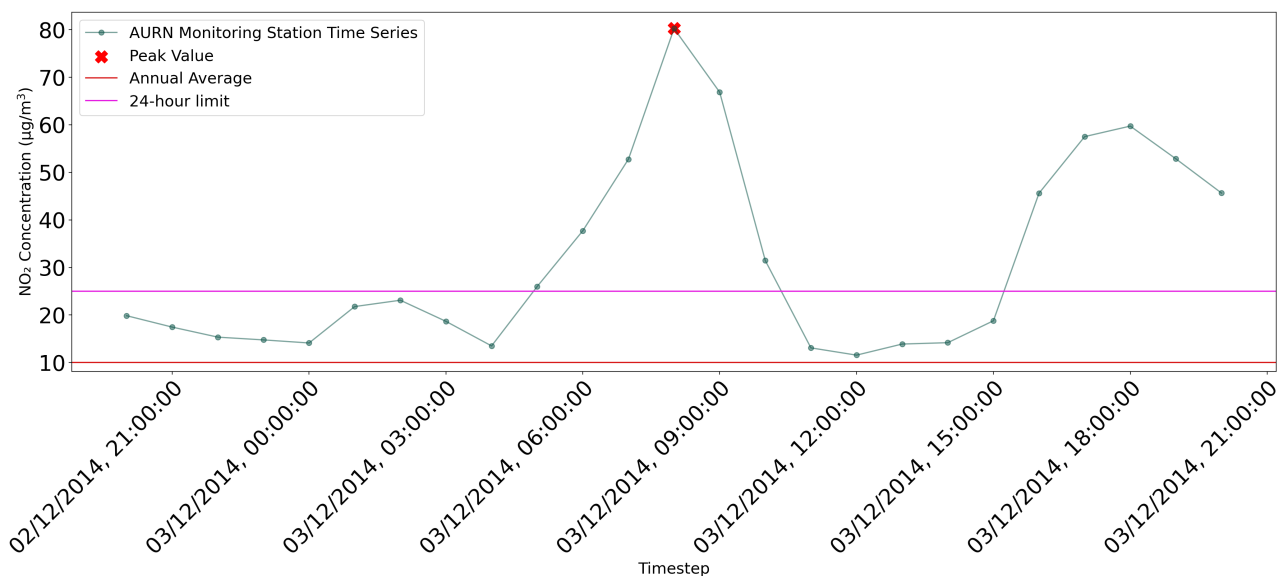
Various methods exist to offer insight into air pollution concentrations in a given location. The most robust and straightforward method available involves specialized equipment designed to provide direct measurements of air pollution concentrations. In-situ measuring equipment can be broadly categorized into two groups: high-quality stationary monitoring stations discussed in Section 1 and more mobile low-cost air quality sensors [14].

While high-quality fixed monitoring stations provide a reliable method of obtaining air pollution concentration data, their deployment on a large scale is prohibitively expensive. In 2018, the UK had 165 high-quality monitoring

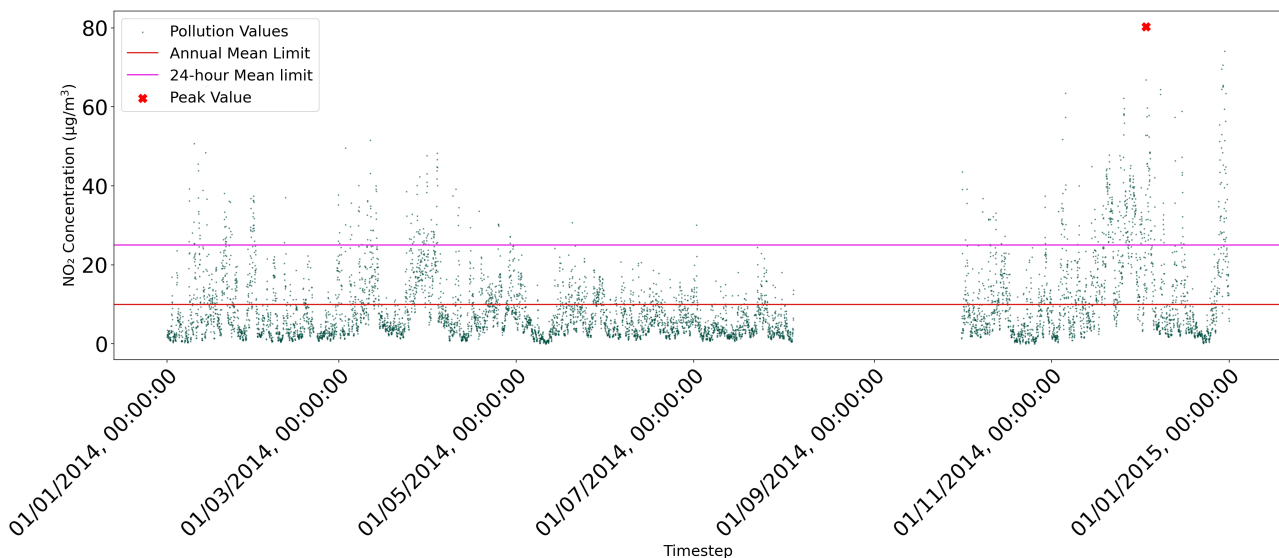
¹<https://uk-air.defra.gov.uk/networks/network-info?view=aurn>

²https://uk-air.defra.gov.uk/networks/site-info?site_id=LEOM

³UK-AIR Annual Modelled Background Air Pollution Data.



(a) **Leominster day air pollution readings surrounding the 2014-2018 peak.** Shown is the peak value for the Leominster AURN monitoring station spanning 2014-2018, recorded at 08:00 on 03/12/2014. Presented alongside the peak value is the 24-hour window surrounding the peak, along with the annual and 24-hour limit averages.



(b) **Leominster 2014 air pollution readings.** Presented are all ambient air pollution measurements for NO₂ at the Leominster for the year 2014. Emphasized is the peak value, which is further examined in Figure 1a, along with the annual and 24-hour average limits.

Figure 1: Leominster AURN monitoring station NO₂ measurements. Figure 1a shows how the peak air pollution reading for NO₂ at the Leominster station dramatically exceeds the 24-hour limit, even more so for the annual limit, showing how there can be periods of quite extreme pollution in the context of the annual limits. Figure 1b shows how there can be extended periods where the air pollution levels are below and exceed the designated limits and the relation of the monitoring station peak to all available data for the station in 2014.

stations online across the country within its premier monitoring network. Notably, a majority of these monitoring stations are situated in urban areas, comprising 144 urban and 21 rural stations. The strategic decision of where to position these monitoring stations carries the potential to exacerbate inequality between urban and rural areas, potentially fostering a divide between rural and urban communities in terms of insight into air pollution where they live and work [15], particularly when considering that O₃ air pollution can often be worse in rural locations [16, 17].

The emergence of low-cost sensors has made it possible to monitor air pollution concentrations over a larger geographic area. However, we see two critical problems with low-cost sensors. One such issue is the quality of the sensors themselves, which can be influenced by changes in atmospheric composition and meteorological conditions, or provide false signals if other air pollutants are present in high concentrations [18]. Another issue is the quality control that is conducted on the sensors, such as the calibration checks that go into ensuring that the measurement

is made under the same conditions, such as the height at which the measurement is taken, affecting the reading that is produced, potentially making comparisons between different low-cost sensors and even the same sensor between locations more challenging [19]. There is research being conducted to help combat the issues facing low-cost sensors; it is still an open challenge but rapidly improving [20]. For now, low-cost air pollution sensors are only suitable for raising awareness rather than applications requiring higher accuracy, such as epidemiological studies or compliance with air quality legislation [21].

An ex-situ indirect measurement of air pollution concentrations can be achieved with remote sensing. Sentinel 5P [22] is an ESA satellite platform that can provide insight into air pollution concentrations at a vast spatial extent. However, a major challenge associated with the use of Sentinel 5P is the issue of data completeness. Two primary drivers contribute to missing data from the Sentinel 5P platform. The first challenge arises from the platform's orbit, which follows a near-polar, sun-synchronous path [23]. This orbit causes the platform to consistently pass over a region at a similar time each day. While this characteristic is advantageous for comparing locations, it complicates the provision of insight into air pollution concentrations across an entire day. As a result, questions such as the difference between rush hour and midnight air pollution concentrations become difficult to answer. Another factor contributing to data gaps is environmental conditions that may lead to a specific reading not passing quality control, resulting in missing measurements on certain days [24]. Another remote sensing platform is the recently operational TEMPO [25], which provides hourly air pollution concentration measurements. However, TEMPO shares similar limitations with Sentinel 5P and only offers coverage over North America. While remote sensing is a valuable tool in certain circumstances, it cannot provide a complete picture of air pollution concentrations. This comprehensive understanding is crucial for designing effective interventions to tackle air pollution.

2.2 Modelling Air Pollution

As it is evident that all methods of measuring air pollution concentrations have drawbacks, models have been extensively utilized to complement real-world observations. Various types of model frameworks exist, each offering distinct benefits and drawbacks.

There are two widely used air pollution model frameworks: Lagrangian and Eulerian. Lagrangian models track individual air parcels (or particles) moving through the atmosphere. Each parcel is associated with a set of equations of motion, making the parcel the focal point of the model as it moves through space and time [26]. On the other hand, Eulerian models do not concentrate on a single air parcel; instead, they divide the atmosphere into regions, using fixed points or cells to represent specific locations. The goal is to understand the concentrations of air pollutants at these specific locations at different times [27]. Lagrangian models are particularly well-suited for studying problems where a specific pollution source is of interest, such as the ash emitted from a volcano [28].

On the other hand, an Eulerian model is well-suited for studying the spatial distribution and long-term trends of air pollutants, albeit at the expense of not being able to provide specific information about a given source and pollutant. Consequently, this work will primarily focus on Eulerian models, as they provide the necessary data for conducting the analyses and assessments discussed in Section 1.

Statistical Eulerian models, such as Land use regression (LUR), exist as a method for creating stochastic air pollution models. LUR incorporates a variety of predictors, including meteorological, terrain, land use, and road network data [29]. Another paradigm of Eulerian air pollution models is represented by mechanistic models, such as GEOS-Chem [30]. These models are open source and available for use, providing comprehensive spatial coverage of air pollution concentrations. However, they demand a high level of expertise in the domain field for interrogation due to their complexity. Additionally, these models come with extensive requirements for supporting infrastructure, with a GEOS-Chem 4.00°x5.00° degree standard simulation requiring 15GB of RAM⁴.

A rapidly emerging area is the use of deterministic models to address the current gap within the existing suite of models, providing high-resolution air pollution concentration data both temporally and spatially; this empowers stakeholders to make informed decisions concerning air pollution. Several models in this category are based on data-driven supervised machine learning, where a target vector, typically representing air pollution concentrations, is estimated from a feature vector, such as meteorological variables (e.g., wind speed). The model's objective is to learn the relationship between the target and feature vectors in situations where both are available, enabling subsequent predictions of target vectors when only the feature vector is available. In the scientific literature, numerous studies utilize machine learning techniques to forecast air pollution concentrations [31, 32, 33]. However, a limitation exists, as this approach requires air pollution concentration data from the location being predicted before the time predicted. Therefore, there is a need for historical air pollution data to be available. For example, a forecasting model will use air pollution concentration data from T-X to estimate air pollution at time T, where X is some defined time, such as 1/3/9 hours. If historical air pollution concentrations are used, it restricts the method's applicability to locations where an air pollution monitoring station exists.

Existing studies have tackled the problem of estimating air pollution concentrations in locations without monitoring stations. However, the studies focus either on small geographical areas, such as the Bay of Algeciras (Spain) with hourly temporal resolution [34] or a large geographical area with low temporal resolution, such as monthly [35]. Some work has been able to achieve higher spatial coverage with daily temporal resolution [36, 37]. As such,

⁴<https://geos-chem.readthedocs.io/en/stable/gcc-guide/01-startup/memory.html>

this work presents a model combining these aspects, predicting hourly temporal resolution concentrations across England’s large geographical area, a considerable challenge due to the variance of air pollution concentrations in locations covered.

This manuscript aims to use machine learning to produce data similar to an Eulerian model framework. While traditionally, the concentration is resolved over an area in an Eulerian model, the model presented here can be considered an approach of using machine learning as a synthetic monitoring station. The process that is followed for the model is answering the question of the air pollution concentration reading of a monitoring station that experiences the environmental conditions described by the input data. The model takes the training data to learn the relationship between environmental conditions and air pollution, allowing us to use the environmental conditions that are known in all locations across the England and make predictions of air pollution concentrations that are not so readily available, providing a complete picture of air pollution concentrations in the England. Compared with other deterministic methods, such as mechanistic models, a key benefit of the approach is the improvement in computational speed. In contrast, more traditional Eulerian models involve spatial dependencies between grids, where, for example, two adjacent grids impact each other. The framework presented in this work, however, treats each synthetic monitoring station as independent from one another. This approach offers a significant speedup in computation through the parallelization of predictions, while also enabling more accessible exploration of data by predicting air pollution locations independently. This novel approach is a key contribution of this work, utilizing machine learning to underpin a scalable estimation of ambient air pollution concentrations. Importantly, this approach is linearly scalable concerning computational complexity, allowing stakeholders to employ a model capable of predicting air pollution concentrations at any spatial and temporal resolution.

3 Data

The data-driven supervised machine learning model this paper proposes for air pollution concentration prediction is based on two primary sets of data: feature vectors and target vectors. In the case of air pollution concentration estimation, the target vector is the air pollution concentration itself, the data to be estimated, and the feature vector represents the data used to make predictions, for example, the wind speed. The model aims to understand the relationship between the feature and target vectors, e.g., what is the given NO_x concentration at given wind speeds?

3.1 Target Vector: Air Pollution Concentrations

We obtained air pollution data for our study from the UK Automatic Urban and Rural Network (AURN) using the OpenAir package [38]. Our study focuses on seven pollutants: Nitrogen Oxide (NO), Nitrogen Dioxide (NO_2), Nitrogen Oxides (NO_x), Particles $< 10\mu\text{m}$ (PM_{10}), Particles $< 2.5\mu\text{m}$ ($\text{PM}_{2.5}$), Ozone (O_3), and Sulphur Dioxide (SO_2). All air pollutants are measured in micrograms per cubic meter ($\mu\text{g}/\text{m}^3$). All types of monitoring stations were included in the study. The number of station types per pollutant varied, resulting in different data point distributions, as shown in Table 1, with apparent gaps in some locations for certain air pollutants, such as Suburban Industrial for PM_{10} , $\text{PM}_{2.5}$, and SO_2 . Clear spatial differences exist in the locations of monitoring stations. Figure S2 shows the spatial distribution of all AURN monitoring stations used in this study across three high-level environmental area classifications.

Each environmental area has a representative area over which the station’s measurements relate [39]. Urban stations are defined as representative of a few square kilometres (km^2), suburban stations cover tens of square kilometres, and rural stations encompass at least 1,000 square kilometres. Each station within the network also has a location type that specifies the primary source of air pollution at the station. Background stations are strategically located to ensure that no single source or street significantly influences the readings at the station. Instead, the measurements reflect an integrated contribution from all sources upwind. Traffic stations are located so that the measurements represent a street segment of at least 100 meters, and industrial stations have a representative area of 250 square meters (m^2).

The monitoring station location was abstracted to the closest grid centroid for ease of creating the needed datasets. Consequently, there is some distance between the true location and the location where we created the feature vector for the monitoring station. This abstraction of location provided a common framework, reducing the computation required to build the associated feature and target vectors, and facilitating a more straightforward interpretation of the framework. While the AURN monitoring station guidelines specify a minimal representative sample area, and the maximum abstraction distance across the monitoring network locations was 399 meters for the London Hackney monitoring station, we deemed this to be a worthwhile tradeoff. Full details of the abstraction distance can be found in Supplementary Material Table S3. It is noteworthy that as the spatial resolution increases, the associated errors will decrease, leading to an improvement in the approach. Eventually, the error from abstracting the location of the monitoring station will be eliminated when the abstracted distance is below the monitoring station representative sample area. However, this comes at the cost of considerable additional computational expenses. Therefore, the experiments in this study represent a lower bound for the framework’s performance, as any operational deployment could utilize increased spatial resolution for potential performance improvement.

For the study, we used the years 2014-2016 as the training set, 2017 as the validation set, and 2018 as the test set. To be included in the study, a station needed to have at least one measurement in each of these sets.

We conducted preprocessing on the collected air pollution concentration data. While UK-AIR performs some data validation [40], we undertook additional preprocessing steps. The initial step involved removing negative values, which are possible in the UK-AIR dataset [41]. The number of observations removed per air pollutant due to the presence of negative concentrations is detailed in Table S2. The distribution of the positive air pollution concentration values can vary widely across air pollutants and exhibit apparent differences between different environmental locations of monitoring stations. This variability raises the question of how to identify outliers, alongside the issue of developing a model that can handle target vectors with stark differences in distribution. For example, O₃ is the only air pollutant with a non-zero-inflated distribution, with the skewing between distributions for different environmental classifications for each air pollutant showing varying degrees of skew, as depicted in KDE plots in Figure S3.

Points that are distant from the mean have the potential not to be genuine outliers, but rather data points generated by different phenomena compared with the other data points in the distribution. We aimed to identify and remove both outliers and anomalies within the dataset. The challenge in identifying outliers lies in the context of the dataset, where a single urban traffic data point within the context of rural background monitoring station data points might be flagged as an outlier using established methods like IQR [42]. We were also cognizant of the potential presence of anomalies in the dataset. We recognized that a single localized event could drive a high-value concentration data point. While this reading might be accurate, it does not align with the AURN monitoring stations’ purpose, where concentrations are intended to represent a larger geographic area. Consequently, we considered identifying and removing these values beyond the scope of this work and proceeded with the study, acknowledging the presence of outliers and anomalous observations within the dataset that we could not explicitly identify. As such, we decided not to remove any such data points from the dataset.

Pollutant Name	Urban Background	Urban Traffic	Rural Background	Suburban Background	Urban Industrial	Suburban Industrial
NO _x	40	41	11	3	6	2
NO ₂	40	41	11	3	6	2
NO	40	41	11	3	6	2
O ₃	32	3	13	2	3	1
PM ₁₀	17	22	2	0	5	0
PM ₂₅	30	15	2	2	4	0
SO ₂	9	1	5	0	3	0

Table 1: **AURN monitoring station counts by environmental classification per air pollutant.** The number of stations for each pollutant within the UK AURN network within England is shown. It can be seen that there is an unequal distribution across the different environment types, alongside some pollutants such as SO₂, missing some environmental types completely.

3.2 Feature Vectors

The data considered in this study can be categorized into different dataset families, each containing a set of distinct but related datasets describing a phenomenon associated with air pollution concentrations. Addressing the temporal and spatial resolution differences between the datasets was a key challenge in creating a consistent feature vector to estimate the air pollution target vector. The common framework employed consisted of 355,827 1km² grids covering the extent of the England land mass. England was chosen as the study area since it was a common geographical region in all the datasets examined during this study, as illustrated in Figure S1. For the study, seven different dataset families were used, each providing a set of datasets describing a range of related phenomena that correlate with air pollution concentrations. Across all dataset families, there are 152 feature vector elements, with Figure 2 showing example feature vectors across England for each dataset family.

Transport Infrastructure Structural Properties, 28 features. Transport Infrastructure has been shown to provide information concerning air pollution concentrations [43]. We used Open Street Maps [44] to create annual snapshots of 14 transport infrastructure networks, from motorways⁵ to residential⁶ roads. Using the road network, we calculated two sets of feature vectors. One detailing the distance to each road type from the grid centroid, and the second detailing the total length of the given road type within the grid. Further details on the process conducted can be seen in Section S1.3.

⁵Open Street Maps Motorway Highway Classification.

⁶Open Street Maps Motorway Residential Classification.

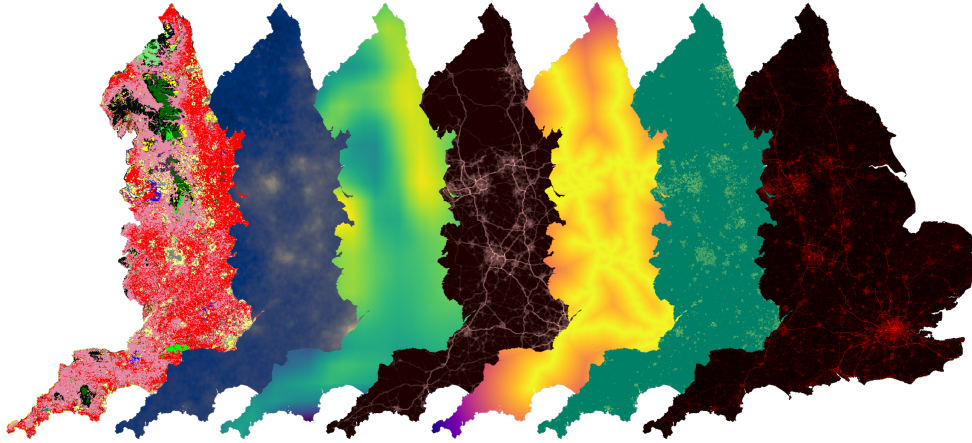


Figure 2: **Example feature vector dataset from each dataset family.** From left to right, the example datasets are the majority land use classification for each grid (geographic family, discussed in Section S1.8), Sentinel 5P NO₂ measurements (remote sensing family, discussed in Section S1.6), 100m U component of wind (meteorological family, discussed in Section S1.5), NAEI SNAP sector 7 (road transport) NO_x emissions (emissions family, discussed in Section S1.7), road infrastructure distance from the nearest motorway and total length of residential road per grid (transport infrastructure structural properties family, discussed in Section S1.3), and the car and taxis score (transport use family, discussed in Section S1.4).

Transport Infrastructure Use, 5 features. Vehicles themselves are a primary driver of air pollution through multiple processes. Road vehicles exhaust gas air pollutants such as NO_x and SO₂ [45] alongside causing PM air pollution [46]. Further vehicles can cause air pollution through traffic resuspension [47] and fuel spillage and evaporation [48]. Within England, only traffic counts from point locations detailing daily traffic flows across different road types for key vehicle types such as Cars and Heavy Goods vehicles (HGVs) were available from the Department of Transportation [49]. Using OpenStreetMaps, we created a spatially complete dataset by providing the average daily traffic flow by road type per meter across the UK. We then used a spatial microsimulation using data from the UK Census (providing sociodemographic details of different regions of the UK) [50] and the UK Time Use Survey (providing details of how different sociodemographic groups travel, both temporally and by which transportation mode) [51] to spatially distribute the daily traffic counts to produce an hourly spatially complete dataset of traffic counts. Complete details of the process are covered in Section S1.4.

Meteorology, 11 features. Meteorological phenomena play a pivotal role in air pollution concentrations. Wind advects air pollution both to and from locations of interest through horizontal transport [52, 53]. Temperature can have a range of impacts on air pollution, impacting temperature inversions [54], the production of O₃ air pollution [55] and the removal of air pollution by plants [56]. UV radiation directly impacts O₃ production [57]. The removal of air pollution from the atmosphere via deposition by precipitation is notable [58], alongside wash-off from surfaces [59, 60]. Pressure can also influence air pollution concentrations, either by vertical mixing in low-pressure systems [61] or high-pressure systems, causing an accumulation of air pollution concentrations near the ground through a lack of vertical mixing and advection [62]. Further, O₃ production is increased at higher pressures [63]. The boundary layer also influences air pollution concentrations through vertical mixing within the layer. Larger boundary layer heights tend to produce less concentrated air pollution at the surface. For smaller boundary layer heights, the inverse is true. [64, 65, 66]. We retrieved data from the ECMWF Re-Analysis Version 5 (ERA5) dataset [67]. ERA5 is a global dataset that details the environmental conditions at equal space points, at 0.25°x0.25° hourly resolution. We choose the variables commonly associated with air pollution concentrations in the scientific literature. We interpolated across the study area to provide a value for each 1km² grid centroid; the details of the process of creating the dataset can be seen in Section S1.5.

Remote Sensing, 5 features. While there are limitations to the data produced by remote sensing, as discussed in Section 2.1, they provide valuable insight into air pollution concentrations between locations. We used monthly averages of Sentinel 5P data [22] to ensure that all locations had a measurement value. Further details of the feature vector are discussed in Section S1.6.

Emissions, 77 features. Emissions of air pollutants are the primary driver of a wide range of air pollutant concentrations. The emissions are classified into 11 SNAP (Selected Nomenclature for Air Pollutant) sectors denoting the emissions source, with particular details discussed in Section S1.7. The first sector "Combustion Energy Production and Transformation" (SNAP 1) includes power generation which can produce air pollutants such as SO₂ [68, 69]. Road vehicles exhaust gas air pollutants such as CO, CO₂, NO_x, SO₂ [45] and are included in the "Road Transport" category (SNAP 7). SNAP 8, "Other Transport and Mobile Machinery" includes shipping which emits NO_x, PM, CO₂ and VOCs [70], particularly SO_x from the marine fuels which has a high sulfur content [71]. Organic waste in landfills ("Waste Treatment and Disposal", SNAP 9) can produce VOCs, a precursor to O₃ [72]. Agriculture emissions (part of SNAP 10, "Agriculture, Forestry and Land Use Change"), comprise a large source of air pollutants, for example 39% of global PM_{2.5} is caused by ammonia from livestock manure and urine and synthetic nitrogen fertilisers [73]. Other emission sectors are "Combustion in Commercial, Institutional, Residential and Agriculture" (SNAP 2), "Combustion in Industry" (SNAP 3), "Production Processes" (SNAP 4), "Extraction and Distribution of Fossil Fuels" (SNAP 5), "Solvent Use" (SNAP 6) and "Nature" (SNAP 11).

Land Use, 22 features. The land use composition of a given area is related to air pollution concentrations, such as throughout greenspace [74, 75] and urbanisation [76, 77]. Land use composition profiles were created for each grid using the UKCEH 25m Land Cover Maps [78]. Details of the process and the different land use types are discussed in Section S1.8.

Temporal Aspects, 4 features. Air pollution displays various temporal cyclical elements, including diurnal cycles caused by rush hour for NO₂ [79], UV radiation for O₃ [80], and boundary layer height for all pollutants [81]. Weekly trends also emerge due to the working week affecting transportation and industrial emissions for NO_x [82], with similar patterns observed for PM [83]. Seasonal cycles for PM are evident due to winter residential heating [84], with similar factors contributing to an increase in SO₂ [85]. Furthermore, winter has a higher probability of adverse meteorological conditions, which reduces vertical mixing [86]. Additionally, colder temperatures and reduced sunlight in winter months affect O₃ production [53]. Consequently, the hour, day of the week, week number, and month were all included as elements in the feature vector.

The following section justifies the inclusion of such a broad range of different datasets by exploring the relationship between the feature vector and the air pollution concentrations at AURN monitoring stations. This analysis highlights the differences between types of air pollution and variations experienced at different environmental types for a single type of air pollution, ensuring robust estimation of air pollution concentrations across all environment types found in England.

4 Feature Selection

4.1 Air Pollution and Feature Vectors

Air pollution can be attributed to various sources, with different processes influencing its concentration, as discussed in Section 3.2. The issue of different drivers of air pollution is further complicated when considering that at different locations, the key phenomena driving the pollution concentrations are different, as detailed within the AURN environment classification discussed in Section 3.1. This tangled web of sources, such as road transport, and sinks, such as wind speed, makes it challenging to identify a common set of datasets that can provide insight into all the air pollutants of interest. Therefore, this section aims to untangle the relationship between the different air pollutants and monitoring station environment types to provide insight into the different feature vectors and their relationship with the air pollutant measurements. This provides insight into the benefit of each dataset, detailed in Section 3.2.

Figure 3 shows the average Spearman correlation coefficient across all monitoring stations for NO_x and O₃. These figures depict the ten highest magnitude feature vector elements in both directions. The differences in the contributing sources of air pollution for a given pollutant are evident and appear to support the scientific literature regarding the relationship between different air pollutants and their sources and sinks.

For example, NO_x has the highest positive Spearman correlation coefficient with the emissions dataset, particularly SNAP sectors 1 and 2, indicating a strong relationship between energy production and transformation emissions and the commercial, institutional, residential, and agriculture sectors. It is also notable that the highest magnitude negative Spearman correlation belongs to the sinks, namely wind speed and the boundary layer height, as expected.

In contrast, O₃ presents a very different situation compared to NO_x; the highest magnitude correlation is inverse. Both wind speed and boundary layer height have a high positive magnitude Spearman correlation, highlighting that the same phenomenon can have a completely opposite relationship on the concentrations of air pollutants. It also follows that the correlation between "Downward UV Radiation At Surface" and O₃ has a positive correlation, given that O₃ is produced under sunlight by the precursors of NO_x and Volatile Organic Compounds (VOCs) [87], highlighting that more sunlight results in more O₃ being produced.

Figure 4 illustrates the relationship between feature vectors for Rural Background and Urban Traffic monitoring station environment classifications (discussed in Section 3.1) for the air pollutant NO_x. Each subclassification of

monitoring stations indicates the primary contributor to the measured air pollution. Background stations have no single primary source, while traffic stations are primarily driven by traffic.

For the Urban Traffic station, the strongest positive correlation across air pollutants is with SNAP Sector 7, denoting road transport emissions. Notably, there is a strong relationship with SNAP Sector 6 NMVOCs, indicating solvent use for NMVOCs. This might be explained by the small number of data points for monitoring stations (41 Urban Traffic stations), alongside emissions data being based on extensive scaling depending on the hour, week, and month of interest [88]. The potential for confounding variables, such as NMVOC emissions arising from vapor from petrol [88], makes the 0.014 magnitude difference in relationship strength negligible. The current data quality is suitable for identifying general trends rather than pinpointing the most substantial relationship by sector.

The transport use dataset exhibits a positive but weaker Spearman correlation with the Urban Traffic site, with an average score of 0.36 across the five datasets. In contrast, the Rural Background sites for the transport use datasets have an average of 0.05. This aligns with the literature, showing a clear signal for increased traffic near an Urban Traffic monitoring site and increased NO_x concentrations. It also agrees with the AURN environment classification, with a still positive but significantly reduced magnitude correlation.

As the AURN environment classification is based on the primary emitters closest to the station, it then follows that both station types have the same feature vector for the highest negative magnitude Spearman correlation with the expected boundary layer height and wind, namely the meteorological variables that are present across all monitoring stations, and the sinks in the case of NO_x .

4.2 Inter Feature Vectors

While there is considerable existing literature about the relationship between different air pollutants and the phenomena covered in the datasets used in this study, considerably less literature covers the relationship between the phenomena comprising the feature vector. This section aims to understand the relationship between the different feature vectors to address the issue of multicollinearity, which can have significant implications for the machine learning approach implemented.

The Spearman correlation coefficient was again used to calculate the relationship between each pair of feature vectors. Figure 5 is a heatmap representing the Spearman correlation coefficient value for every pairing. There are no air pollution monitoring stations for some feature vectors—nine feature vectors for the emissions dataset family and four in the geographic dataset family. The lack of target vector data at some key feature vector locations presents the first significant problem with any model developed: not all environmental condition types experienced within England have observations. For example, there are no air pollution concentration data for the Land Use classification of Saltwater, representing a scenario in which the model has no exposure.

From the heatmap in Figure 5, it is clear that multicollinearity is present between some features, for example between different species within the same emissions sector. Two main concerns were identified with the complete set of feature vectors: the implications on model interpretation depending on the model chosen and the redundant information between features. The model interpretation would impact future stakeholder engagement, and redundant features would make the hyperparameter search more complex. Therefore, we considered removing features entirely or creating a new set of features through dimensionality reduction. However, as stakeholder engagement with the model was an essential aspect of any operational model, and losing the semantic meaning of features would be detrimental to model interpretation, we decided against creating a new set of features.

Hierarchical clustering was performed between the Spearman correlation of the feature vectors, allowing us to create a more complex method of grouping together feature vectors. Figure 6 shows the clustering results. The linkage distance provides a consistent metric across all feature vectors to explore the similarity of features and provide clusters of features depending on the value of the linkage distance provided. Figure 6 shows how related some of the feature vectors are; for example, the 100m and 10m components of wind in both directions are highly correlated and therefore have a very low linkage distance. There are also more complex relations between the feature vectors, such as within the transport use datasets. Still, there are differences within the data set, such as car and taxi and bus and coach being highly related but not to the same degree as HGVs. The motivation for performing hierarchical clustering is to allow for a subset of features to be selected that provide the same information as one another, aiding model interpretation. In the case above, the idea is that including the 100m U component of wind provides the same information as the 10m U component of wind, so there isn't a need to include both.

Table S7 shows the number of clusters at varying linkage distances, where increasing the linkage distance results in fewer clusters as the information provided between datasets isn't required to be as strong. As including redundant feature vectors increases the computation costs of creating and using the model rather than impacting the performance of the predictions, we decided to keep all feature vectors when training the model. The intention is to provide a baseline performance of a machine learning model that utilises all the datasets covered while allowing for an understanding by individual stakeholders of the redundant feature through the hierarchical clustering performed, allowing them to subset the datasets as desired for their particular use case. Using all the feature vectors does mean, however, that a machine learning approach that is robust to multicollinearity needs to be chosen. The second issue of model interpretability implications is discussed in Section 5.1.

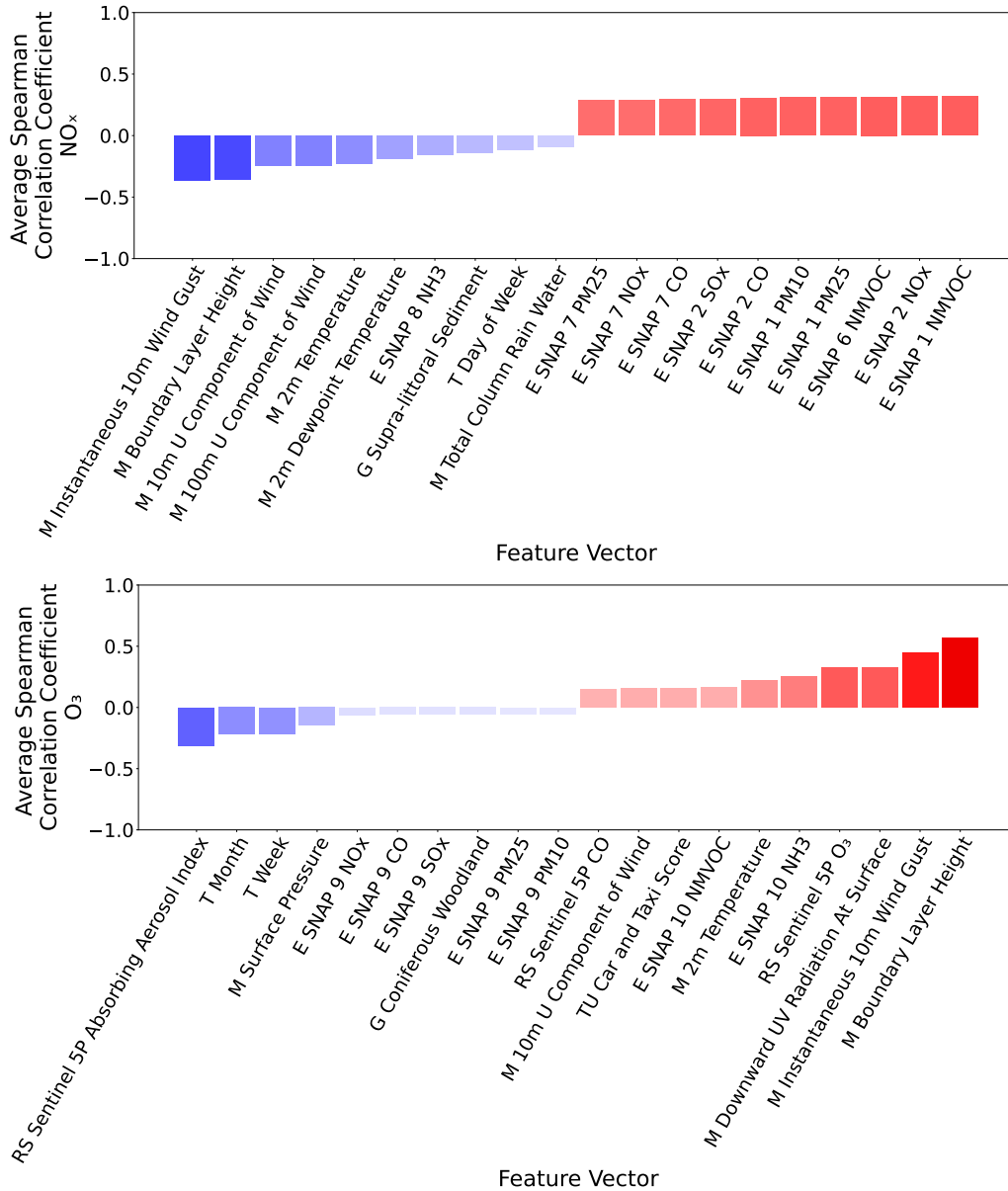


Figure 3: **Spearman correlation coefficients overall mean for all pollutants.** The mean Spearman correlation coefficients for NO_x and O₃ across all the environmental classifications of the AURN network for the ten most extreme, both positive and negative, for the feature vectors are shown. The sources and sinks of the air pollutants are different, aligning with the scientific literature (Section 3.2), with NO_x being highly positively correlated with emission features, whereas O₃ exhibits such a relationship mainly with meteorological features, such as wind gusts. Regarding negative correlations, the two air pollutants exhibit counter relationships, with NO_x having a negative correlation with the meteorological. The analysis highlights how the relationships between a particular phenomenon and a given air pollutant can be widely different in strength.

5 Modelling

Section 5 starts by describing the reasoning behind different modelling choices. The model's performance in two critical scenarios is then explored: forecasting and estimating missing stations. Forecasting aims to answer the question of, given a location the model has already seen, how well the model performs when estimating a future year it has not. The estimating of a missing station then experiments with understanding model performance when predicting air pollution at a location it has never seen before. The model's performance on peak concentrations is also analysed, a critical situation for the model to perform well. Finally, a justification for including such a wide range of datasets is motivated by experimenting with a model that predicts based on one dataset family.

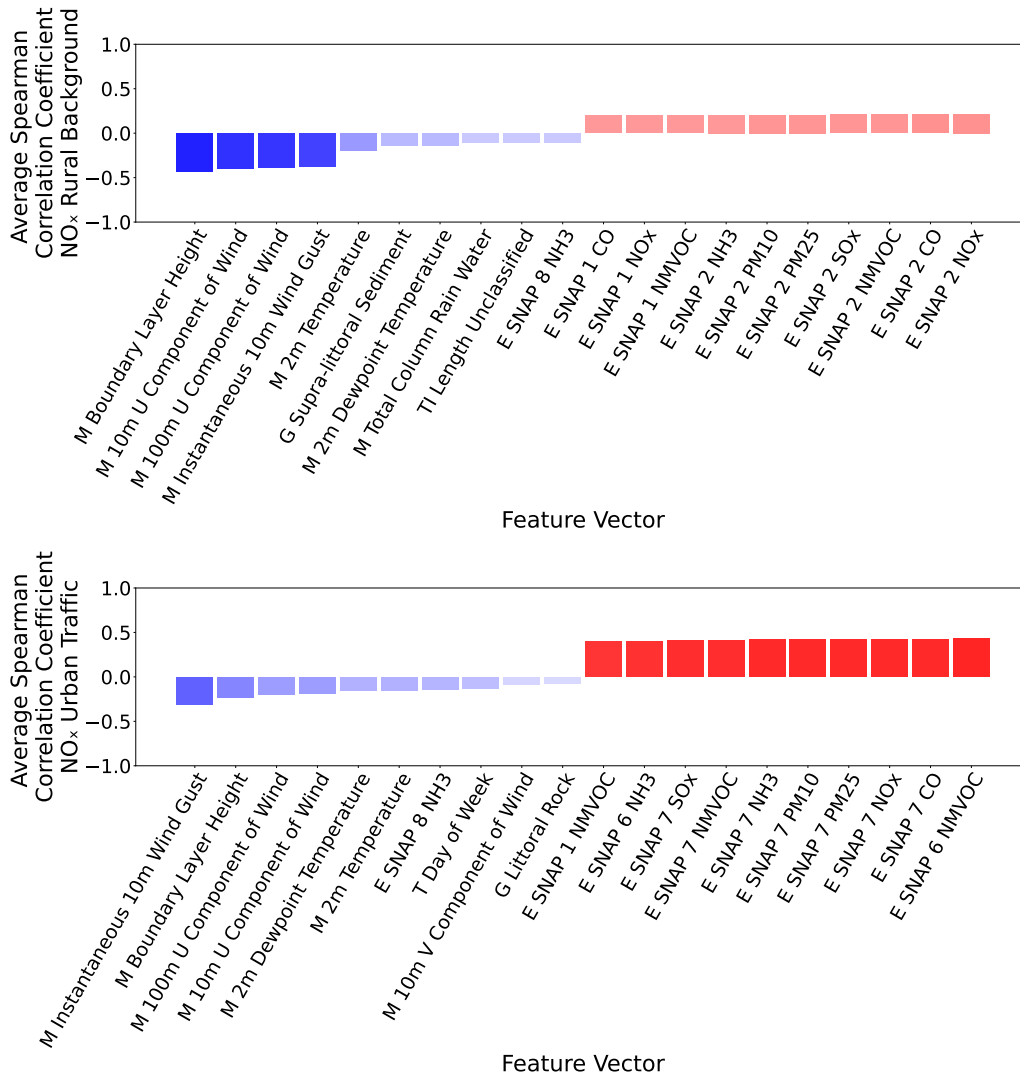


Figure 4: **Spearman correlation coefficients for NO_x monitoring station environmental subclassification locations, Rural Background and Urban Traffic.** While Figure 3 highlights the difference between phenomena and air pollutants, there exists a further difference between environmental subclassifications. For the Urban Traffic monitoring stations, it can be seen that the primary positive correlations are related to road transport as would be expected (the strong relationship with Solvent Use is likely an artefact of the scaling performed and discussed in Section 3.2 and S1.7, alongside a limited sample size of 41 stations). In contrast, the Rural Background monitoring stations show a strong relationship with emissions from the residential sector, highlighting that the sources and sinks for an air pollutant depend on the air pollutant itself and the location of interest.

5.1 Model Design and Training

The first consideration when choosing the model framework was the need for the model to be robust to multiple uninformative and redundant features. As discussed in Sections 4.1 and 4.2, uninformative features exist for various reasons. Some features are uninformative for specific air pollutants, such as the transport use features with O₃. Features can also be uninformative for specific environmental locations of monitoring stations, as seen in Section 4.1 for rural background NO_x stations. Multicollinearity further compounds the issue, allowing multiple features to extract the same information about air pollution measurements, as discussed in Section 4.2. The second consideration when choosing the model was for it to be robust to outliers and anomalies, as discussed in Section 3.1. The model we chose to use was LightGBM, a gradient-boosting algorithm based on decision trees.

LightGBM [89] was identified as a machine learning approach that could address the concerns raised in the study through various techniques while also providing state-of-the-art performance on tabular prediction problems. LightGBM is a gradient-boosting decision tree (GBDT) algorithm where an ensemble of decision trees is trained in sequence, with the n+1 decision tree fitting the residuals of the first n decision trees, learning the difference between the actual target vector and the weighted sum of predictions of the first n decision trees.

LightGBM allows us to mitigate the impact of uninformative and redundant features on training time through the

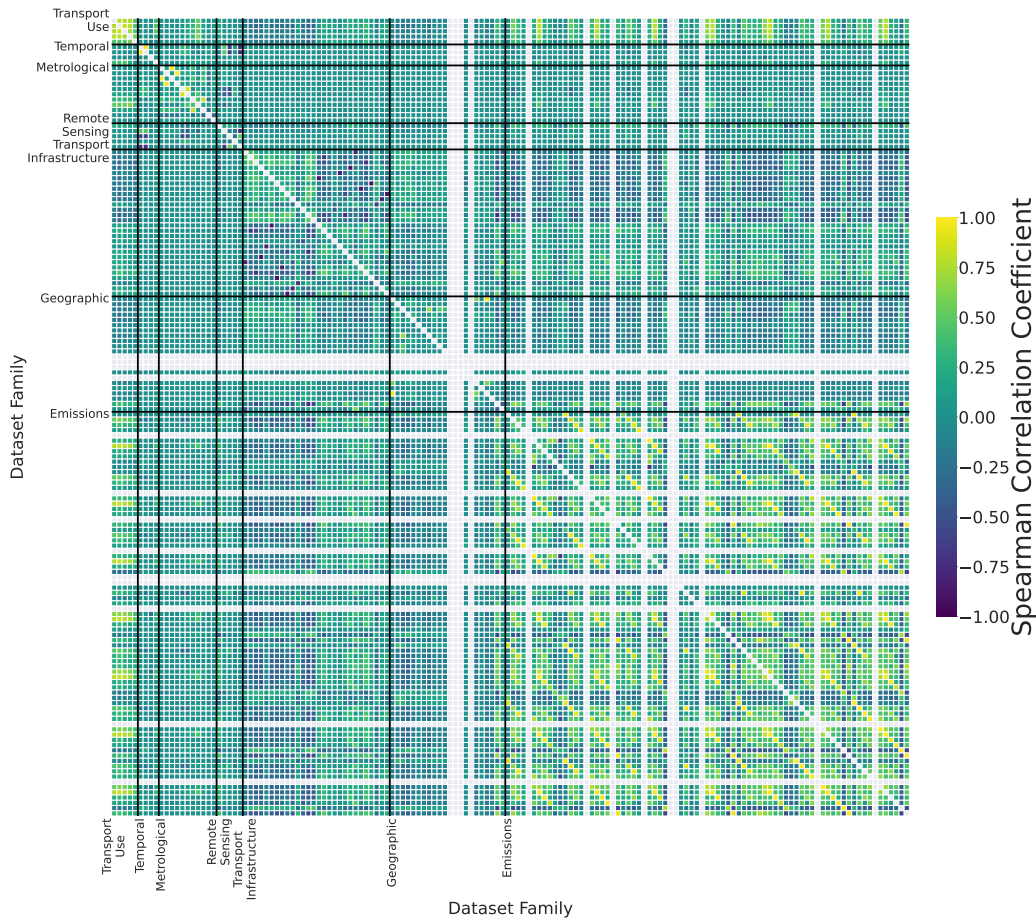


Figure 5: **Spearman correlation heatmap between all feature vectors.** The grey lines throughout the heatmap show the data points missing from the dataset, phenomena with no monitoring stations across all pollutants, including four geographic features and nine emissions features.

tree-building algorithm. The approach that LightGBM takes when building the decision trees is to split observations based on the feature vector values, looking for the best possible split regarding information gain and reducing the uncertainty regarding the target vector. This involves grouping homogenous instances of data points, such as instances where there is high transport use at a monitoring station that is measuring high concentration readings for NO_x .

One of the core issues with our air pollution training data is that many data points within the datasets repeat the same information due to the cyclical nature of air pollution measurements, causing a considerable amount of bloat in the datasets. The standard approach to identifying split points within a GBDT is the pre-sorted algorithm where all possible split points are explored, an approach which, in this use case, would be highly costly regarding computation and memory. LightGBM helps tackle this issue by using histograms when performing the splits, where continuous variables are put into discrete bins, changing the computational cost from being dependent on the number of data points to the number of discrete bins created.

The second concern identified when exploring the datasets was the presence of outliers and anomalies within the dataset. LightGBM inherently tackles this problem via decision trees being the underlying learner within the model. The decision tree's goal is to group homogenous data instances, and there is an ability to set a minimum number of data instances that comprise a valid leaf on the decision tree via the "minimum data in leaf" model parameter.

The "minimum data in leaf" parameter allows for a minimum threshold of homogeneous data points for the LightGBM algorithm to view as a set of data points that should be learned from and used in predictions. Concerning the air pollution prediction problem as a notional example, say there is a high wind speed and low traffic count but a high air pollution concentration reading, which only occurs once in the dataset; LightGBM will not create a leaf for this data instance. The scenario described could plausibly happen if a single air pollution emitter passes by the station, causing an artificially high measurement that would not represent the geographic area intended for the station as outlined by the AURN documentation, as discussed in Section 3.1.

There are, however, some trade-offs to the LightGBM solutions presented above. The feature importances given for the feature vectors via the model will likely be misleading due to the multicollinearity present. For example, the most extreme case seen in the hierarchical clustering of multicollinearity is for the wind speeds at 10m and 100m,



Figure 6: **Dendrogram depicting hierarchical clustering of feature vectors.** The lower the linkage distance between feature vectors, the more correlated the features are, indicating that they provide similar information. Table S7 details the number of clusters for different linkage distances.

where both features exhibit a strong correlation, meaning that we can extract information about air pollution from either feature. Therefore, during model building, in the split performed, the model would use only the 10m or 100m component of the wind direction, as they would present the same information gain about the target variable as each other. As the feature importance given by LightGBM is based on the number of times a feature vector is used, the total number of times the two feature vectors are used may be split across the two features, reducing the feature importance given to each one. The feature importances given must be analyzed considering the clusters presented in Table S7, treating each of the clusters' feature importances together, or a more sophisticated technique of model interrogation used, such as SHAP [90].

A key consideration during the model design was the choice of the loss function. The loss function represents the error of a given prediction, in this case, quantifying the difference between the prediction and the actual air pollution concentration measurement of a model, thereby allowing for comparisons between models and subsequent choice of the optimal model. The choice of the loss function in this situation was between the mean absolute error (MAE) and the mean squared error (MSE) [91]. The MAE would help reduce the influence of higher air pollution measurements on the model present due to the known presence of outliers and anomalies within the dataset. However, these high air pollution measurements are of vital interest within the context of air pollution, even if they are potentially erroneous. So, a tradeoff of potentially overfitting on these higher values was seen as a worthwhile tradeoff, and as such, the MSE was chosen as the loss function. The underlying premise is that $10\mu\text{g}/\text{m}^3$ is more than twice as bad for human health than $5\mu\text{g}/\text{m}^3$, so using the MSE is more appropriate given the domain in which the model would be used, supporting the existing literature that there is a non-linear relationship between the detrimental effects of air pollution concentrations [92, 93].

As an air pollution concentration can never measure less than zero, we trained the model on the log transformation of the target vector. We added a small constant of 1×10^{-7} to the target vector and then performed the log transformation due to the presence of 0 concentration measurements within the dataset. The log transformation and addition ensured that the model would never predict a negative value as the model output, as the reverse transformation of calculating the exponential and subtracting 1×10^{-7} was performed on the output. A further hyperparameter explored during model training was L2 regularization [94]. Including L2 regularization helps distribute the weights within the decision tree, encouraging the weights to be closer to 0 but keeping all feature vectors, ensuring that no single feature vector drives predictions, which is key with the considerable number of feature vectors used.

The framework for choosing the model's hyperparameters was a randomised grid search of 40 parameter sets. The parameters we optimized during the randomised search were the L2 regularization and the min data in each leaf already discussed, alongside the number of leaves, the number of trees, and the max depth [95]. The number of leaves search space was given the range of 1,000 to 4,095 [96], with the optimal values being chosen near the centre of this range, validating its choice. The number of trees was controlled via early stopping, where no additional tree would be added after 30 trees had been added without any improvement in the loss function performance. Similarly, the max depth was not limited and left to grow as needed until performance did not improve during training.

Some model parameters were kept constant throughout the search, such as the max bin, kept constant at 255. The max bin refers to the number of discrete bins created for a continuous feature vector. 255 was chosen to ensure that a range of different splits during model training could be created while also helping to reduce training time by allowing data to be stored optimally as an int8 data type. The boosting type used during training was Gradient-based One-Side Sampling (GOSS) [89]. GOSS is a method of boosting that allows the $n+1$ decision tree discussed at the start of this section to be trained on a subsample of the data. The subsample of data chosen is the data that has a large gradient, i.e. the data has yet to learn well from in the model and a random sample of the small gradient data, helping to reduce the amount of data used drastically, and therefore training time. The tradeoff with GOSS is the potential for overfitting when the datasets are small; however, this was not a concern in the context of air pollution.

The final consideration was the grouping and number of models to develop. One possible choice was creating a single unified model with all seven air pollutants comprising the target vector. However, due to the considerable imbalance in the number of data points and the issue of every monitoring station measuring a different subset of pollutants, the number of locations with every air pollutant measured at the same timestamp was minuscule. Another possibility was to create an individual model for each environment type covered in the AURN environment classification, such as Urban Traffic, Rural Background. However, this approach presented the problem of requiring a determination of the environment type of every grid in the study where there wasn't an existing monitoring station. Therefore, we created a single model for each of the different air pollutants mixed with all the different environment types, the benefit of which is simplifying the process of estimating a never before seen location while making use of all of the air pollution observations possible.

During the hyperparameter grid search, data from 2014-2016 was used as the training set, with the validation set being 2017 and 2018 as the test set. We split the dataset temporally to ensure no data leakage and to give an intuitive sense of the performance metrics gathered. We chose the best parameter set based on the model's MSE on the validation set across the parameter sets. Subsequently, using the best parameter set to train a model with both the training and validation set, with performance evaluated using the test set, data the model has never seen. The R^2 score for each model on the different sets was calculated at each stage.

To allow flexibility in extending the model with new data, we deliberately excluded feature vector elements that would identify monitoring station details, such as names or locations. Additionally, we opted not to include lags of air pollution concentrations, like using the concentration at T-1 to estimate the concentration at time T. This

decision enables us to make predictions even in the absence of a specific air pollution measurement, promoting the use of observations as independent entities. This structure facilitates the tabular format, leveraging the state-of-the-art performance of LightGBM. The temporal and spatial independence of observations supports the creation of a lightweight model, conducive to parallel computation for different locations and time points. Our experiments addressed two crucial scenarios, providing insights into the model’s temporal and spatial performance. We assessed its ability to forecast air pollution concentrations into the future (discussed in Section 5.2), and extended the analysis to evaluate the model’s performance in estimating air pollution concentrations in spatial locations not previously encountered (discussed in Section 5.3).

5.2 Filling Temporal Missing Data

The initial set of experiments focused on evaluating the models’ capability to predict future air pollution concentrations at locations already included in the model. These experiments aimed to assess the model’s performance in forecasting scenarios. The achieved performance serves as a conservative estimate for filling in missing data temporally in a given monitoring station’s time series, considering that air pollution concentration readings at the estimated time would be available in an operational hindcast situation.

Table 2 presents the R^2 score for the model developed at each stage, as discussed in Section 5.1. The results illustrate a degradation in the model’s performance as it moves temporally away from the data it was initially optimized for during the randomised parameter grid search. These experiments demonstrate that the model parameters identified during the randomised search remain consistent across the three datasets, with minimal performance loss observed between the validation and test sets. This observation supports the idea that the model is effectively learning the true relationship between the feature and target vectors.

Pollutant Name	Dataset Train Score	Dataset Validation Score	Dataset Test Score
NO ₂	0.85	0.77	0.77
NO _x	0.82	0.75	0.74
NO	0.73	0.67	0.65
O ₃	0.80	0.70	0.67
SO ₂	0.45	0.43	0.30
PM ₁₀	0.51	0.38	0.32
PM _{2.5}	0.55	0.35	0.29

Table 2: R^2 scores depicting forecasting performance (2014-2016 train score, 2017 validation score, 2018 test score). The dataset train score shows the model’s performance in capturing the relationship of the training data shown with the validation showing the performance in 2017 and the test score on 2018 data. The similar performance between the validation and test scores shows that the model optimised during the parameter search is learning the true relationship between the features and air pollution that is robust to data never seen before.

In the best-case scenario, NO₂ shows no drop in performance (rounded to 2 decimal places) between the validation and test sets. The most significant performance decrease is observed in SO₂; however, it’s important to note that this may be influenced by a data issue, as SO₂ has significantly fewer stations (18) compared to NO₂ (103), as detailed in Table 1.

While a benefit of the model presented is the ability to forecast air pollution concentrations into the future, answering the question of what air pollution concentrations at a station will look like in the next year, the adaptable temporal and spatial independence discussed in section 5.1 allows for the model to be used to estimate missing data. Figure 7 shows the model used to estimate the missing data in the NO₂ observations for the Chesterfield Loundsley Green monitoring station from 2014-2018. There are two possible cases for the missing data being filled in. The first is to backdate or postdate the observations depending on when the station came online or was decommissioned. Chesterfield Loundsley Green came online on 01/03/2015 [97], but the model can backdate the observations to 01/01/2014, extending the readings and helping to create a complete dataset. It is also possible to extend the life of a station if it was taken offline by filling in observations since the station was decommissioned [98].

The second situation where the model can fill in missing data is when an issue at the monitoring station or associated infrastructure causes the station to go offline and measurements not to be reported [99]. However, one potential issue with this approach is if there is a particular reason that the site cannot report data, for example, when wind speeds are over a defined speed. This situation would indicate that no data is within the training set concerning this specific situation, indicating the model is extrapolating. However, this is not a concern in this situation as AURN reports the reasoning behind data not being reported, such as a communication issue or an instrument error. It is something, however, to be understood in the context of any future work that uses this framework where this situation could occur. In Figure 7, there are three prolonged periods in which Chesterfield was not reporting NO_x measurements. The model presented can fill in these periods alongside the periods from before the station came

online to create a time series for the station that has all available data as seen in Figure 7 where the real measurements from the station have been augmented with the model output where real measurements are not available.

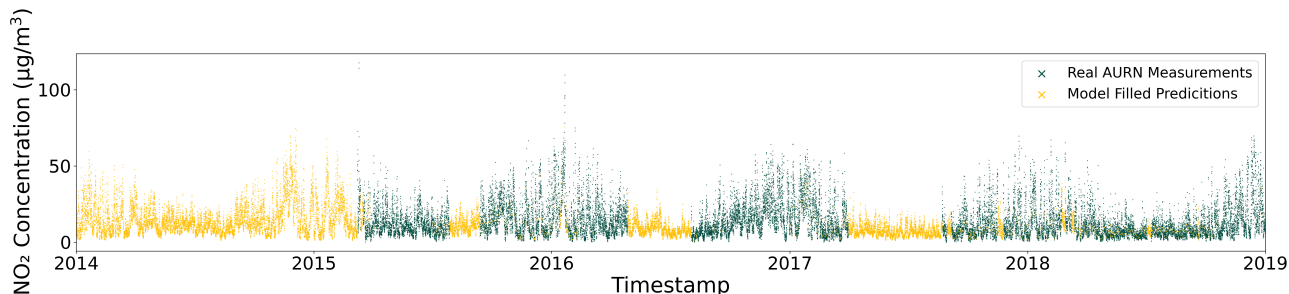


Figure 7: **Chesterfield Loundsley Green NO₂ concentrations augmented dataset, with missing AURN measurements filled with model predictions.** Figure 7 shows that the station’s measurements (green) started in early 2015 with three clear periods of long-term missing data. The model predictions (yellow) can create a complete augmented time series using the model.

5.3 Filling Spatial Missing Data

The second set of experiments that we conducted explored the ability of a model to be trained and predict the complete time series for another station, never seen before. We used 5-fold leave-one-out validation (LOOV) to experiment with this scenario. The results from this experiment provide an understanding of how the model performs when filling in missing air pollution concentration data spatially, a situation akin to using the model as synthetic stations across England at locations where no station has ever existed.

The same experimental design as Section 5.2 was repeated alongside a final step that calculates the LOOV score for every station not included in the training, validation or test set. Table 3 shows that the models trained during the 5-fold LOOV can retain their future predictive performance, with minor differences for the performance of air pollutants across the different subsets of stations used, showing the results from section 5.2 to be robust to changing input datasets. Table 4 shows the LOOV summary statistics for the experiments conducted, based on the R^2 retrieved from the model estimating the complete time series of a monitoring station’s data. Four different summary statistics were considered from the set of LOOV results, namely the mean, median, min and max results. The max LOOV results are positive for all of the pollutants, indicating some merit to this approach across all pollutants. This is further supported by the majority of positive results in the mean and median LOOV for all pollutants apart from SO₂. Of central interest is the LOOV min, where for all pollutants other than PM₁₀ there is a negative R^2 , indicating a prediction across the time series that is worse than simply predicting the average concentration. In this case, a potential hypothesis for the model performance is a lack of data available. The performance of SO₂ supports this hypothesis; the worst out of all pollutants and has the least available data.

Pollutant Name	Dataset Train Score	Dataset Validation Score	Dataset Test Score
NO ₂	0.85	0.77	0.77
NO _x	0.82	0.75	0.74
NO	0.73	0.67	0.65
O ₃	0.81	0.70	0.67
SO ₂	0.46	0.42	0.29
PM ₁₀	0.54	0.38	0.32
PM _{2.5}	0.58	0.34	0.29

Table 3: **R^2 scores depicting forecasting performance for 5-fold leave-one-out-validation.** The experiment conducted aimed to ensure that with different subsets of monitoring stations, the forecasting performance of the model remains robust. Shown with Table 3 having similar performance as the experiment result shown in Table 2, particularly the test score, data the models have never seen before.

Through the definition provided for the AURN station environment types, we know that air pollutant concentrations exhibit different signatures in different locations. There is the possibility of further subclassifications within these environment types. For example, taking the Urban Traffic environment type, there could be a distinction between the Urban Traffic stations within London and outside of London. Particularly for the approach used within this work, a data-driven model, this can have wide-ranging implications. Suppose it does exist that a subset or single

station within the LOOV dataset is unique compared to others, resulting in no similar data present within the training data. In that case, the model presented will fail to replicate the time series measured. This hypothesis is supported as the temporal experiment framework performance is consistent across all the experiments conducted, shown in Figure 2 and Figure 3, with the issue only appearing in the spatial experiments. As a more concrete example of this scenario, the Aston Hill AURN monitoring station is the only monitoring station in the NO_x dataset with no roads nearby, a clearly unique monitoring station in the dataset. This issue is further complicated when considering the results from Section 4.2, where not all feature vector elements have an air pollution monitoring station present, showing clear environment types that have no data available, denoting situations where the model is extrapolating and potentially widely wrong.

The experiment here provides the basis for using the model to create a complete spatial map of pollution across England and Wales with the framework of synthetic stations. In the case of the grid system used in this study, the framework acts as if 355,827 synthetic stations are present at the centroid of each grid, which gives a point sample measurement of the ambient air pollution concentration at a given time. Figure 8 shows the resulting air pollution concentration map we can create from the model, predicting air pollution at every location across England.

Pollutant Name	Estimation LOOV Max	Estimation LOOV Min	Estimation LOOV Mean	Estimation LOOV Median
NO	0.62	-2.28	0.10	0.21
NO ₂	0.70	-1.75	0.25	0.37
NO _x	0.67	-1.46	0.20	0.32
O ₃	0.78	-1.95	0.45	0.62
PM ₁₀	0.59	-0.17	0.35	0.38
PM ₂₅	0.59	0.23	0.45	0.46
SO ₂	0.10	-1.65	-0.20	-0.02

Table 4: **R² scores for missing monitoring stations performance summary statistics for 5-fold leave-one-out-validation.** The summary statistics show the R² for each monitoring station in the study for a model that has never seen the stations’ data before. The approach has clear merit, with all air pollutants having a positive maximum score. However, some monitoring stations have a negative minimum score, driven by their unique nature concerning the feature vectors and phenomena driving the air pollution concentrations at a given location. The mean and median R² scores show that the approach works for most stations for most air pollutants in estimating air pollution concentrations at a missing location.

5.4 Prediction of Peak Values

While the R² score provides a metric for evaluating the overall performance of the model on the entire dataset, a critical consideration in the context of air pollution concentration estimation is the model’s performance during peak concentrations. Given that peak concentrations have the most significant impact on human health and well-being and are the focus of policymakers when designing interventions, it is crucial to assess how well the model performs in these high-concentration scenarios.

We conducted an analysis of the model predictions during peak concentration events observed at each station. Figure 9 illustrates the model’s predictions compared to real-world measurements from AURN monitoring stations. Specifically, Figure 9a focuses on the Leominster monitoring station discussed in Section 1. The visual comparison reveals that while the model did not capture the exact magnitude of the peak concentration at the station, it did exhibit an uptick at the correct time. This raises concerns about the model’s ability to make high-magnitude predictions. However, further investigation indicates otherwise, as evidenced by the Stanford-le-Hope Roadside AURN station, which had a high-magnitude prediction of approximately 140 $\mu\text{g}/\text{m}^3$ for its overall peak concentration reading between 2014-2018.

This prompts the question of whether the model’s prediction for the Leominster peak value was an underprediction or if the peak value itself was an anomalous reading. The percentage difference for the Leominster monitoring station at 03/12/2014 8 AM was 42.5%. In contrast, the mean peak percentage difference across all NO₂ monitoring stations was 22.1% during the Leominster peak, considerably lower than the overall NO₂ average peak distance of 50.72%. The considerable difference in expected peak distance suggests that the Leominster station differed from nearby stations at this time. The performance variation across different pollutants sheds light on a potential issue with the model stemming from the training data, as depicted in Table 5. Notably, O₃ exhibits the best performance in predicting peak concentrations. As outlined in Section 2, meteorological conditions predominantly drive O₃ concentrations. The ERA5 data used in this study stands out as the most robust dataset, featuring temporally and spatially unique data points.

In contrast, other datasets used in the model lack this level of uniqueness, relying on idealized values that may not accurately represent the true variability. For instance, the transport use dataset family follows a common temporal distribution, emissions are scaled, and datasets like transport infrastructure lack sufficient variability. These

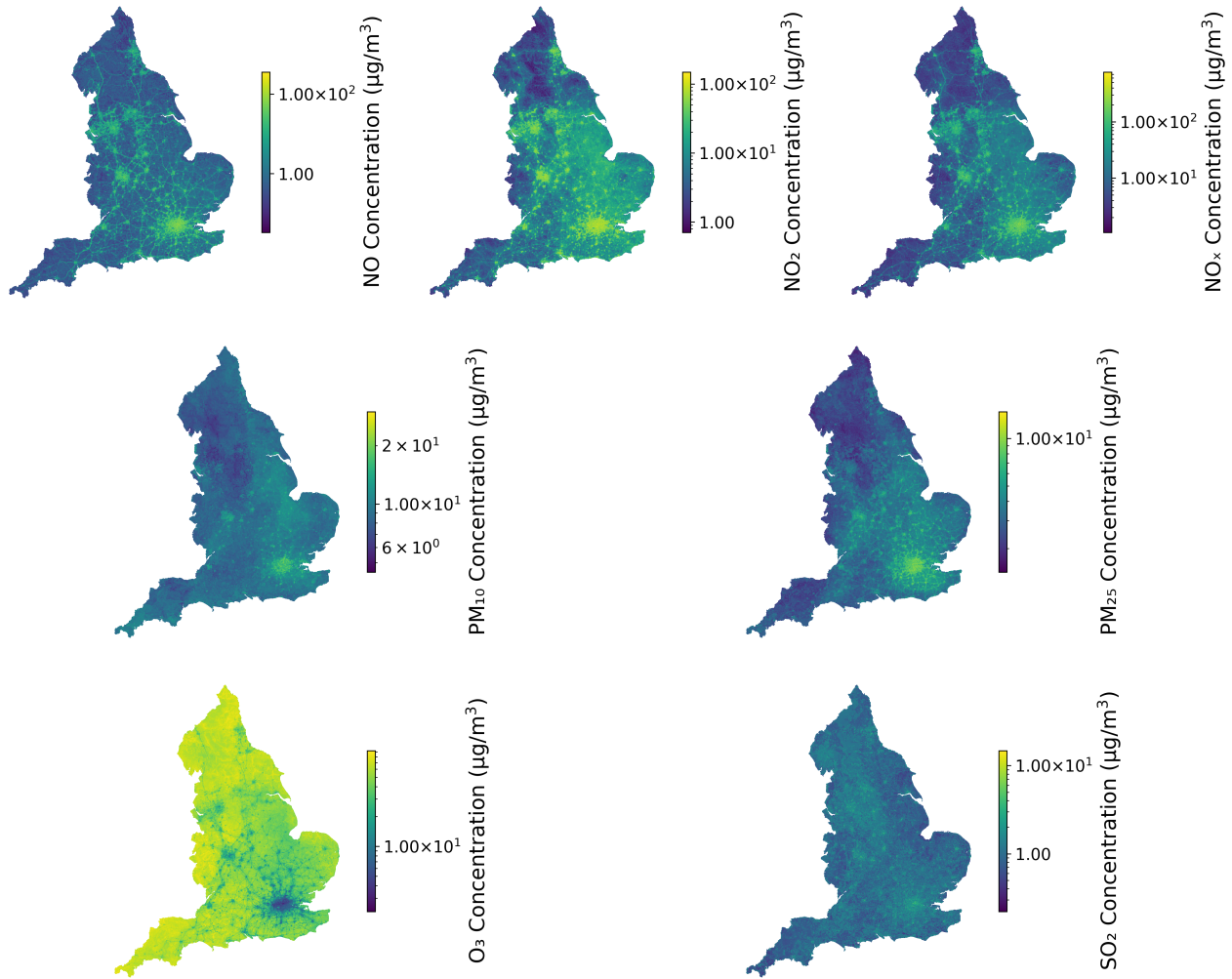


Figure 8: **Full spatial map of England for all pollutants for 8AM on 19/01/2018, chosen arbitrarily as a typical working day away from national holidays in England.** Plotted on a log scale to help highlight the differences within regions in the map.

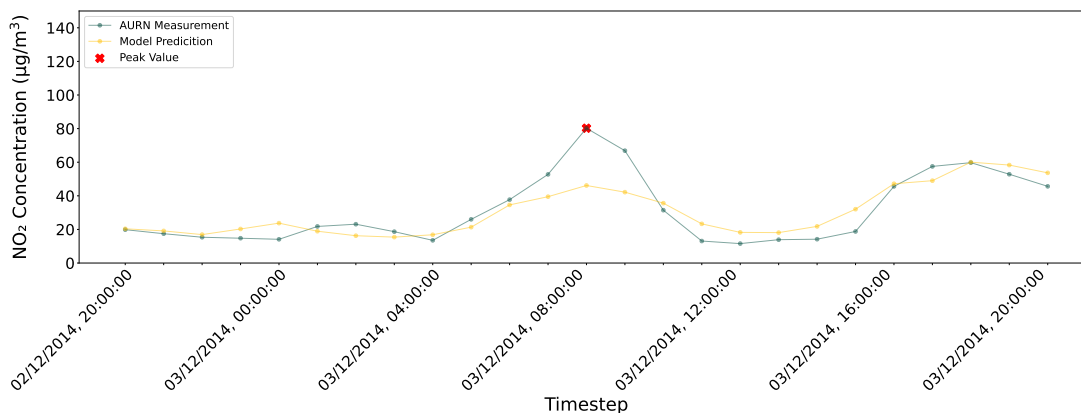
idealized values present an avenue for improving the model by seeking enhanced data representations of phenomena influencing air pollution. Additionally, addressing the potential impact of outlier and anomalous data points could further enhance model performance. The peak distance percentage is defined in Equation 1.

$$\left(\frac{(\text{Measured Peak} - \text{Model Prediction})}{\text{Peak Value}} \right) \times 100 \quad (1)$$

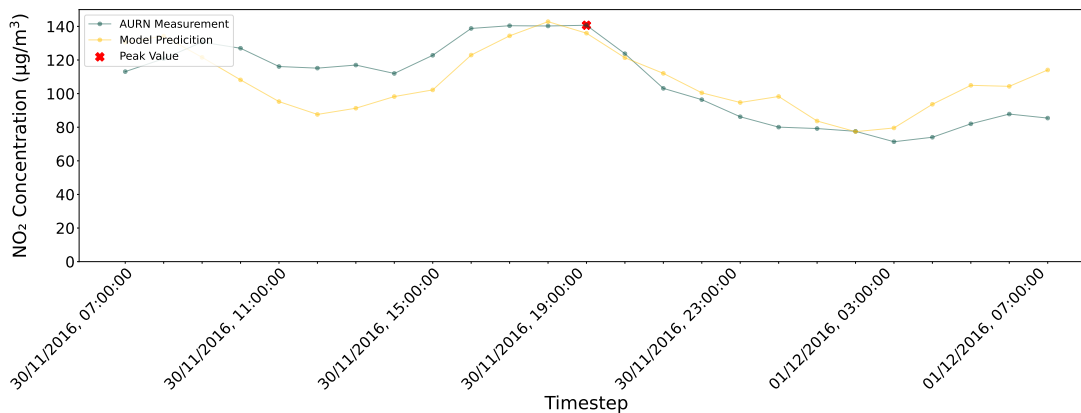
5.5 Data Subsetting

The scalability of the framework has been considered primarily within temporal and spatial resolution dimensions. However, the framework's adaptability extends to different amounts of data, contingent on the availability of specific datasets. Variations in input datasets allow for the development of models tailored to different use cases. For instance, datasets that are only available after historical dates, such as remote sensing, may be excluded when creating models for forecasting purposes. Table S11 provides experiment results for this type of model. Additionally, in situations where a location lacks certain datasets, such as traffic estimates for an entire country, models can be built using only the available datasets. Both meteorological and remote sensing datasets have global availability, making them suitable for creating baseline hindcast models for locations worldwide. Table S10 showcases the performance of such a model.

Further experimentation delved into assessing the performance of each dataset family, as depicted in Table 6. These findings support the concepts presented in Section 4.1, emphasizing that no single dataset alone can achieve a positive mean LOOV score.



(a) Leominster NO₂.



(b) Stanford-le-Hope Roadside NO₂.

Figure 9: Prediction of peak values for NO₂ monitoring stations. In Figure 9a, it is evident that the model failed to capture the peak concentration for the Leominster monitoring station. However, there is a noticeable uptick in the concentration prediction at the correct time, raising concerns about a consistent underestimation by the model. Conversely, Figure 9b illustrates the peak prediction for the Stanford-le-Hope monitoring station. The model not only captures the peak but also yields a magnitude considerably higher than that for Leominster, offering an initial indication that the model may not be systematically underpredicting concentrations.

6 Research Data Output

As part of our ongoing efforts, we plan to release an open-source dataset consisting of two components. The first component is the augmented AURN dataset, as illustrated in Figure 7. This dataset includes model predictions for air pollution concentrations at all AURN monitoring stations for the period 2014-2018, which were utilized in this study. The second component is a comprehensive air pollution concentration map for England, encompassing each air pollutant for the year 2018. This dataset provides a spatial resolution of 1 km² and hourly temporal resolution. We anticipate that this dataset will be of significant interest to various stakeholders, as outlined in Section 1. Moreover, it opens avenues for the research community to explore a diverse range of research topics that were previously constrained, given that current air pollution estimations at this spatial resolution typically operate at the annual temporal level.

The presented dataset opens up diverse research possibilities, with one illustrative example being the examination of air pollution concentration variations across different locations concerning legislation compliance, as discussed in Section 1. Figure 10 showcases a series of heatmaps representing the grids employed in this study. Each grid is colour-coded based on the number of times it exceeded specific concentration thresholds in 2018 at an hourly granularity. The maximum possible number of exceedances per grid is 8760, representing the total hours in 2018.

The thresholds considered include 10µg/m³, aligning with the WHO NO₂ air quality guideline level for the annual temporal period. The second threshold is 25µg/m³, corresponding to the WHO 24-hour aggregate air quality guideline [5]. The third threshold is 40µg/m³, reflecting the UK National Air Quality Guideline annual limit. Lastly, 200µg/m³ represents the UK National Air Quality Guideline hourly target for NO₂ concentrations [7]. While not all these thresholds directly pertain to hourly concentration legislation, they provide a comprehensive set of benchmarks derived from actual legislation, offering insights into the distribution of air pollutants across England.

Pollutant Name	Average Peak Distance Percentage (% of $\mu\text{g}/\text{m}^3$)
O ₃	32.07
NO ₂	50.72
NO _x	63.82
NO	72.32
PM ₂₅	84.21
PM ₁₀	87.37
SO ₂	93.00

Table 5: **Average peak concentrations prediction difference.** The peak percentage difference is calculated according to formula 1. O₃ has the best performance for predicting the peak concentrations across all the monitoring stations, with SO₂ having the worst performance. This ordering presents further evidence that the likely explanation for the model not capturing the peak concentrations is not the model framework itself but rather the input data. SO₂ has by a considerable margin the least amount of data across the air pollutants (Table 1, alongside O₃ being most correlated (Section 4.1) and driven by meteorological phenomena according to the scientific literature (Section 3.2), which given that ERA5 is the highest quality dataset, with unique points spatially and temporally indicates that the difference in data is likely driving the difference in peak concentration estimation performance.

Dataset Family	Dataset Train Score	Dataset Validation Score	Dataset Test Score	Mean LOOV
Emissions	0.46	0.42	0.42	-0.23
Geographic	0.31	0.25	0.29	-0.46
Meteorological	0.15	0.17	0.14	-0.53
Remote Sensing	0.35	0.31	0.36	-0.38
Temporal	0.00	0.03	0.02	-0.64
Transport Infrastructure	0.32	0.29	0.29	-0.41
Transport Use	0.35	0.23	0.16	-0.47

Table 6: **Repeat experiments results of Tables 2 and 4 for models trained on individual dataset families (Section 3.2) for NO₂.** The framework presented can be used on varying amounts of input data, depending on available data, providing a basic understanding of limitations when moving the model between areas, such as being used to predict countries other than England. Table 6 shows that in the case of England, while individual dataset families can forecast into the future, the performance of estimating missing monitoring stations is limited and requires datasets that cover a wide range of phenomena to achieve the same performance as 4.

The analysis reveals compelling insights into air pollution concentration exceedances across various thresholds. It was found that 99.96% of locations surpassed the $10\mu\text{g}/\text{m}^3$ threshold at least once, 63% exceeded the $25\mu\text{g}/\text{m}^3$ threshold at least once, 26.2% exceeded the $40\mu\text{g}/\text{m}^3$ threshold at least once, and only a single grid exceeded the $200\mu\text{g}/\text{m}^3$ threshold at least once. This analysis serves as a valuable tool to pinpoint locations demanding further investigation into air pollution concentration causes and potential interventions at the local level. For instance, the coordinates at latitude 51.5, longitude -0.15, representing a location exceeding the $200\mu\text{g}/\text{m}^3$ threshold with concentration predictions surpassing 10 for every hour in 2018, underscore the need for targeted attention. Moreover, leveraging the temporal precision of the predictions allows for flexible aggregation to various temporal levels stipulated in UK or EU legislation. For instance, aggregating to a 24-hour mean [100] for each grid facilitates a comprehensive assessment of legislation compliance, as depicted in Figure 11.

7 Discussion

We have released two datasets that hold significant value for the scientific community, policymakers, and the public. The comprehensive spatial dataset offers valuable insights into locations where air pollution concentration data might be non-existent at the hourly temporal level. If one were to acquire the data produced by our model through real-world measurements, the cost would amount to £70B⁷ through AURN monitoring stations.

The augmented AURN dataset, generated from this study, provides a complete temporal perspective of all monitoring station measurements across England. This is particularly crucial for compliance assessments related to absolute threshold exceedances, such as NO₂, where a detailed limit of $200\mu\text{g}/\text{m}^3$ should not be exceeded more

⁷Calculated based on 355827 monitoring stations at a cost of £198000 per station, as outlined in Section 1.

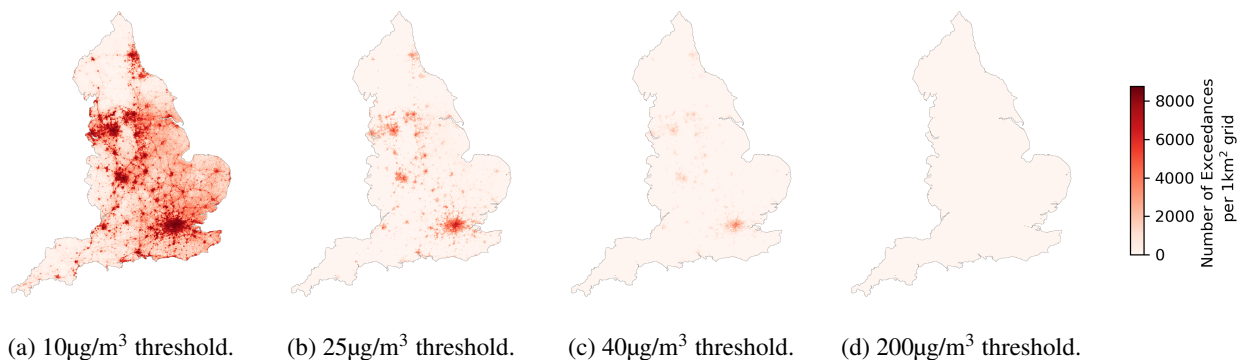


Figure 10: **Count of times that a grid exceeded the outlined thresholds for NO_2 in 2018.** Figure 10a shows the $10\mu\text{g}/\text{m}^3$ threshold where one grid exceeds the threshold for every hour of the year, with 99.6% of grids exceeding the threshold at least once. Figure 10b depicts the counts for the $25\mu\text{g}/\text{m}^3$ where the max count was 8656 exceedances across the year, with 63% of grids exceeding the threshold at least once. Figure 10c uses a threshold of $40\mu\text{g}/\text{m}^3$ where the max count for exceedances was 8,086 across the year, with 26.2% of grids exceeding the threshold at least once. Figure 10d denotes a $200\mu\text{g}/\text{m}^3$ threshold, where only a single grid exceeded the threshold twice across the year. Latitude 51.5, longitude -0.15 was the location that exceeded the threshold, a central London location with the postcode W1G 6JA.

than 18 times a year [7]. Ensuring a complete time series with measurements at each time step is essential when comparing two locations, especially in situations where missing data during peak pollution periods, like NO_x during rush hour, could potentially mask crucial information. This consideration becomes paramount when creating higher temporal resolution statistics through UK AIR⁸.

While the presented model has demonstrated its effectiveness in filling missing data from high-quality air quality monitoring stations, its most significant advantages lie in its potential application to low-cost monitoring sensors and citizen science initiatives. The symbiotic relationship between the model and low-cost sensors addresses a core issue present in both approaches. The model’s performance is notably impacted by a lack of data. In locations where the installation of more expensive AURN-style stations might not be deemed a worthwhile investment, low-cost sensors can be strategically deployed to fill data gaps. These sensors, due to their minimal cost, can be implemented in various locations, enhancing spatial coverage.

Conversely, the model can contribute to overcoming the challenges associated with low-cost sensors, which are often less robust than AURN stations. By leveraging the model, missing data points can be backfilled temporally and spatially, ensuring the generation of a more complete dataset. This collaborative approach is particularly valuable in scenarios where the less frequent deployment of AURN stations results in gaps in the feature vector, as discussed in Section 4.2. An additional advantage is the model’s ability to handle temporally messy data commonly encountered in citizen science initiatives. Unlike AURN monitoring stations that provide data at regular intervals, citizen science datasets may exhibit irregular time stamps (e.g., 10:14, 10:47, and 11:46). The model enables a more sophisticated estimation of air pollution at specific times (e.g., 10:00, 11:00, 12:00), facilitating further analysis such as legislation compliance or integration with other forecasting systems.

Importantly, the model method offers substantial benefits compared to other approaches for filling missing data, such as interpolation, as it takes into account the nuanced patterns present in air pollution concentration time series datasets.

Although the proposed model demonstrates significant advantages, there is a clear pathway to extracting even more benefits from the model framework, given its inherent scalability in both spatial and temporal dimensions. The extension of the method to make predictions at a minute temporal-level is straightforward, and similarly, increasing the spatial resolution grid size to 100m^2 is feasible. This scalable approach empowers researchers by providing the desired data without being constrained by limitations in financial resources for monitoring station placement.

Furthermore, the encoding of the temporal aspect into a tabular format facilitates a substantial acceleration through parallelization. Each timestep and grid within the estimation is independent of one another, enabling the simultaneous calculation of all timesteps and grids. This approach yields a significant speedup over traditional forecasting methods, whether machine-learning or physics-based, that rely on lags from previous timesteps.

From a performance standpoint, the capacity to parallelize estimations becomes pivotal when combined with the scalability of the approach. This combination forms the basis for a computationally effective method of estimating air pollution concentrations at a global level. Future work could extend the experiment conducted in Section 5.3, where air pollution concentrations at one station were estimated using data from other monitoring stations, to a study that analyzes the feasibility of estimating air pollution between countries and their respective air pollution

⁸UK AIR Statistics Using Incomplete Data, denoted by data capture rate.

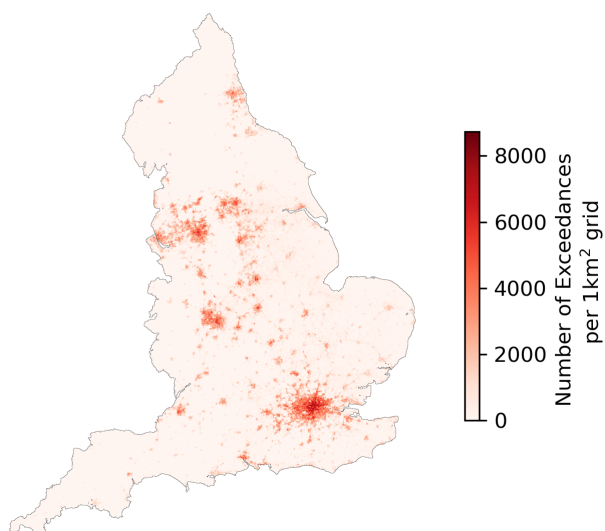


Figure 11: **24-hour mean [100] exceedance counts example.** The threshold used is a mean of $25 \mu\text{g}/\text{m}^3$. As the hourly level is the most common high-resolution temporal level mentioned in air quality legislation, pursuing data at this level allows for a more coarse temporal level to be calculated from the input data, resulting in the dataset providing complete legislation coverage no matter the resolution of interest.

monitoring networks. The potential benefit of this analysis is to help reduce inequalities between countries concerning monitoring stations, enabling the design of interventions based on air pollution without the need for high-cost, dedicated monitoring station networks to be implemented by a country's government.

While the datasets employed in this study successfully estimated air pollution concentrations under a variety of conditions, there remains room for improvement in the input feature vectors. Presently, the model does not consider variations associated with specific days, such as distinct travel patterns on bank holidays compared to regular weekdays. Incorporating local knowledge into the model, such as categorizing whether a day is a bank holiday or another national holiday, would enhance the model's understanding of unique circumstances on special days, such as Bonfire Night in the UK, known to have considerable impact on air pollution concentrations [101]. Additionally, some feature vectors used in the model will improve over time as technology advances, enabling improved model performance. For example, remote sensing of trace gases over Europe will improve with the Sentinel-4 missions, which are currently scheduled for launch in 2024, on the MTG-s Satellite [102]. Sentinel-4 will provide hourly temporal resolution, with a spatial resolution of 8km for much of northern Europe for O_3 , NO_2 , SO_2 , and aerosol optical depth [103].

In addition to incorporating additional knowledge into the model, a thorough analysis of the training data used in the study is crucial to ensure comprehensive coverage of all scenarios, minimizing the need for extrapolation during model estimations. For instance, as discussed in Section 4.2, there are environmental conditions where no air pollution concentration measurements are available. Future work could focus on analyzing missing scenarios in the training data, identifying locations where additional air pollution monitoring stations should be placed. When combined with low-cost sensors, this approach could form the basis for a dynamic mobile monitoring network to identify areas where the model predictions are most uncertain.

In summary, we believe this work holds significant importance for a broad audience, addressing critical challenges outlined in the United Nations (UN) Sustainable Development Goals (SDGs). The work presented empowers decision-makers with high-quality data for crucial indicators (UN SDG 3.9.1, 11.6.2) for essential goals such as Good Health and Well-being (SDG 3) and Sustainable Cities and Communities (SDG 11). The contribution to SDG 3 is evident in reallocating resources from monitoring air pollution to clean air initiatives, providing estimates in all regions, not just those with monitoring stations. Simultaneously, the research contributes to SDG 11 by advancing the understanding of the relationship between urban and rural air pollution.

References

- [1] Office for Health Improvement and Disparities. (2022) Air pollution: applying All Our Health. Accessed on: 29/11/2023. [Online]. Available: <https://www.gov.uk/government/publications/air-pollution-applying-all-our-health/air-pollution-applying-all-our-health>

- [2] AEA Technology, Aug 2006, https://uk-air.defra.gov.uk/assets/documents/reports/cat06/0608141644-386_Purchasing_Guide_for_AQ_Monitoring_Equipment_Version2.pdf "Accessed on: 08/2022 [Online]".
- [3] George Eustice and Lord Goldsmith of Richmond Park. (2021) Environment Bill. Accessed on: 29/11/2023. [Online]. Available: <https://bills.parliament.uk/bills/2593>
- [4] UK-AIR. (2019) Modelled air quality data. Accessed on: 29/11/2023. [Online]. Available: <https://uk-air.defra.gov.uk/data/modelling-data>
- [5] World Health Organisation. (2021) What are the WHO Air quality guidelines? Accessed on: 29/11/2023. [Online]. Available: <https://www.who.int/news-room/feature-stories/detail/what-are-the-who-air-quality-guidelines>
- [6] World Health Organization, *WHO global air quality guidelines: particulate matter (PM_{2.5} and PM₁₀), ozone, nitrogen dioxide, sulfur dioxide and carbon monoxide*. World Health Organization, 2021.
- [7] King's Printer of Acts of Parliament. (2010) The Air Quality Standards Regulations 2010. Accessed on: 29/11/2023. [Online]. Available: <https://www.legislation.gov.uk/uksi/2010/1001/contents/made>
- [8] E. Assessment, "Guidelines for exposure assessment," *Federal Register*, vol. 57, no. 104, pp. 22 888–938, 1992.
- [9] B. Zou, J. G. Wilson, F. B. Zhan, and Y. Zeng, "Air pollution exposure assessment methods utilized in epidemiological studies," *Journal of Environmental Monitoring*, vol. 11, no. 3, pp. 475–490, 2009.
- [10] R. W. Atkinson, A. Analitis, E. Samoli, G. W. Fuller, D. C. Green, I. S. Mudway, H. R. Anderson, and F. J. Kelly, "Short-term exposure to traffic-related air pollution and daily mortality in london, uk," *Journal of exposure science & environmental epidemiology*, vol. 26, no. 2, pp. 125–132, 2016.
- [11] G. Konstantinoudis, T. Padellini, J. Bennett, B. Davies, M. Ezzati, and M. Blangiardo, "Long-term exposure to air-pollution and covid-19 mortality in england: a hierarchical spatial analysis," *Environment international*, vol. 146, p. 106316, 2021.
- [12] V. É. Molnár, E. Simon, B. Tóthmérész, S. Ninsawat, and S. Szabó, "Air pollution induced vegetation stress—the air pollution tolerance index as a quick tool for city health evaluation," *Ecological Indicators*, vol. 113, p. 106234, 2020.
- [13] A. P. Tai, M. V. Martin, and C. L. Heald, "Threat to future global food security from climate change and ozone air pollution," *Nature Climate Change*, vol. 4, no. 9, pp. 817–821, 2014.
- [14] Y. Kang, L. Aye, T. D. Ngo, and J. Zhou, "Performance evaluation of low-cost air quality sensors: A review," *Science of The Total Environment*, vol. 818, p. 151769, 2022.
- [15] A. Rosofsky, J. I. Levy, A. Zanobetti, P. Janulewicz, and M. P. Fabian, "Temporal trends in air pollution exposure inequality in massachusetts," *Environmental research*, vol. 161, pp. 76–86, 2018.
- [16] W. N. Stasiuk Jr and P. E. Coffey, "Rural and urban ozone relationships in new york state," *Journal of the Air Pollution Control Association*, vol. 24, no. 6, pp. 564–568, 1974.
- [17] Belgian Interregional Environment Agency. (2024) Why are ozone concentrations higher in rural areas than in cities? Accessed on: 05/01/2024. [Online]. Available: <https://www.irceline.be/en/documentation/faq/why-are-ozone-concentrations-higher-in-rural-areas-than-in-cities>
- [18] UK-AIR, DEFRA. (2021) 'Low-cost' pollution sensors - understanding the uncertainties. Accessed on: 29/11/2023. [Online]. Available: <https://uk-air.defra.gov.uk/research/aqeg/pollution-sensors/understanding-uncertainties.php>
- [19] F. Concas, J. Mineraud, E. Lagerspetz, S. Varjonen, X. Liu, K. Puolamäki, P. Nurmi, and S. Tarkoma, "Low-cost outdoor air quality monitoring and sensor calibration: A survey and critical analysis," *ACM Transactions on Sensor Networks (TOSN)*, vol. 17, no. 2, pp. 1–44, 2021.
- [20] A. C. Rai, P. Kumar, F. Pilla, A. N. Skouloudis, S. Di Sabatino, C. Ratti, A. Yasar, and D. Rickerby, "End-user perspective of low-cost sensors for outdoor air pollution monitoring," *Science of The Total Environment*, vol. 607-608, pp. 691–705, Dec. 2017. [Online]. Available: <https://linkinghub.elsevier.com/retrieve/pii/S0048969717316935>
- [21] N. Castell, F. R. Dauge, P. Schneider, M. Vogt, U. Lerner, B. Fishbain, D. Broday, and A. Bartonova, "Can commercial low-cost sensor platforms contribute to air quality monitoring and exposure estimates?" *Environment International*, vol. 99, pp. 293–302, Feb. 2017. [Online]. Available: <https://linkinghub.elsevier.com/retrieve/pii/S0160412016309989>
- [22] J. P. Veefkind, I. Aben, K. McMullan, H. Förster, J. De Vries, G. Otter, J. Claas, H. Eskes, J. De Haan, Q. Kleipool *et al.*, "Tropomi on the esa sentinel-5 precursor: A gmes mission for global observations of the atmospheric composition for climate, air quality and ozone layer applications," *Remote sensing of environment*, vol. 120, pp. 70–83, 2012.
- [23] European Space Agency - Copernicus. (2023) Sentinel, Missions, Sentinel 5P - Orbit. Accessed on: 29/11/2023. [Online]. Available: <https://sentinels.copernicus.eu/web/sentinel/missions/sentinel-5p/orbit>

- [24] ——. (2017) Sentinel-5 Precursor Calibration and Validation Plan for the Operational Phase. Accessed on: 29/11/2023. [Online]. Available: <https://sentinels.copernicus.eu/documents/247904/2474724/Sentinel-5P-Calibration-and-Validation-Plan.pdf>
- [25] P. Zoogman, X. Liu, R. Suleiman, W. Pennington, D. Flittner, J. Al-Saadi, B. Hilton, D. Nicks, M. Newchurch, J. Carr *et al.*, “Tropospheric emissions: Monitoring of pollution (tempo),” *Journal of Quantitative Spectroscopy and Radiative Transfer*, vol. 186, pp. 17–39, 2017.
- [26] A. Eliassen, “Aspects of lagrangian air pollution modelling,” in *Air Pollution Modeling and Its Application III*. Springer, 1984, pp. 3–21.
- [27] Daewon W. Byun, Avraham Lacser, Robert Yamartino, and Paolo Zannetti, “Chapter 10 eulerian dispersion models,” 2003.
- [28] M. de’Michieli Vitturi, A. Neri, T. Esposti Ongaro, S. Lo Savio, and E. Boschi, “Lagrangian modeling of large volcanic particles: Application to vulcanian explosions,” *Journal of Geophysical Research: Solid Earth*, vol. 115, no. B8, 2010.
- [29] G. Hoek, R. Beelen, K. De Hoogh, D. Vienneau, J. Gulliver, P. Fischer, and D. Briggs, “A review of land-use regression models to assess spatial variation of outdoor air pollution,” *Atmospheric environment*, vol. 42, no. 33, pp. 7561–7578, 2008.
- [30] D. K. Henze, A. Hakami, and J. H. Seinfeld, “Development of the adjoint of geos-chem,” *Atmospheric Chemistry and Physics*, vol. 7, no. 9, pp. 2413–2433, 2007. [Online]. Available: <https://acp.copernicus.org/articles/7/2413/2007/>
- [31] B. S. Freeman, G. Taylor, B. Gharabaghi, and J. Thé, “Forecasting air quality time series using deep learning,” *Journal of the Air & Waste Management Association*, vol. 68, no. 8, pp. 866–886, 2018.
- [32] Q. Tao, F. Liu, Y. Li, and D. Sidorov, “Air pollution forecasting using a deep learning model based on 1d convnets and bidirectional gru,” *IEEE access*, vol. 7, pp. 76 690–76 698, 2019.
- [33] K. Harishkumar, K. Yogesh, I. Gad *et al.*, “Forecasting air pollution particulate matter (pm2. 5) using machine learning regression models,” *Procedia Computer Science*, vol. 171, pp. 2057–2066, 2020.
- [34] S. Van Roode, J. Ruiz-Aguilar, J. González-Enrique, and I. Turias, “An artificial neural network ensemble approach to generate air pollution maps,” *Environmental monitoring and assessment*, vol. 191, pp. 1–15, 2019.
- [35] C.-C. Chen, Y.-R. Wang, H.-Y. Yeh, T.-H. Lin, C.-S. Huang, and C.-F. Wu, “Estimating monthly pm2. 5 concentrations from satellite remote sensing data, meteorological variables, and land use data using ensemble statistical modeling and a random forest approach,” *Environmental Pollution*, vol. 291, p. 118159, 2021.
- [36] Q. He, T. Ye, M. Zhang, and Y. Yuan, “Enhancing the reliability of hindcast modeling for air pollution using history-informed machine learning and satellite remote sensing in china,” *Atmospheric Environment*, p. 119994, 2023.
- [37] J. Li, H. Zhang, C.-Y. Chao, C.-H. Chien, C.-Y. Wu, C. H. Luo, L.-J. Chen, and P. Biswas, “Integrating low-cost air quality sensor networks with fixed and satellite monitoring systems to study ground-level pm2. 5,” *Atmospheric Environment*, vol. 223, p. 117293, 2020.
- [38] D. C. Carslaw and K. Ropkins, “openair — An R package for air quality data analysis,” *Environmental Modelling and Software*, vol. 27–28, no. 0, pp. 52–61, 2012.
- [39] UK-AIR. (2023) Site environment types - Background Station. Accessed on: 29/11/2023. [Online]. Available: <https://uk-air.defra.gov.uk/networks/site-types>
- [40] DEFRA, Department for Environment Food and Rural Affairs. (2017) The Air Quality Data Validation and Ratification Process. Accessed on: 29/11/2023. [Online]. Available: https://uk-air.defra.gov.uk/assets/documents/Data_Validation_and_Ratification_Process_Apr_2017.pdf
- [41] ——. (2023) Air quality statistics in the UK, 1987 to 2022 - Background. Accessed on: 29/11/2023. [Online]. Available: <https://www.gov.uk/government/statistics/air-quality-statistics/background>
- [42] T. Crosby, “How to detect and handle outliers,” 1994.
- [43] L. J. Berrisford, E. Ribeiro, and R. Menezes, “Estimating ambient air pollution using structural properties of road networks,” *arXiv preprint arXiv:2207.14335*, 2022.
- [44] J. Bennett, *OpenStreetMap*. Packt Publishing Ltd, 2010.
- [45] L. Watkins, “Air pollution from road vehicles,” 1991.
- [46] F. Yan, E. Winijkul, S. Jung, T. C. Bond, and D. G. Streets, “Global emission projections of particulate matter (pm): I. exhaust emissions from on-road vehicles,” *Atmospheric Environment*, vol. 45, no. 28, pp. 4830–4844, 2011.
- [47] F. Amato, X. Querol, C. Johansson, C. Nagl, and A. Alastuey, “A review on the effectiveness of street sweeping, washing and dust suppressants as urban pm control methods,” *Science of the total environment*, vol. 408, no. 16, pp. 3070–3084, 2010.

- [48] A. Haagen-Smit, "Urban air pollution," *Advances in Geophysics*, vol. 6, pp. 1–18, 1959.
- [49] Department of Transport, UK Government. (2023) Road Traffic Stations - About. Accessed on: 29/11/2023. [Online]. Available: <https://roadtraffic.dft.gov.uk/about>
- [50] O. for National Statistics, "2011 census aggregate data," 2017. [Online]. Available: <https://www.ons.gov.uk/census/2011census>
- [51] J. Sullivan O., Gershuny, "United kingdom time use survey, 2014-2015," 2023. [Online]. Available: <https://beta.ukdataservice.ac.uk/datacatalogue/doi/?id=8128#1>
- [52] X. Jurado, N. Reiminger, J. Vazquez, and C. Wemmert, "On the minimal wind directions required to assess mean annual air pollution concentration based on cfd results," *Sustainable Cities and Society*, vol. 71, p. 102920, 2021. [Online]. Available: <https://www.sciencedirect.com/science/article/pii/S2210670721002079>
- [53] R. Cichowicz, G. Wielgosiński, and W. Fetter, "Dispersion of atmospheric air pollution in summer and winter season," *Environmental monitoring and assessment*, vol. 189, pp. 1–10, 2017.
- [54] J. Wallace, D. Corr, and P. Kanaroglou, "Topographic and spatial impacts of temperature inversions on air quality using mobile air pollution surveys," *Science of the total environment*, vol. 408, no. 21, pp. 5086–5096, 2010.
- [55] B. J. Bloomer, J. W. Stehr, C. A. Piety, R. J. Salawitch, and R. R. Dickerson, "Observed relationships of ozone air pollution with temperature and emissions," *Geophysical research letters*, vol. 36, no. 9, 2009.
- [56] D. J. Nowak, P. J. McHale, M. Ibarra, D. Crane, J. C. Stevens, and C. J. Luley, "Modeling the effects of urban vegetation on air pollution," *Air pollution modeling and its application XII*, pp. 399–407, 1998.
- [57] B. J. Finlayson-Pitts and J. N. Pitts Jr, "Atmospheric chemistry. fundamentals and experimental techniques," 1986.
- [58] O. Jolliet and M. Hauschild, "Modeling the influence of intermittent rain events on long-term fate and transport of organic air pollutants," *Environmental science & technology*, vol. 39, no. 12, pp. 4513–4522, 2005.
- [59] Q. Yuan, H. B. Guerra, and Y. Kim, "An investigation of the relationships between rainfall conditions and pollutant wash-off from the paved road," *Water*, vol. 9, no. 4, p. 232, 2017.
- [60] X. Xu, X. Yu, L. Bao, and A. R. Desai, "Size distribution of particulate matter in runoff from different leaf surfaces during controlled rainfall processes," *Environmental Pollution*, vol. 255, p. 113234, 2019.
- [61] G. Ning, S. Wang, S. H. L. Yim, J. Li, Y. Hu, Z. Shang, J. Wang, and J. Wang, "Impact of low-pressure systems on winter heavy air pollution in the northwest sichuan basin, china," *Atmospheric Chemistry and Physics*, vol. 18, no. 18, pp. 13 601–13 615, 2018.
- [62] F. M. Vukovich, "A note on air quality in high pressure systems," *Atmospheric Environment (1967)*, vol. 13, no. 2, pp. 255–265, 1979.
- [63] H. Hippler, R. Rahn, and J. Troe, "Temperature and pressure dependence of ozone formation rates in the range 1–1000 bar and 90–370 k," *The Journal of chemical physics*, vol. 93, no. 9, pp. 6560–6569, 1990.
- [64] Y. Xiang, T. Zhang, J. Liu, L. Lv, Y. Dong, and Z. Chen, "Atmosphere boundary layer height and its effect on air pollutants in beijing during winter heavy pollution," *Atmospheric Research*, vol. 215, pp. 305–316, 2019.
- [65] F. Davies, D. Middleton, and K. Bozier, "Urban air pollution modelling and measurements of boundary layer height," *Atmospheric environment*, vol. 41, no. 19, pp. 4040–4049, 2007.
- [66] Y. Xiang, T. Zhang, J. Liu, L. Lv, Y. Dong, and Z. Chen, "Atmosphere boundary layer height and its effect on air pollutants in beijing during winter heavy pollution," *Atmospheric Research*, vol. 215, pp. 305–316, 2019.
- [67] H. Hersbach, "The era5 atmospheric reanalysis." in *AGU fall meeting abstracts*, vol. 2016, 2016, pp. NG33D–01.
- [68] F. Chaaban, T. Mezher, and M. Ouwayjan, "Options for emissions reduction from power plants: an economic evaluation," *International journal of electrical power & energy systems*, vol. 26, no. 1, pp. 57–63, 2004.
- [69] Q. Shi and J. Wu, "Review on sulfur compounds in petroleum and its products: State-of-the-art and perspectives," *Energy & Fuels*, vol. 35, no. 18, pp. 14 445–14 461, 2021.
- [70] J. J. Corbett and P. Fischbeck, "Emissions from ships," *Science*, vol. 278, no. 5339, pp. 823–824, 1997.
- [71] L. Tao, D. Fairley, M. J. Kleeman, and R. A. Harley, "Effects of switching to lower sulfur marine fuel oil on air quality in the san francisco bay area," *Environmental science & technology*, vol. 47, no. 18, pp. 10 171–10 178, 2013.
- [72] A. T. Nair, J. Senthilnathan, and S. S. Nagendra, "Emerging perspectives on voc emissions from landfill sites: Impact on tropospheric chemistry and local air quality," *Process safety and environmental protection*, vol. 121, pp. 143–154, 2019.
- [73] B. Gu, L. Zhang, R. Van Dingenen, M. Vieno, H. J. Van Grinsven, X. Zhang, S. Zhang, Y. Chen, S. Wang, C. Ren *et al.*, "Abating ammonia is more cost-effective than nitrogen oxides for mitigating pm2.5 air pollution," *Science*, vol. 374, no. 6568, pp. 758–762, 2021.

- [74] D. J. Nowak *et al.*, “The effects of urban trees on air quality,” *USDA Forest Service*, pp. 96–102, 2002.
- [75] D. J. Nowak, D. E. Crane, and J. C. Stevens, “Air pollution removal by urban trees and shrubs in the united states,” *Urban forestry & urban greening*, vol. 4, no. 3-4, pp. 115–123, 2006.
- [76] A. J. Arnfield, “Street design and urban canyon solar access,” *Energy and buildings*, vol. 14, no. 2, pp. 117–131, 1990.
- [77] M. F. Yassin, “Impact of height and shape of building roof on air quality in urban street canyons,” *Atmospheric Environment*, vol. 45, no. 29, pp. 5220–5229, 2011.
- [78] C. Rowland, R. Morton, L. Carrasco, G. McShane, A. O’neil, and C. Wood, “Land cover map 2015 (vector, gb),” *NERC Environmental Information Data Centre*, vol. 10, 2017.
- [79] D. L. Goldberg, S. C. Anenberg, G. H. Kerr, A. Mohegh, Z. Lu, and D. G. Streets, “Tropomi no2 in the united states: A detailed look at the annual averages, weekly cycles, effects of temperature, and correlation with surface no2 concentrations,” *Earth’s future*, vol. 9, no. 4, p. e2020EF001665, 2021.
- [80] J. Garland and R. Derwent, “Destruction at the ground and the diurnal cycle of concentration of ozone and other gases,” *Quarterly Journal of the Royal Meteorological Society*, vol. 105, no. 443, pp. 169–183, 1979.
- [81] T. Su, Z. Li, and R. Kahn, “Relationships between the planetary boundary layer height and surface pollutants derived from lidar observations over china: regional pattern and influencing factors,” *Atmospheric Chemistry and Physics*, vol. 18, no. 21, pp. 15 921–15 935, 2018.
- [82] S. Beirle, U. Platt, M. Wenig, and T. Wagner, “Weekly cycle of no 2 by gome measurements: a signature of anthropogenic sources,” *Atmospheric Chemistry and Physics*, vol. 3, no. 6, pp. 2225–2232, 2003.
- [83] J. K. Gietl and O. Klemm, “Analysis of traffic and meteorology on airborne particulate matter in münster, northwest germany,” *Journal of the Air & Waste Management Association*, vol. 59, no. 7, pp. 809–818, 2009.
- [84] X. Feng, Q. Li, Y. Zhu, J. Wang, H. Liang, and R. Xu, “Formation and dominant factors of haze pollution over beijing and its peripheral areas in winter,” *Atmospheric Pollution Research*, vol. 5, no. 3, pp. 528–538, 2014.
- [85] K. Meng, X. Xu, X. Cheng, X. Xu, X. Qu, W. Zhu, C. Ma, Y. Yang, and Y. Zhao, “Spatio-temporal variations in so2 and no2 emissions caused by heating over the beijing-tianjin-hebei region constrained by an adaptive nudging method with omi data,” *Science of the total environment*, vol. 642, pp. 543–552, 2018.
- [86] Q. Li, H. Zhang, X. Jin, X. Cai, and Y. Song, “Mechanism of haze pollution in summer and its difference with winter in the north china plain,” *Science of The Total Environment*, vol. 806, p. 150625, 2022. [Online]. Available: <https://www.sciencedirect.com/science/article/pii/S004896972105703X>
- [87] United States Environmental Protection Agency. (2023) Ground-level Ozone Basics. Accessed on: 29/11/2023. [Online]. Available: <https://www.epa.gov/ground-level-ozone-pollution/ground-level-ozone-basics>
- [88] UK National Atmospheric Emissions Inventory (NAEI). (2023) Pollutant information: Non Methane VOC. Accessed on: 29/11/2023. [Online]. Available: https://naei.beis.gov.uk/overview/pollutants?pollutant_id=9#:~:text=NMVOCs%20are%20emitted%20to%20air,over%20a%20large%20spatial%20scale.
- [89] G. Ke, Q. Meng, T. Finley, T. Wang, W. Chen, W. Ma, Q. Ye, and T.-Y. Liu, “Lightgbm: A highly efficient gradient boosting decision tree,” *Advances in neural information processing systems*, vol. 30, 2017.
- [90] S. M. Lundberg and S.-I. Lee, “A unified approach to interpreting model predictions,” in *Advances in Neural Information Processing Systems 30*, I. Guyon, U. V. Luxburg, S. Bengio, H. Wallach, R. Fergus, S. Vishwanathan, and R. Garnett, Eds. Curran Associates, Inc., 2017, pp. 4765–4774. [Online]. Available: <http://papers.nips.cc/paper/7062-a-unified-approach-to-interpreting-model-predictions.pdf>
- [91] T. O. Hodson, “Root-mean-square error (rmse) or mean absolute error (mae): When to use them or not,” *Geoscientific Model Development*, vol. 15, no. 14, pp. 5481–5487, 2022.
- [92] L. Yang, J. Yang, M. Liu, X. Sun, T. Li, Y. Guo, K. Hu, M. L. Bell, Q. Cheng, H. Kan *et al.*, “Nonlinear effect of air pollution on adult pneumonia hospital visits in the coastal city of qingdao, china: A time-series analysis,” *Environmental Research*, vol. 209, p. 112754, 2022.
- [93] B. Zhao, S. Wang, D. Ding, W. Wu, X. Chang, J. Wang, J. Xing, C. Jang, J. S. Fu, Y. Zhu *et al.*, “Nonlinear relationships between air pollutant emissions and pm2. 5-related health impacts in the beijing-tianjin-hebei region,” *Science of the Total Environment*, vol. 661, pp. 375–385, 2019.
- [94] A. E. Hoerl and R. W. Kennard, “Ridge regression: Biased estimation for nonorthogonal problems,” *Technometrics*, vol. 12, no. 1, pp. 55–67, 1970.
- [95] Microsoft. (2023) LightGBM - Parameters. Accessed on: 29/11/2023. [Online]. Available: <https://lightgbm.readthedocs.io/en/latest/Parameters.html>
- [96] Salil Mishra. (2023) Hyper parameter optimization - suggested parameter grid · ISSUE #695 · Microsoft/LIGHTGBM. Accessed on: 29/11/2023. [Online]. Available: <https://github.com/microsoft/LightGBM/issues/695>

- [97] UK-AIR, DEFRA. (2023) Site Information for Chesterfield Loundsley Green(UKA00604) - Defra, UK. Accessed on: 29/11/2023. [Online]. Available: https://uk-air.defra.gov.uk/networks/site-info?site_id=CHLG
- [98] ——. (2023) Closed AURN Monitoring Sites. Accessed on: 29/11/2023. [Online]. Available: <https://uk-air.defra.gov.uk/networks/aurn-sites>
- [99] ——. (2023) Interactive monitoring networks map. Accessed on: 29/11/2023. [Online]. Available: <https://uk-air.defra.gov.uk/interactive-map>
- [100] ——. (2023) FAQ - What is the definition of Running annual mean and Running 8hr mean. . Accessed on: 29/11/2023. [Online]. Available: <https://uk-air.defra.gov.uk/air-pollution/faq?question=20>
- [101] M. P. Adams, M. D. Tarn, A. Sanchez-Marroquin, G. C. Porter, D. O’Sullivan, A. D. Harrison, Z. Cui, J. Vergara-Temprado, F. Carotenuto, M. A. Holden *et al.*, “A major combustion aerosol event had a negligible impact on the atmospheric ice-nucleating particle population,” *Journal of Geophysical Research: Atmospheres*, vol. 125, no. 22, p. e2020JD032938, 2020.
- [102] ESA. (2024) Introducing MTG. Accessed on: 04/01/2024. [Online]. Available: https://www.esa.int/Applications/Observing_the_Earth/Meteorological_missions/meteosat_third_generation/Introducing_MTG
- [103] EUMETSAT. (2024) Sentinel-4. Accessed on: 04/01/2024. [Online]. Available: <https://www.eumetsat.int/sentinel-4>

Supplementary Materials for the manuscript entitled
**A Framework for Scalable Ambient Air Pollution Concentration
Estimation**

January 18, 2024

arXiv:2401.08735v1 [stat.AP] 16 Jan 2024

S1 Data Details

This section details the preprocessing and transformations to create a consistent dataset for training the data-driven supervised machine learning model.

S1.1 Common Data Format

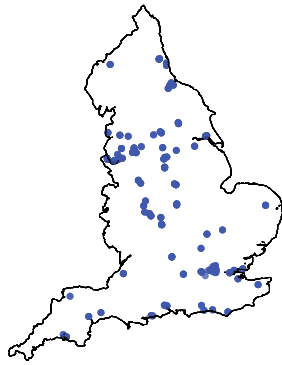
As the model framework is Eulerian [1], the first decision was the grid framework, taking into context the modifiable areal unit problem (MAUP) [2] for the grids in which the aggregation for predictors would be taken. The decision was made to use the same framework as existing air pollution concentration datasets, particularly the UK Modelled Background Annual dataset [3].



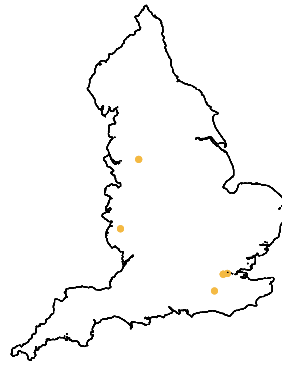
Supplementary Figure S1: **1km² land grids For England.** The land grids covering the area of the England land mass provide the common framework for aggregating the datasets and providing estimates of ambient air pollution, a total of 355,827 point locations at the centroid of each grid for which measurements are sampled.

S1.2 Air Pollution Concentrations

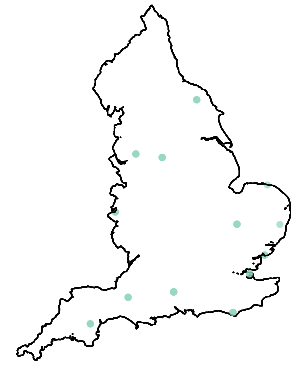
Detailed are the supporting analysis and figures for the air pollution concentration data. Included are the spatial distribution of the AURN network monitoring stations for each top-level environmental classification in Figure S2, kernel distributions for each air pollutant concentration dataset Figure S3, and the abstracted distance of each AURN monitoring station from its real location in the model framework Table S3.



(a) 91 Unique Urban Station Locations



(b) 5 Unique Suburban Station Locations



(c) 13 Unique Rural Station Locations

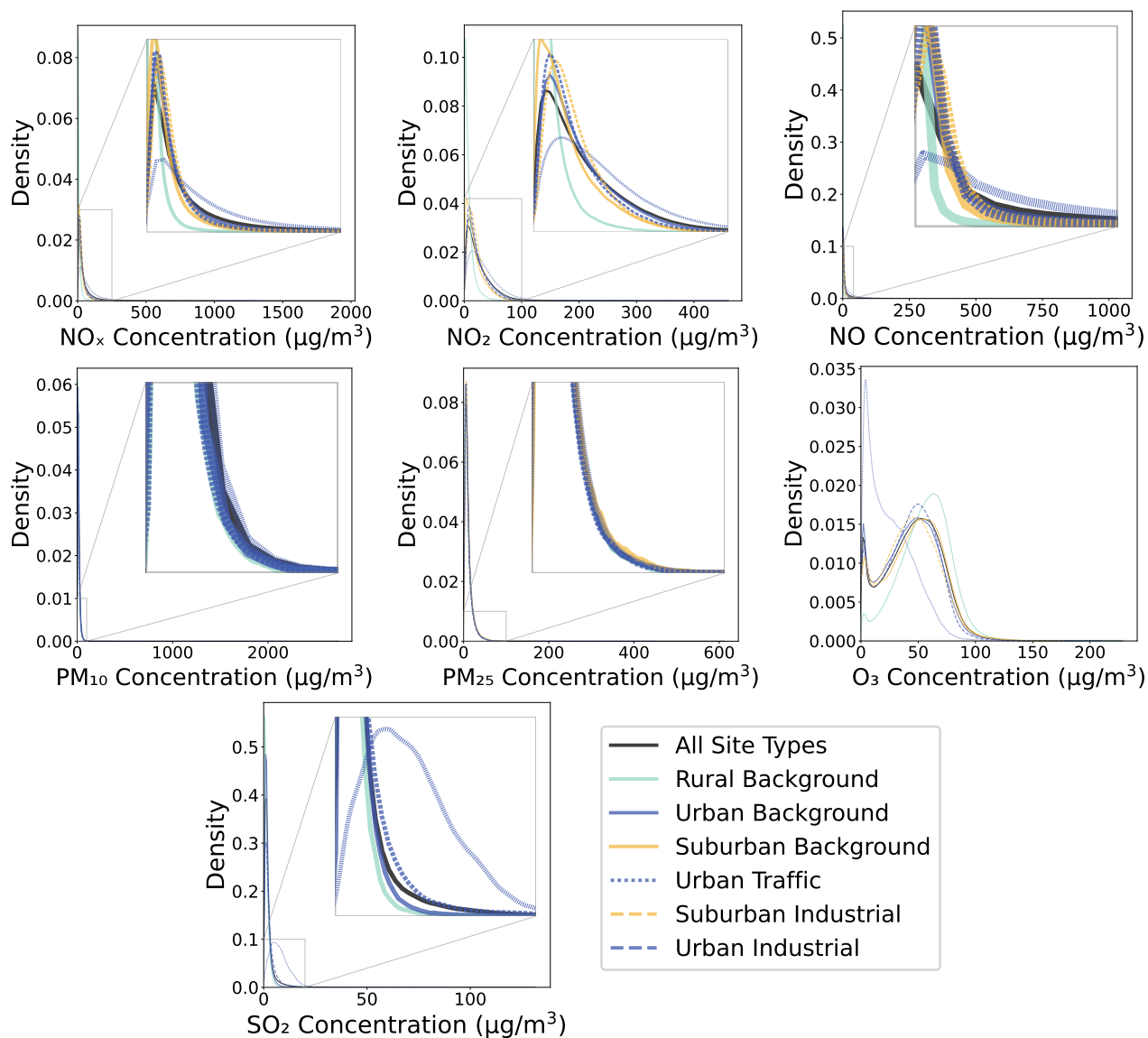
Supplementary Figure S2: **Spatial distribution and classification of monitoring stations within England.** The Automatic Urban and Rural Network (AURN) stations are divided into 3 classes: urban, suburban, and rural. The urban stations are then further divided into background, traffic and industrial, suburban into background and industrial and rural background. Note the inequality of station numbers; most of the stations are in urban settings.

AURN Site Name	Peak Value Timestamp	Peak Value ($\mu\text{g}/\text{m}^3$)	Peak Day Average ($\mu\text{g}/\text{m}^3$)	Peak Year Average ($\mu\text{g}/\text{m}^3$)
London Marylebone Road	10/06/2016 15:00:00	321.9	139.7	89.1
Sandy Roadside	01/03/2018 16:00:00	336.7	43.2	26.6
Luton A505 Roadside	19/01/2016 08:00:00	362.7	176.9	49.8
Camden Kerbside	15/02/2016 18:00:00	385.3	124.4	65.9
Manchester Piccadilly	13/09/2014 15:00:00	456.8	69.9	40.5

Supplementary Table S1: **AURN NO₂ monitoring station peak values between 2014-2018 with associated year daily mean peak and annual mean; for the year in which the peak measurement occurs.** These five monitoring stations show how there is not a simple relationship between the peak value, the peak daily average and the overall peak year average. London Marylebone Road station never has a peak as intense as Manchester Piccadilly but does experience consistently higher pollution across the year and similarly has a higher peak daily mean. However, Sandy Roadside has a higher overall peak than London Marylebone Road but a considerably lower peak day and year mean. The five stations have highlighted how multiple averages and a finer temporal scale are needed to uncover the intricacies of air pollution experienced at a single location.

Pollutant Name	Number Of Values	Number of Negative Values	Percentage of Negative Values (%)
NO _x	3855871	235	0.01
NO ₂	3855760	2697	0.07
NO	3859339	2078	0.05
O ₃	2198186	659	0.03
PM ₁₀	1646086	3743	0.23
PM _{2.5}	2004487	23,515	1.17
SO ₂	683276	1016	0.15

Supplementary Table S2: **AURN negative data point summary.** Negative data points within the AURN air pollution concentrations were removed from the dataset as the only form of preprocessing performed on the dataset. Negative concentrations can't exist, and their presence in the dataset indicates a fault with the instruments at the monitoring station.



Supplementary Figure S3: **KDE for air pollution measurements.** The kernel distribution estimation plots for each air pollutant show the distribution of concentration values. For PM₁₀ and PM_{2.5}, the distribution of values appears to remain constant across all sub classifications of the monitoring station, whereas NO_x, NO₂, NO and SO₂ appear to have different concentrations at different environmental locations. All air pollutants other than O₃ have a right skew, indicating a tendency for no air pollution to be the norm in the atmosphere, with pollution emitted and then subsequently dispersed, reducing the concentration measured.

AURN Station Name	Station Environment Type	Station Latitude	Station Longitude	Grid Centroid Latitude	Grid Centroid Longitude	Station Distance From Grid Centroid (m)
Plymouth Tavistock Road	Urban Traffic	50.4	-4.1	50.4	-4.1	8.7
Aston Hill	Rural Background	52.5	-3.0	52.5	-3.0	18.2
Salford Eccles	Urban Background	53.5	-2.3	53.5	-2.3	27.4
Eastbourne	Urban Background	50.8	0.3	50.8	0.3	31.7
Leamington Spa Rugby Road	Urban Traffic	52.3	-1.5	52.3	-1.5	32.4
Birkenhead Borough Road	Urban Traffic	53.4	-3.0	53.4	-3.0	35.0
Blackpool Marton	Urban Background	53.8	-3.0	53.8	-3.0	35.1
Wharfedale	Rural Background	54.6	-2.5	54.6	-2.5	38.1
London Brent	Urban Background	51.6	-0.3	51.6	-0.3	39.6
London Bridge Place	Urban Background	51.5	-0.1	51.5	-0.1	46.7
Liverpool Queen's Drive Roadside	Urban Traffic	53.4	-3.0	53.4	-3.0	47.1
Lullington Heath	Rural Background	50.8	0.2	50.8	0.2	54.1
Great Dun Fell	Rural Background	54.7	-2.5	54.7	-2.5	59.1
Birmingham A4540 Roadside	Urban Traffic	52.5	-1.9	52.5	-1.9	59.2
Scunthorpe Town	Urban Industrial	53.6	-0.6	53.6	-0.6	63.4
Rotherham Centre	Urban Background	53.4	-1.4	53.4	-1.4	65.8
London Westminster	Urban Background	51.5	-0.1	51.5	-0.1	67.1
Wigan Centre	Urban Background	53.5	-2.6	53.5	-2.6	68.3
Tower Hamlets Roadside	Urban Traffic	51.5	-0.0	51.5	-0.0	70.3
Middlesbrough	Urban Industrial	54.6	-1.2	54.6	-1.2	72.0
Immingham Woodlands Avenue	Urban Background	53.6	-0.2	53.6	-0.2	73.1
Billingham	Urban Industrial	54.6	-1.3	54.6	-1.3	87.2
London Bromley	Urban Traffic	51.4	0.0	51.4	0.0	90.8
Bury Roadside	Urban Traffic	53.5	-2.3	53.5	-2.3	91.1
Cambridge	Urban Traffic	52.0	0.0	52.0	0.0	96.4
London Teddington	Urban Background	51.4	-0.3	51.4	-0.3	96.8
London Cromwell Road 2	Urban Traffic	51.5	-0.2	51.5	-0.2	98.3
Reading London Road	Urban Traffic	51.5	-0.9	51.5	-0.9	98.5
Leeds Pottermewton	Urban Background	53.8	-1.5	53.8	-1.5	98.8
London Haringey Priory Park South	Urban Background	51.6	-0.1	51.6	-0.1	100.3
Birmingham East	Urban Background	52.5	-1.8	52.5	-1.8	103.7
Birmingham Acoccks Green	Urban Background	52.4	-1.8	52.4	-1.8	111.4
Charlton Mackrell	Rural Background	51.1	-2.7	51.1	-2.7	112.6
Northampton	Urban Background	52.3	-0.9	52.3	-0.9	114.1
Saltash Callington Road	Urban Traffic	50.4	-4.2	50.4	-4.2	114.1
Bottesford	Rural Background	52.9	-0.8	52.9	-0.8	114.4
Leamington Spa	Urban Background	52.3	-1.5	52.3	-1.5	116.0
Hove Roadside	Urban Traffic	50.8	-0.2	50.8	-0.2	119.5
Oxford Centre Roadside	Urban Traffic	51.8	-1.3	51.8	-1.3	120.5
Walsall Alumwell	Urban Background	52.6	-2.0	52.6	-2.0	121.3
Sandwell Oldbury	Urban Background	52.5	-2.0	52.5	-2.0	124.0
Coventry Allesley	Urban Background	52.4	-1.6	52.4	-1.6	124.1
Sunderland Wessington Way	Urban Traffic	54.9	-1.4	54.9	-1.4	125.6
Manchester Town Hall	Urban Background	53.5	-2.2	53.5	-2.2	128.6
Sunderland	Urban Background	54.9	-1.4	54.9	-1.4	128.9
Sheffield Centre	Urban Background	53.4	-1.5	53.4	-1.5	129.6
Bristol Old Market	Urban Traffic	51.5	-2.6	51.5	-2.6	133.3
Hartlepool St Abbs Walk	Urban Background	54.7	-1.2	54.7	-1.2	137.5
Southampton A33	Urban Traffic	50.9	-1.5	50.9	-1.5	137.5
Liverpool Speke	Urban Industrial	53.3	-2.8	53.3	-2.8	145.6
Bradford Centre	Urban Background	53.8	-1.7	53.8	-1.7	145.8
Doncaster A630 Cleveland Street	Urban Traffic	53.5	-1.1	53.5	-1.1	148.5
London Bloomsbury	Urban Background	51.5	-0.1	51.5	-0.1	151.1
London Southwark	Urban Background	51.5	-0.1	51.5	-0.1	151.2
Liverpool Centre	Urban Background	53.4	-3.0	53.4	-3.0	152.3
Thurrock	Urban Background	51.5	0.3	51.5	0.3	154.7
Chesterfield Loundsley Green	Urban Background	53.2	-1.5	53.2	-1.5	155.2
Northampton Kingshorpe	Urban Background	52.3	-0.9	52.3	-0.9	162.9
Derby St Alkmund's Way	Urban Traffic	52.9	-1.5	52.9	-1.5	165.7
Brentford Roadside	Urban Traffic	51.5	-0.3	51.5	-0.3	169.5
Birmingham Ladywood	Urban Background	52.5	-1.9	52.5	-1.9	169.8
Sheffield Barnsley Road	Urban Traffic	53.4	-1.5	53.4	-1.5	170.0
Market Harborough	Rural Background	52.6	-0.8	52.6	-0.8	172.2
Northampton Spring Park	Urban Background	52.3	-0.9	52.3	-0.9	174.4
Canterbury	Urban Background	51.3	-1.1	51.3	-1.1	179.1
Redcar	Suburban Background	54.6	-1.1	54.6	-1.1	180.7
Burton-on-Trent Hominglow	Urban Background	52.8	-1.6	52.8	-1.6	182.9
Bristol Centre	Urban Background	51.5	-2.6	51.5	-2.6	183.9
Ladybower	Rural Background	53.4	-1.8	53.4	-1.8	186.5
Norwich Lakenfields	Urban Background	52.6	1.3	52.6	1.3	187.6
Sheffield Devonshire Green	Urban Background	53.4	-1.5	53.4	-1.5	188.2
Blackburn Accrington Road	Urban Traffic	53.7	-2.5	53.7	-2.5	191.7
London Cromwell Road	Urban Traffic	51.5	-0.2	51.5	-0.2	192.5
Wirral Tranmere	Urban Background	53.4	-3.0	53.4	-3.0	194.8
Sibton	Rural Background	52.3	1.5	52.3	1.5	195.1
Bristol St Paul's	Urban Background	51.5	-2.6	51.5	-2.6	195.4
Lincoln Canwick Road	Urban Traffic	53.2	-0.5	53.2	-0.5	195.6
Weybourne	Rural Background	53.0	1.1	53.0	1.1	196.5
Carlisle Roadside	Urban Traffic	54.9	-2.9	54.9	-2.9	196.9
Blackburn Darwen Roadside	Urban Traffic	53.7	-2.5	53.7	-2.5	197.9
London N. Kensington	Urban Background	51.5	-0.2	51.5	-0.2	199.4
Southwark Roadside	Urban Traffic	51.5	-0.1	51.5	-0.1	199.4
Stockport Shaw Heath	Urban Background	53.4	-2.2	53.4	-2.2	201.0
Stanford-le-Hope Roadside	Urban Traffic	51.5	0.4	51.5	0.4	201.8
High Muffles	Rural Background	54.3	-0.8	54.3	-0.8	204.0
Camden Kerbside	Urban Traffic	51.5	-0.2	51.5	-0.2	209.0
Leominster	Suburban Background	52.2	-2.7	52.2	-2.7	209.5
York Fishergate	Urban Traffic	54.0	-1.1	54.0	-1.1	209.5
Leicester University	Urban Background	52.6	-1.1	52.6	-1.1	210.4
Honiton	Urban Background	50.8	-3.2	50.8	-3.2	211.2
West Bromwich Kenrick Park	Urban Background	52.5	-2.0	52.5	-2.0	211.4
Sandwell West Bromwich	Urban Background	52.5	-2.0	52.5	-2.0	216.6
Hull Centre	Urban Background	53.7	-0.3	53.7	-0.3	217.1
Oldbury Birmingham Road	Urban Traffic	52.5	-2.0	52.5	-2.0	217.7
Leeds Headingley Kerbside	Urban Traffic	53.8	-1.6	53.8	-1.6	222.4
Nottingham Centre	Urban Background	53.0	-1.1	53.0	-1.1	224.5
Wigan Leigh	Urban Background	53.5	-2.5	53.5	-2.5	224.5
Lincoln Roadside	Urban Traffic	53.2	-0.5	53.2	-0.5	225.3
Southend-on-Sea	Urban Background	51.5	0.7	51.5	0.7	225.5
Chesterfield	Urban Background	53.2	-1.4	53.2	-1.4	226.9
Coventry Memorial Park	Urban Background	52.4	-1.5	52.4	-1.5	228.1
Plymouth Centre	Urban Background	50.4	-4.1	50.4	-4.1	228.9
Bradford Mayo Avenue	Urban Traffic	53.8	-1.8	53.8	-1.8	229.6
Swindon Walcot	Urban Background	51.6	-1.8	51.6	-1.8	232.0
Rugeley	Urban Background	52.8	-1.9	52.8	-1.9	232.8
Warrington	Urban Industrial	53.4	-2.6	53.4	-2.6	233.0
London Harlington	Urban Industrial	51.5	-0.4	51.5	-0.4	233.9
Bromley Roadside	Urban Traffic	51.4	0.0	51.4	0.0	234.1

(a) AURN station real distance from the centroid distance.

AURN Station Name	Station Environment Type	Station Latitude	Station Longitude	Grid Centroid Latitude	Grid Centroid Longitude	Station Distance From Grid Centroid (m)
London Honor Oak Park	Urban Background	51.4	-0.0	51.4	-0.0	234.5
Salthash Roadside	Urban Traffic	50.4	-4.2	50.4	-4.2	234.5
Ealing Horn Lane	Urban Traffic	51.5	-0.3	51.5	-0.3	236.0
Bolton	Urban Background	53.6	-2.4	53.6	-2.4	237.4
Hull Holderness Road	Urban Traffic	53.8	-0.3	53.8	-0.3	238.3
Sheffield Tinsley	Urban Background	53.4	-1.4	53.4	-1.4	238.6
Widnes Milton Road	Urban Traffic	53.4	-2.7	53.4	-2.7	240.2
London Bexley	Suburban Background	51.5	0.2	51.5	0.2	240.7
Newcastle Cradlewell Roadside	Urban Traffic	55.0	-1.6	55.0	-1.6	242.3
Cambridge Roadside	Urban Traffic	52.2	0.1	52.2	0.1	243.8
Central London	Urban Background	51.5	-0.1	51.5	-0.1	244.1
Chesterfield Roadside	Urban Traffic	53.2	-1.5	53.2	-1.5	244.9
Manchester South	Suburban Industrial	53.4	-2.2	53.4	-2.2	245.9
Haringey Roadside	Urban Traffic	51.6	-0.1	51.6	-0.1	246.6
Stoke-on-Trent Centre	Urban Background	53.0	-2.2	53.0	-2.2	246.6
Luton A505 Roadside	Urban Traffic	51.9	-0.5	51.9	-0.5	248.1
Chilworth	Suburban Background	51.0	-1.4	51.0	-1.4	248.9
Norwich Centre	Urban Background	52.6	1.3	52.6	1.3	249.2
Hounslow Roadside	Urban Traffic	51.5	-0.3	51.5	-0.3	251.6
London Haringey	Urban Background	51.6	-0.1	51.6	-0.1	251.9
Featherstone	Urban Background	53.7	-1.4	53.7	-1.4	255.0
York Bootham	Urban Background	54.0	-1.1	54.0	-1.1	256.3
Stockton-on-Tees Eaglescliffe	Urban Traffic	54.5	-1.4	54.5	-1.4	256.5
London Harrow	Suburban Background	51.6	-0.4	51.6	-0.3	257.7
Wicken Fen	Rural Background	52.3	0.3	52.3	0.3	258.0
Birmingham Tyburn	Urban Background	52.5	-1.8	52.5	-1.8	259.8
Bristol East	Urban Background	51.5	-2.6	51.5	-2.6	259.8
Scunthorpe	Urban Industrial	53.6	-0.6	53.6	-0.6	260.5
Leeds Centre	Urban Background	53.8	-1.5	53.8	-1.5	261.7
Southampton Centre	Urban Background	50.9	-1.4	50.9	-1.4	262.4
Stewartby	Urban Industrial	52.1	-0.5	52.1	-0.5	262.7
London Marylebone Road	Urban Traffic	51.5	-0.2	51.5	-0.2	263.1
Brighton Preston Park	Urban Background	50.8	-0.1	50.8	-0.2	263.1
Leicester Centre	Urban Background	52.6	-1.1	52.6	-1.1	265.6
Hull Freetown	Urban Background	53.7	-0.3	53.7	-0.3	266.2
Borehamwood Meadow Park	Urban Background	51.7	-0.3	51.7	-0.3	267.8
Dewsbury Ashworth Grove	Urban Background	53.7	-1.6	53.7	-1.6	267.9
Wolverhampton Centre	Urban Background	52.6	-2.1	52.6	-2.1	268.2
Stockton-on-Tees Yarm	Urban Traffic	54.5	-1.4	54.5	-1.4	270.0
Stockport	Urban Background	53.4	-2.2	53.4	-2.2	273.3
Birmingham Kerbside	Urban Traffic	52.3	-1.9	52.3	-1.9	273.7
Shaw Crompton Way	Urban Traffic	53.6	-2.1	53.6	-2.1	275.1
Telford Hollinswood	Urban Background	52.7	-2.4	52.7	-2.4	278.6
Bury Whitefield Roadside	Urban Traffic	53.6	-2.3	53.6	-2.3	281.6
Walsall Willenhall	Urban Background	52.6	-2.0	52.6	-2.0	282.4
Stockton-on-Tees A1305 Roadside	Urban Traffic	54.6	-1.3	54.6	-1.3	282.7
Chilbolton Observatory	Rural Background	51.1	-1.4	51.2	-1.4	283.5
Wray	Rural Background	54.1	-2.6	54.1	-2.6	283.8
Bristol Temple Way	Urban Traffic	51.5	-2.6	51.5	-2.6	284.6
Sutton Roadside	Urban Traffic	51.4	-0.2	51.4	-0.2	287.4
Blackpool	Urban Background	53.8	-3.0	53.8	-3.0	288.6
Yarner Wood	Rural Background	50.6	-3.7	50.6	-3.7	288.8
Exeter Roadside	Urban Traffic	50.7	-3.5	50.7	-3.5	289.2
London UCL	Urban Background	51.5	-0.1	51.5	-0.1	290.5
Harwell	Rural Background	51.6	-1.3	51.6	-1.3	290.6
Coventry Binley Road	Urban Traffic	52.4	-1.5	52.4	-1.5	292.1
St Helens Linkway	Urban Traffic	53.5	-2.7	53.5	-2.7	292.3
Horley	Suburban Industrial	51.2	-0.2	51.2	-0.2	293.0
Barnstaple A39	Urban Traffic	51.1	-4.0	51.1	-4.0	293.2
Manchester Piccadilly	Urban Background	53.5	-2.2	53.5	-2.2	295.1
Walsall Woodlands	Urban Background	52.6	-2.0	52.6	-2.0	297.2
Southwark A2 Old Kent Road	Urban Traffic	51.5	-0.1	51.5	-0.1	297.4
Birmingham Tyburn Roadside	Urban Traffic	52.5	-1.8	52.5	-1.8	297.4
London Islington	Urban Background	51.5	-0.1	51.5	-0.1	298.2
Rochester Stoke	Rural Background	51.3	0.6	51.5	0.6	299.0
London Harrow Stanmore	Urban Background	51.6	-0.3	51.6	-0.3	299.9
Manchester Sharston	Suburban Industrial	53.4	-2.2	53.4	-2.2	302.0
Storrington Roadside	Urban Traffic	50.9	-0.4	50.9	-0.4	302.0
Stevenage	Suburban Background	51.9	-0.2	51.9	-0.2	305.3
Sunderland Silksworth	Urban Background	54.9	-1.4	54.9	-1.4	305.4
Newcastle Centre	Urban Background	55.0	-1.6	55.0	-1.6	305.5
London Lewisham	Urban Background	51.4	-0.0	51.4	-0.0	305.7
Stoke-on-Trent A50 Roadside	Urban Traffic	53.0	-2.1	53.0	-2.1	306.6
London A3 Roadside	Urban Traffic	51.4	-0.3	51.4	-0.3	309.0
Norwich Forum Roadside	Urban Traffic	52.6	1.3	52.6	1.3	310.6
London Teddington Bushy Park	Urban Background	51.4	-0.3	51.4	-0.3	313.7
Leicester A594 Roadside	Urban Traffic	52.6	-1.1	52.6	-1.1	314.9
Barnsley 12	Urban Background	53.6	-1.5	53.6	-1.5	319.3
Chatham Roadside	Urban Traffic	51.4	0.5	51.4	0.5	320.8
West London	Urban Background	51.5	-0.2	51.5	-0.2	323.2
Glazebury	Rural Background	53.5	-2.5	53.5	-2.5	323.4
Barnsley	Urban Background	53.6	-1.5	53.6	-1.5	323.6
Barnsley Gawber	Urban Background	53.6	-1.5	53.6	-1.5	326.0
Brighton Roadside	Urban Traffic	50.8	-0.1	50.8	-0.1	326.4
Crew Coppenhall	Urban Background	53.1	-2.5	53.1	-2.5	330.3
Reading New Town	Urban Background	51.5	-0.9	51.5	-0.9	330.9
Bircoates	Urban Background	53.4	-1.1	53.4	-1.1	332.9
Worthing A27 Roadside	Urban Traffic	50.8	-0.4	50.8	-0.4	335.7
Canmock A5190 Roadside	Urban Traffic	52.7	-2.0	52.7	-2.0	336.5
Bath Roadside	Urban Traffic	51.4	-2.4	51.4	-2.4	338.6
London Sutton	Suburban Background	51.4	-0.2	51.4	-0.2	338.8
St Osyth	Rural Background	51.8	1.0	51.8	1.1	340.3
Birmingham Centre	Urban Background	52.5	-1.9	52.5	-1.9	342.6
London Wandsworth	Urban Background	51.5	-0.2	51.5	-0.2	342.8
Christchurch Barrack Road	Urban Traffic	50.7	-1.8	50.7	-1.8	346.4
London Hillingdon	Urban Background	51.5	-0.5	51.5	-0.5	347.8
Somerton	Rural Background	51.0	-2.7	51.0	-2.7	347.8
Nottingham Western Boulevard	Urban Traffic	53.0	-1.2	53.0	-1.2	350.0
Preston	Urban Background	53.8	-2.7	53.8	-2.7	356.2
Norwich Roadside	Urban Traffic	52.6	1.3	52.6	1.3	356.6
Oxford St Ebbes	Urban Background	51.7	-1.3	51.7	-1.3	357.6
London Eltham	Suburban Background	51.5	0.1	51.4	0.1	359.7
Coventry Centre	Urban Background	52.4	-1.5	52.4	-1.5	363.9
Reading	Urban Background	51.5	-1.0	51.5	-1.0	364.6
Sandy Roadside	Urban Traffic	52.1	-0.3	52.1	-0.3	370.1
Bournemouth	Urban Background	50.7	-1.8	50.7	-1.8	384.3
Bath A4 Roadside	Urban Traffic	51.4	-2.4	51.4	-2.4	385.3
London Hackney	Urban Background	51.6	-0.1	51.6	-0.1	399.8

(b) AURN station real distance from the centroid distance (cont.). For each AURN monitoring station used within the study, the station's latitude and longitude are given, alongside the abstracted location of the station within the study, denoted by the grid centroids latitude and longitude. The station distance then gives the difference between the stations true location and the location used within the study.

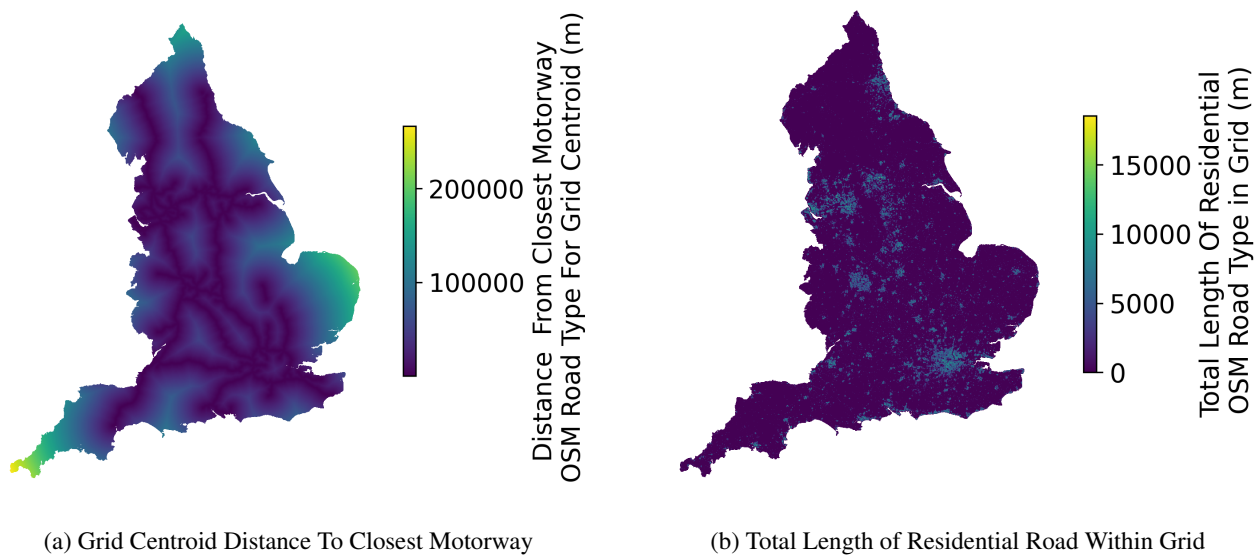
Supplementary Table S3

S1.3 Transport Infrastructure Structural Properties

Open Street Maps was used as the data set to build the transport infrastructure feature vector. Open Street Maps provides a high level of detail on the road location and the type of road, alongside providing a historical dataset that allows for historical roads to be acquired across years. Due to the computational cost of retrieving the feature vector for the transport infrastructure in a grided format, and the minimal change to the road infrastructure itself on a fine temporal level, especially hourly, we decided to take yearly snapshots of the road infrastructure. A possible improvement to the method would be to take more frequency snapshots of the road network at the expense of additional computation if desired. The snapshot of the road network used was the road network structural on the first day of the year. We then used this snapshot of the road network to create a feature vector for the following year of timestamps within the feature vector.

The first set of feature vectors concerning transport infrastructure structural properties detailed each grid's distance to the closest road type within the study in meters. Figure S4a shows the feature vector for the distance to the closet motorway in 2018. The second set of feature vectors created concerning transport infrastructure structural properties details the total length in meters of each analysed road type for every grid within the study. Figure S4b shows the total residential road length in meters in all grids for 2018.

The highway types analysed for creating the feature vector for the transport infrastructure structural properties dataset family included Residential, Footway, Service, Primary, Path, Cycleway, Tertiary, Secondary, Unclassified, Trunk, Track, Motorway, Pedestrian and Living Street. Figure S4 provide an example of the full transport infrastructural properties dataset for the distance to the closet motorway and the total length of residential road for each grid.



Supplementary Figure S4: **Example complete England transport infrastructure structural properties datasets.** A feature vector element is created for the distance to the closest and the total length of the specific road type. 14 different road types are analysed, resulting in 28 feature vector elements contributed by the transport infrastructure structural properties dataset family.

S1.4 Transport Infrastructure Use

Traffic counts from point locations across England were used to estimate the daily traffic flow across given types of roads across different regions within England. The traffic counts used were part of the Department of Transport (DfT) Road usage data included in the annual average daily flow (AADF), major and minor roads dataset [4]. The AADF dataset estimates a range of different transport methods, with the following aggregate transport types being used in the study:

1. Bicycle Count
2. Car and Taxi Count
3. Bus and Coach Score
4. Light Goods Van (LGV)
5. Heavy Goods Vehicle (HGV)

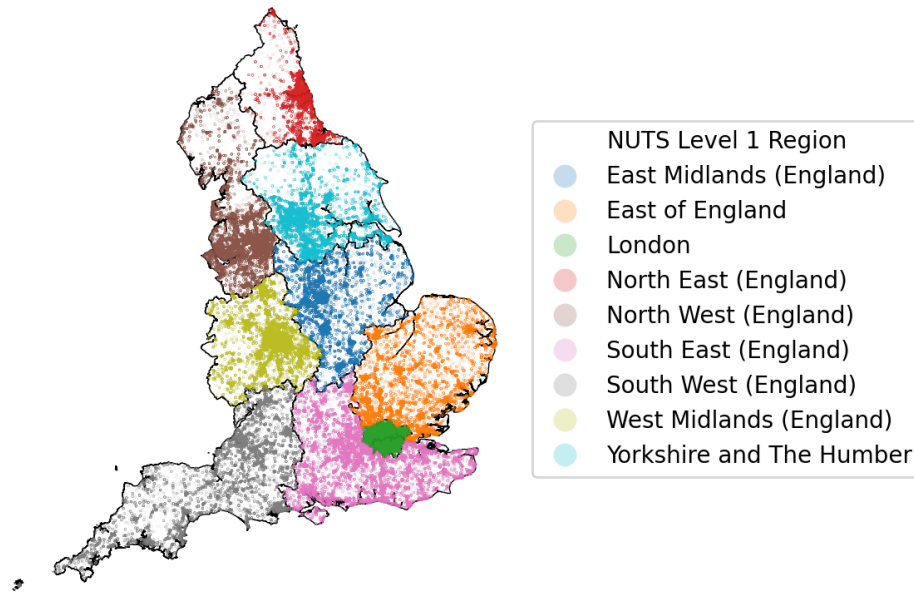
The first step was to create a mean traffic flow per road type. The DfT AADF dataset gives traffic flow estimates on major and minor roads, from motorways to rural areas, including single-lane roads with passing bays [5]. In the transport infrastructural properties dataset family, we included 14 road types, with road types such as cycleways. As the AADF dataset only includes road types suitable for motor vehicles, there was a need to reduce the road types to only those related to the major and minor roads defined by DfT. Therefore, from the OpenStreetMap dataset, we included only the ten road types: motorway, trunk, primary, secondary, tertiary, unclassified, residential, living_street, service, and track. We then matched the sample location from the AADF to the closest OpenStreetMaps road type to calculate a mean for the daily traffic flow for that road.

As road type usage can be substantially different across England, such as a residential road in central London and a small town in the Midlands having widely different traffic flows, we created means for each road type within a set of defined geographic regions. The geographic boundary we chose for this aggregation of sample locations was the NUTS Level 1 Regions, seen in Figure S5. Smaller region sizes of Local Authority Districts, with 371 geographic regions, were also trialled; however, some of the 10 OpenStreetMaps road types had no estimates for the mean traffic flow. Therefore, we used the coarser but more comprehensive aggregation of the NUTS boundary.

The next step was calculating the road network within each grid used within the study. Figure S6 shows the road infrastructure within a single 1km² grid in South Cambridgeshire at location Latitude 52.218, Longitude -0.07. We then calculated the total road length for each road type for each grid. Table S4 shows the total road length for each road type for the grid shown in Figure S6 alongside the number of traffic counts within the DfT dataset for that road type within that NUTS 1 region, in this case, the East of England region. Each road type's mean traffic flow per transport method was multiplied by the overall length of that road type to estimate the traffic flow for that transport method across that road type within the 1km² grid. Each of the road types multiplication was then summed to provide an overall estimate for the traffic of each transport method across the whole road network within that grid, with Table S5 showing the overall traffic score for each transport method for the grid shown in Figure S6.

The traffic flow score in Table S5 gives an estimate of traffic flow at the daily level. However, an estimate of traffic flow based on an hourly level was desired for the analysis of rush hour traffic. To achieve this, we temporally distributed the daily traffic flow based on a spatial microsimulation of the UK Time Use Survey [6]. The UK Time Use Survey provides data on how 11421 individuals spent their time across the UK during weekdays, Saturdays and Sundays. One of the options for how they could specify how they were spending their time was for travelling, which included details of the transport method they were using. Profiling of travel habits was made possible as each participant has associated socio-demographic data. Using the UK census [7], we used a spatial microsimulation [8] to create a synthetic population of England. The input UK census data was the 7201 Middle Layer Super Output Area (MSOA) aggregate socio-demographic statistics. The spatial microsimulation provided a synthetic population for each MSOA that included data on when they would travel based on the UK Time Use Survey. We then created aggregate travel times for each MSOA region. Figure S7 shows the travel profile for MSOA South Cambridgeshire 020, the MSOA that allowed an understanding of what times of day for a weekday, Saturday and Sunday individuals within a given MSOA travel by transport method. The travel profile seen in Figure S7 was then used to temporally distribute the daily traffic flow score for each grid within that MSOA. The grid shown in Figure S6 is within the NUTS region East of England and MSOA South Cambridgeshire 020. As such, the travel profiles in Figure S7 were used to distribute the daily traffic flows in Table S5 temporally to produce the hourly traffic estimates.

Figure S8 shows the difference in traffic score for grids within a London subset. As seen in the figure, each day exhibits a unique signal, with the weekday seeing the highest travel, followed by Saturday and finally Sunday. Figure S9 shows how the traffic flow within a grid for each transport method differs depending on the road types present within the grid. The figure depicts the most significant traffic flow for HGVs on the arterial lines into London and the M25 ring road around central London. In contrast, bicycle use is most prominent in central London. Figure S10 shows the full transport use dataset across all of the land grids, with the white land grids representing grids within the study area with no roads present. Hence, no traffic flow estimate has been made.



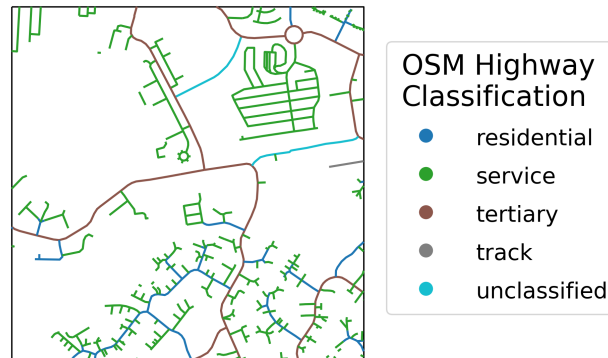
Supplementary Figure S5: **Department for Transport point locations for Annual Average Daily Flow (AADF) of traffic.** Shown are the point sample locations for traffic counts along roads within England that the Department of Transport conducted, giving an annual average daily flow for various transport types. The points are slightly transparent to allow insight into where multiple points overlap, alongside being coloured by corresponding NUTS 1 region, indicating groups of point samples used to calculate an average flow for that region.

Total Road Length (m)	OSM Highway Classification	Traffic Count Counts	Mean Pedal Cycles Traffic	Mean Cars and Taxis Traffic	Mean Bus and Coaches Traffic	Mean LGV Traffic	Mean HGV Traffic
2238.1	residential	448.0	73.2	3954.9	38.9	659.8	129.3
10,138.2	service	180.0	127.2	13,983.9	102.5	2701.8	1033.9
3220.2	tertiary	366.0	60.5	4356.0	33.1	769.7	224.6
99.5	track	58.0	15.8	14,115.8	64.2	3318.3	2036.2
587.6	unclassified	305.0	25.6	3604.1	18.9	742.6	342.6

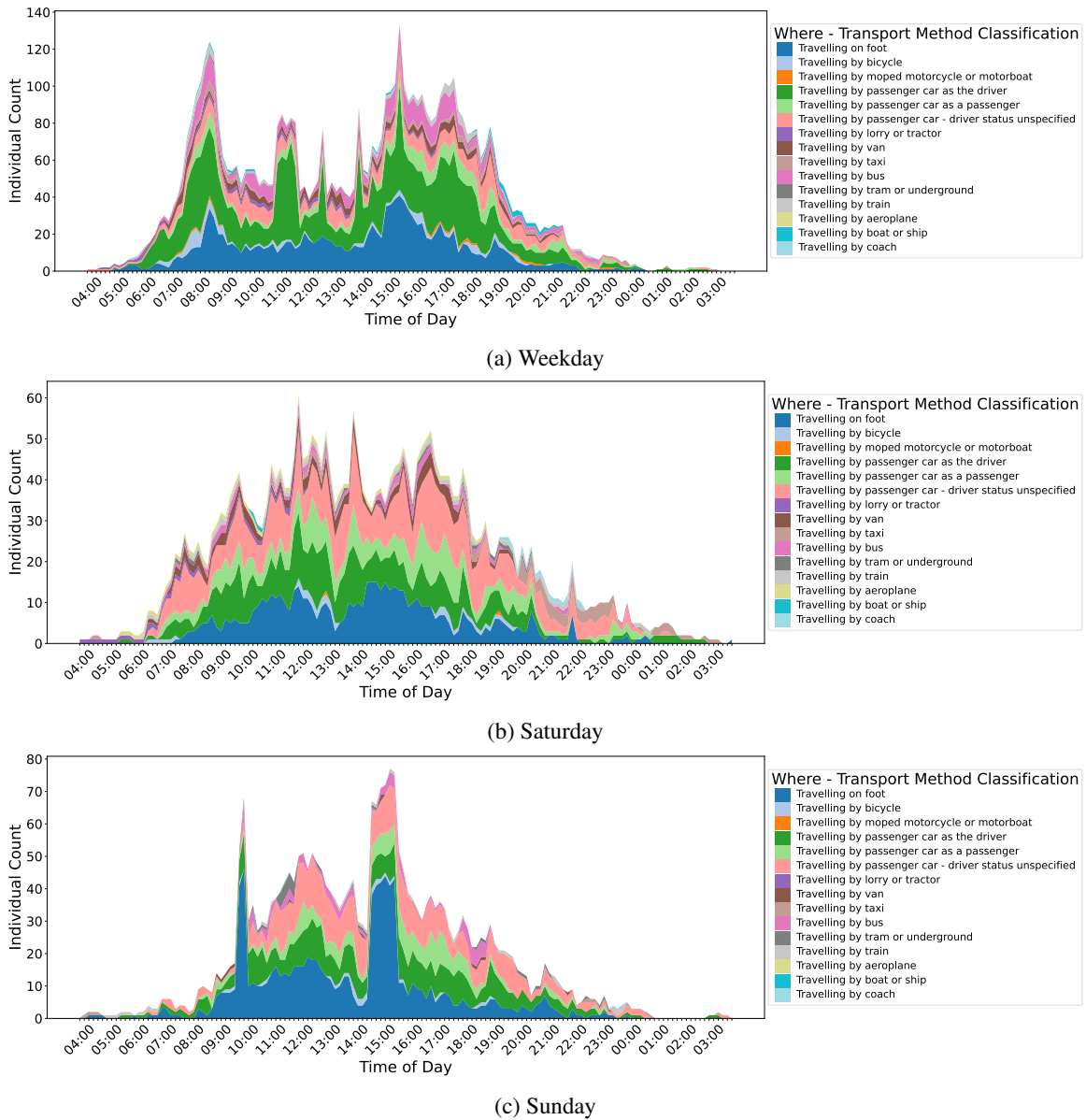
Supplementary Table S4: **Mean traffic count per road for East of England, with summary data road network length for Figure S6** The summary data for the road network within a single grid within the East of England is shown, corresponding to the visualisation in Figure S6. The table provides the data used to create the overall grid score for the grid shown in Table S5. To create the grid score, the sum of the multiplication of the length of the road type and the average traffic flow on that road type gives a single number indicating the traffic for that transport type across the road network within the grid.

OSM Highway Classification	Grid Score
Pedal Cycles	1,664,894
Cars and Taxis	168,171,555
Bus and Coaches	1,250,190
LGV	32,113,165
HGV	11,897,900

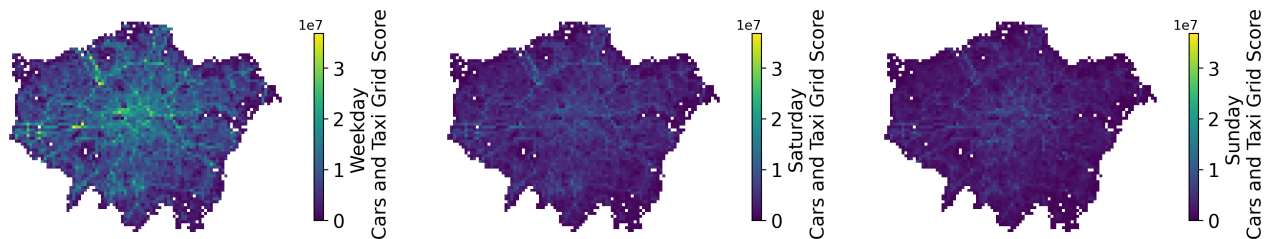
Supplementary Table S5: **Traffic flow average for road types for grid with centroid [52.218, -0.07] in South Cambridgeshire.** The overall grid score for each transport method for the grid is visualised in Figure S6. The grid score provides an overall indication of the traffic across all road types within the grid.



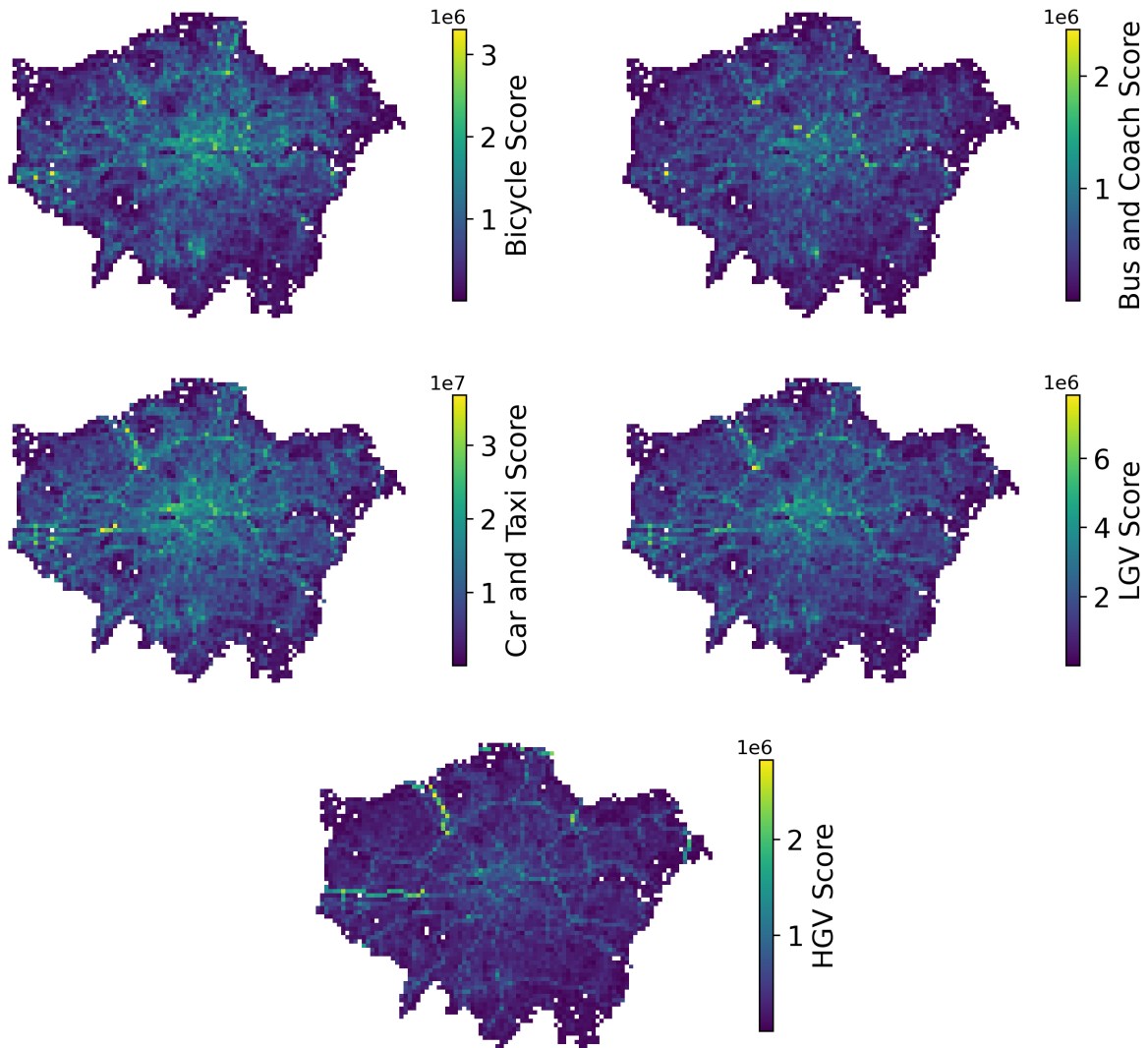
Supplementary Figure S6: **Road network infrastructure for a single grid with centroid [52.218, -0.07] in South Cambridgeshire.** The sub-road networks are shown for each of the five road types within the 1km² grid.



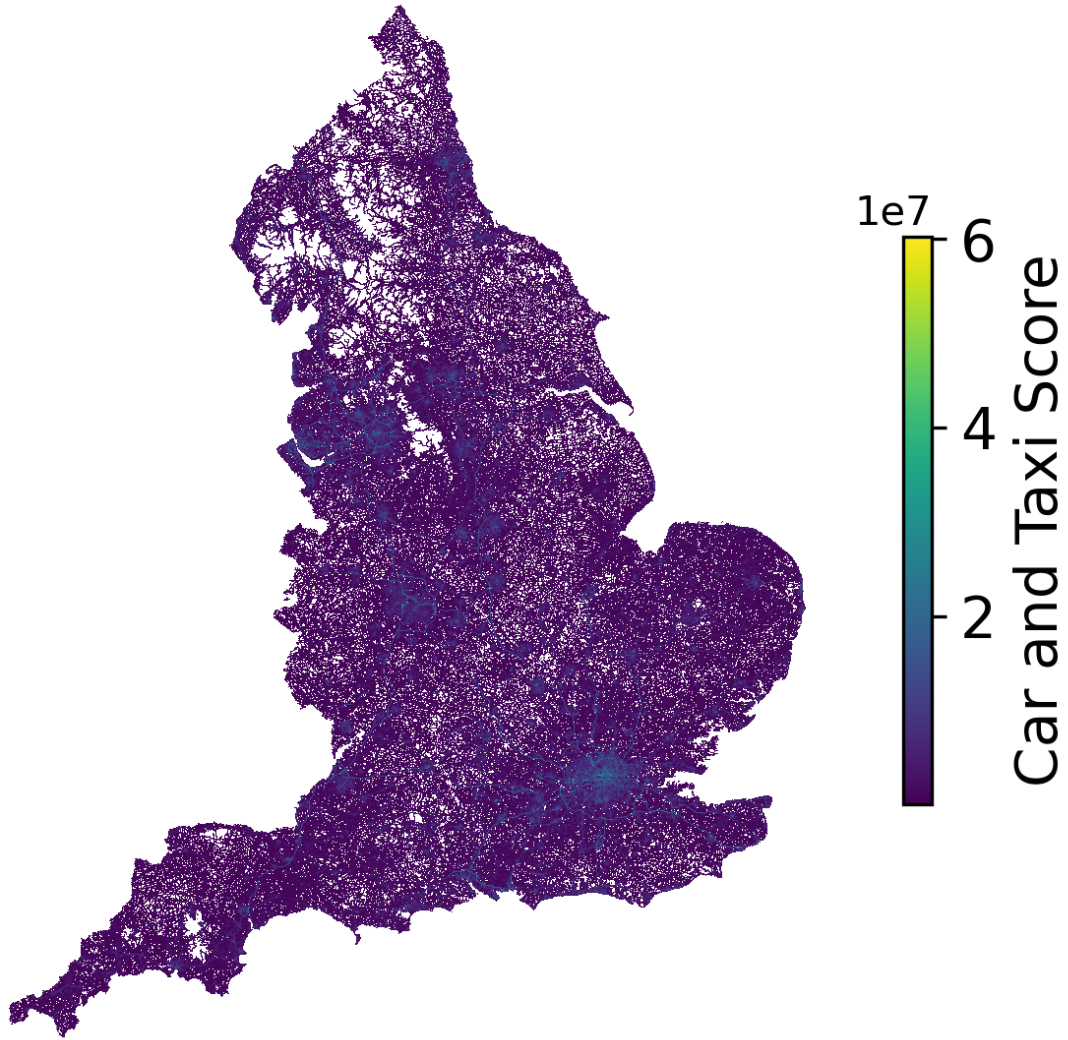
Supplementary Figure S7: **Spatial microsimulation for South Cambridgeshire 020 shows the proportion of different travel methods for all individuals travelling at the given time.** Of note are the different scales of the plots—total number of individuals taking a journey Weekday: 32622, Saturday: 16850, Sunday: 13857. Interestingly, even though Saturday has a higher overall number of individuals travelling, the peak on Sunday is higher.



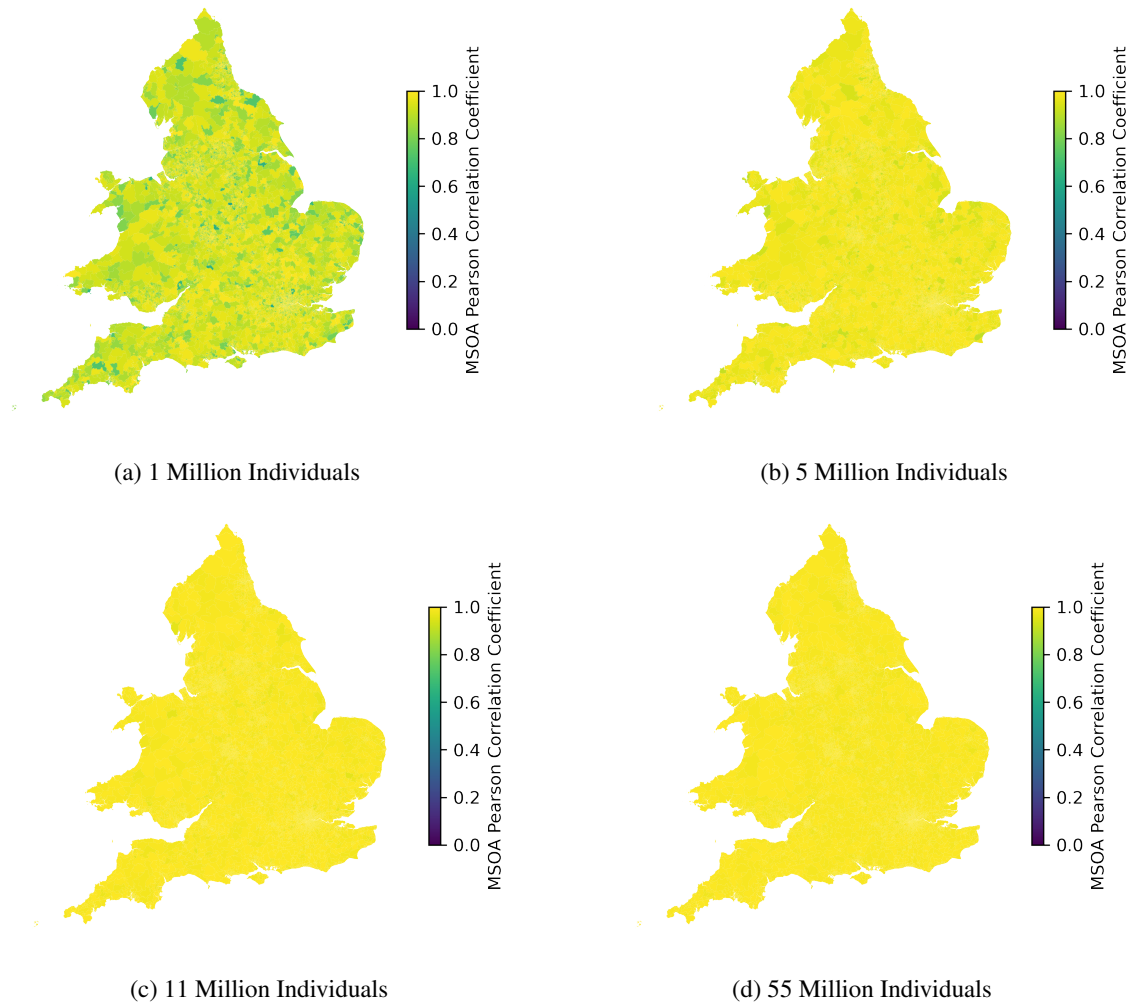
Supplementary Figure S8: **Temporal distribution of traffic grid score within London at 08AM on 1st, 2nd and 3rd June 2018 for cars and taxis.**



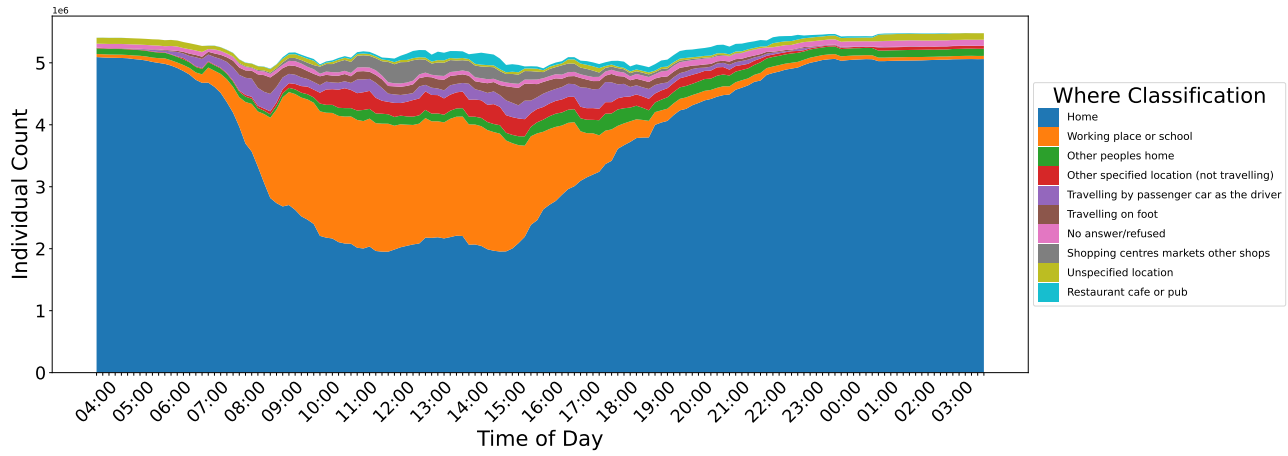
Supplementary Figure S9: **Transport use dataset for central London.** The transport use grids across central London help to highlight the difference in road usage across different road types across the five transport methods. Bicycle usage is more substantial in central London, with cars and taxis pervasive throughout and HGVs using the arterial main roads coming into the city.



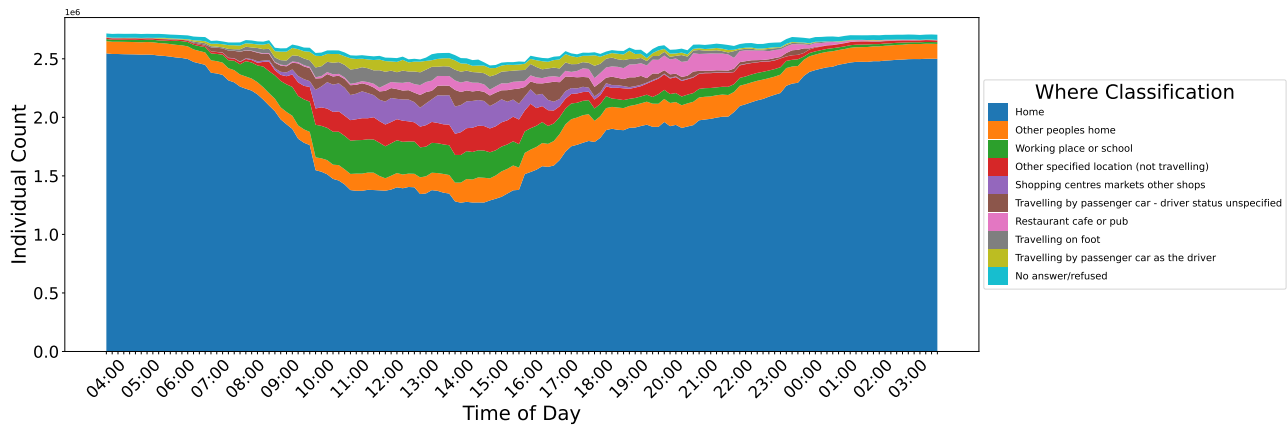
Supplementary Figure S10: **Example complete England transport use dataset for Car and Taxi Score.** Of note is that not every grid is present within the figures, as not every 1km² grid within the study has any road infrastructure. The final feature vector for estimating the air pollution concentration is filled with zeros as those grids have no traffic.



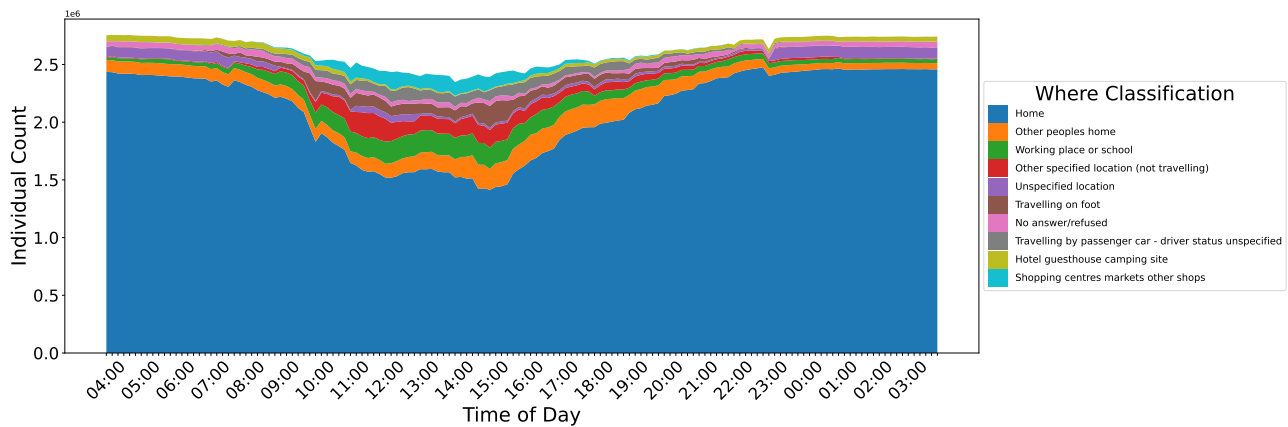
Supplementary Figure S11: **Pearson correlation coefficients across the MSOA regions used during the spatial microsimulation for different total numbers of simulated individuals.** During the spatial microsimulation, the number of individuals to be created was experimented with, intending to achieve a desirable Pearson Correlation coefficient across all MSOA regions ensuring model validity in population representation [9] while reducing the memory and computation burden associated with creating all individuals across the UK. While the simulation of all 55 million individuals in the UK resulted in a good pearson score, it was computationally expensive; as such, 11 million individuals were chosen to be simulated with the Pearson correlation being maintained at above 0.8 while significantly reducing computational costs.



(a) Weekday



(b) Saturday

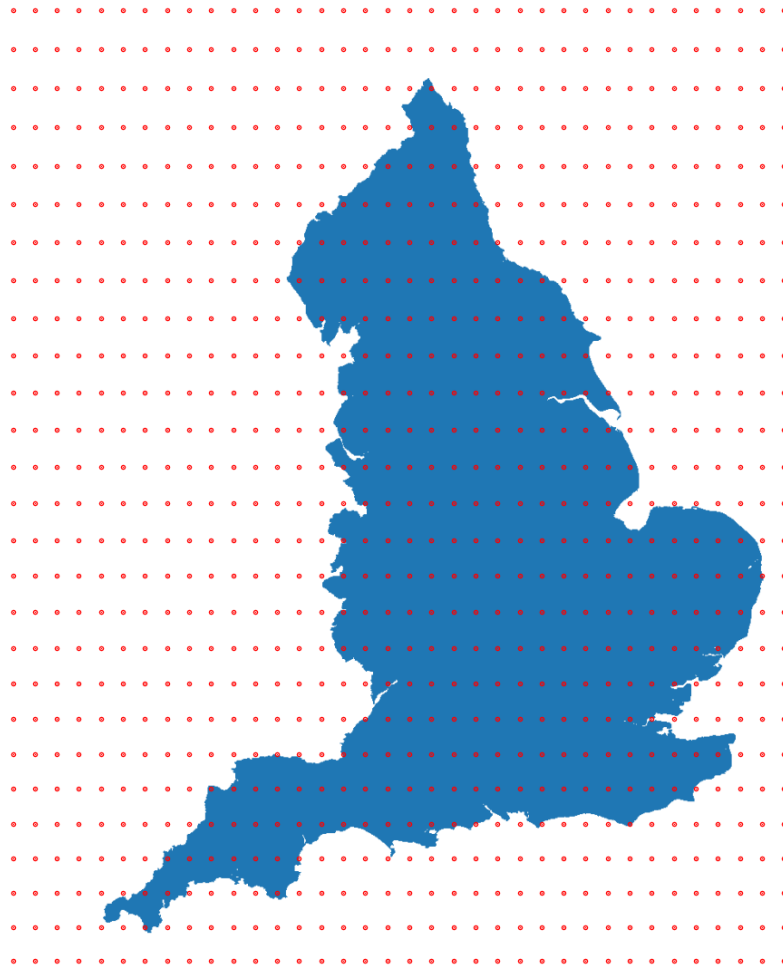


(c) Sunday

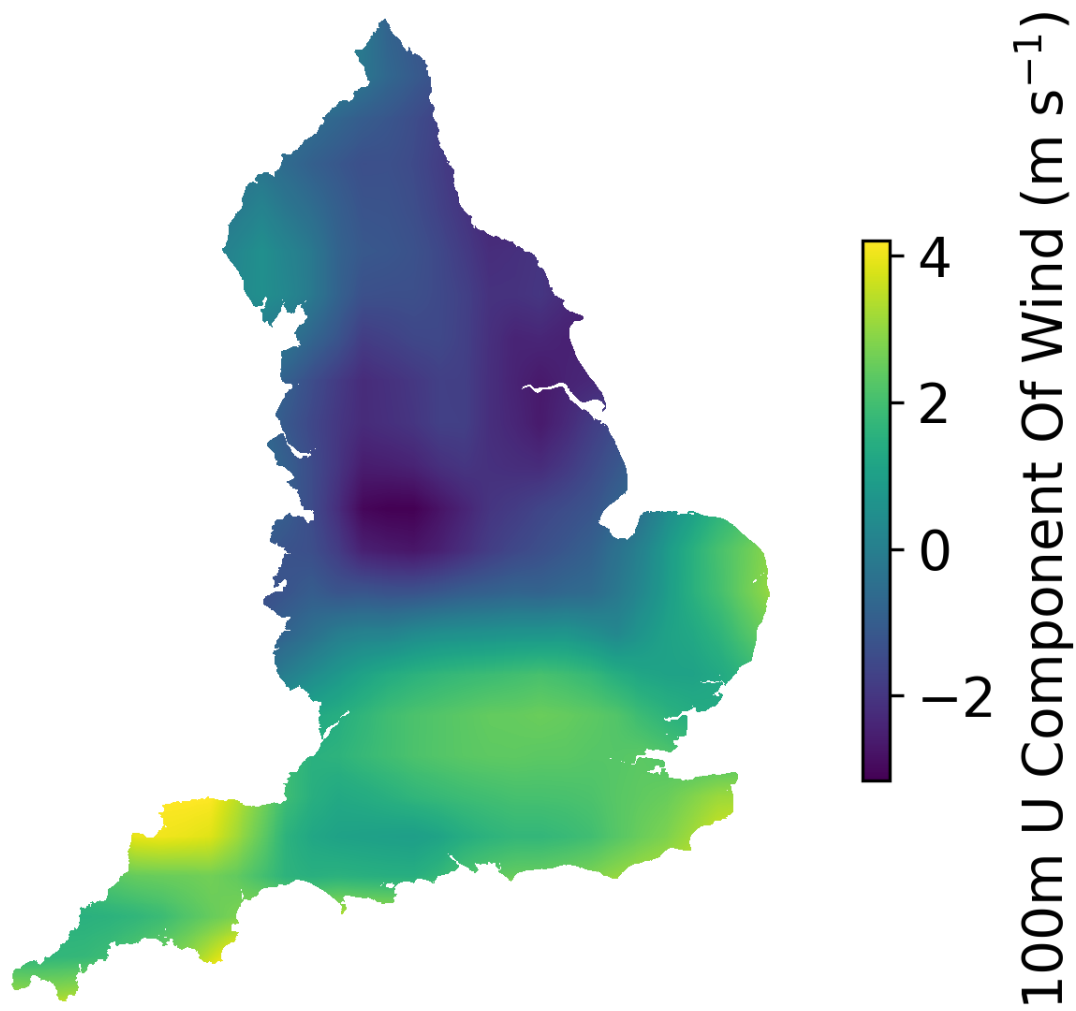
Supplementary Figure S12: UK Time Use stack plots showing where individuals are across all the major location categories included in the dataset.

S1.5 Meteorological

We retrieved meteorological data from the ECMWF Re-analysis version 5 (ERA5) dataset [10]. ERA5 is a global dataset that details the environmental conditions at a range of point locations worldwide. There are 100s of variables available through the data set; we chose a subset of 11 based on meteorological variables detailed as being strongly associated with air pollution concentration in the existing literature. The subset of 11 variables to include was the 100m and 10m U component of wind, the 100m and 10m V component of wind, 2m dewpoint temperature, 2m temperature, boundary layer height, downwards UV radiation at the surface, the instantaneous 10m wind gust, surface pressure and total column rainwater. To create the feature vector, the point locations within the ERA5 dataset seen in Figure S13 were interpolated across the study area to determine the variable value at each of the 1km² grid centroid. The resulting interpolated values at the grid centroids for a meteorological variable used, 100m U Component of Wind, are shown in Figure S14.



Supplementary Figure S13: **The blue region denotes the area of interest presented in Figure S1 with the red points showing the ERA5 sample locations across the UK.**



Supplementary Figure S14: Example complete England meteorological dataset from ERA5 for the 100m U Component of Wind feature vector.

S1.6 Remote Sensing

Google Earth Engine [11] derived datasets from Sentinel 5P [12] measurements comprised the remote sensing dataset family. The temporal period of datasets used was from 01-02-2019 to 01-03-2020, which allowed all available datasets from the Sentinel 5P platform to be studied. To ensure that all of the grids within the study area have a value for each timestamp, we aggregated the sentinel 5P datasets to the monthly mean temporal level. The grid would be interpolated from neighbouring values if any values were missing from the monthly aggregate, which was not the case for the variables used in the final study: NO₂, CO, HCHO, O₃, and the Absorbing Aerosol Index. Table S6 shows the number of missing data points across the study area for each month's different variables of consideration from Sentinel 5P. Methane (CH₄) was missing many data points and was therefore excluded from the dataset.

The process produced a spatially complete map of air pollution concentrations for each month of the year, which was then backfilled to other periods from before the Sentinel 5P platform came online to indicate typical air pollution concentrations during each month. Figure S15 shows the complete spatial map of the remote sensing dataset produced for June for NO₂.

Month	2019	2020	2021	2022	Monthly Median Overall	Monthly Median Overall Interpolated	Month	2019	2020	2021	2022	Monthly Median Overall	Monthly Median Overall Interpolated
1.00	-	100.00	99.66	100.00	100.00	100.00	1.00	-	100.00	73.88	96.09	100.00	100.00
2.00	100.00	100.00	100.00	-	100.00	100.00	2.00	100.00	100.00	100.00	-	100.00	100.00
3.00	100.00	100.00	100.00	-	100.00	100.00	3.00	100.00	100.00	100.00	-	100.00	100.00
4.00	100.00	100.00	100.00	-	100.00	100.00	4.00	100.00	100.00	100.00	-	100.00	100.00
5.00	100.00	100.00	100.00	-	100.00	100.00	5.00	100.00	100.00	100.00	-	100.00	100.00
6.00	100.00	100.00	100.00	-	100.00	100.00	6.00	100.00	100.00	100.00	-	100.00	100.00
7.00	100.00	99.92	100.00	-	100.00	100.00	7.00	100.00	100.00	100.00	-	100.00	100.00
8.00	100.00	100.00	100.00	-	100.00	100.00	8.00	100.00	100.00	100.00	-	100.00	100.00
9.00	100.00	100.00	100.00	-	100.00	100.00	9.00	100.00	100.00	100.00	-	100.00	100.00
10.00	100.00	99.87	100.00	-	100.00	100.00	10.00	100.00	99.98	100.00	-	100.00	100.00
11.00	100.00	100.00	100.00	-	100.00	100.00	11.00	100.00	100.00	100.00	-	100.00	100.00
12.00	100.00	99.98	100.00	-	100.00	100.00	12.00	99.95	0.99	0.25	-	99.99	100.00

(a) NO₂

(b) HCHO

Month	2019	2020	2021	2022	Monthly Median Overall	Monthly Median Overall Interpolated	Month	2019	2020	2021	2022	Monthly Median Overall	Monthly Median Overall Interpolated
1.00	-	100.00	100.00	100.00	100.00	100.00	1.00	-	100.00	100.00	100.00	100.00	100.00
2.00	100.00	100.00	100.00	-	100.00	100.00	2.00	100.00	100.00	100.00	-	100.00	100.00
3.00	100.00	100.00	100.00	-	100.00	100.00	3.00	100.00	100.00	100.00	-	100.00	100.00
4.00	100.00	100.00	100.00	-	100.00	100.00	4.00	100.00	100.00	100.00	-	100.00	100.00
5.00	100.00	100.00	100.00	-	100.00	100.00	5.00	100.00	100.00	100.00	-	100.00	100.00
6.00	100.00	100.00	100.00	-	100.00	100.00	6.00	100.00	100.00	100.00	-	100.00	100.00
7.00	100.00	100.00	100.00	-	100.00	100.00	7.00	100.00	100.00	100.00	-	100.00	100.00
8.00	100.00	100.00	100.00	-	100.00	100.00	8.00	100.00	100.00	100.00	-	100.00	100.00
9.00	100.00	100.00	100.00	-	100.00	100.00	9.00	100.00	100.00	100.00	-	100.00	100.00
10.00	100.00	100.00	100.00	-	100.00	100.00	10.00	100.00	100.00	100.00	-	100.00	100.00
11.00	100.00	100.00	100.00	-	100.00	100.00	11.00	100.00	100.00	100.00	-	100.00	100.00
12.00	100.00	100.00	100.00	-	100.00	100.00	12.00	100.00	100.00	100.00	-	100.00	100.00

(c) O₃

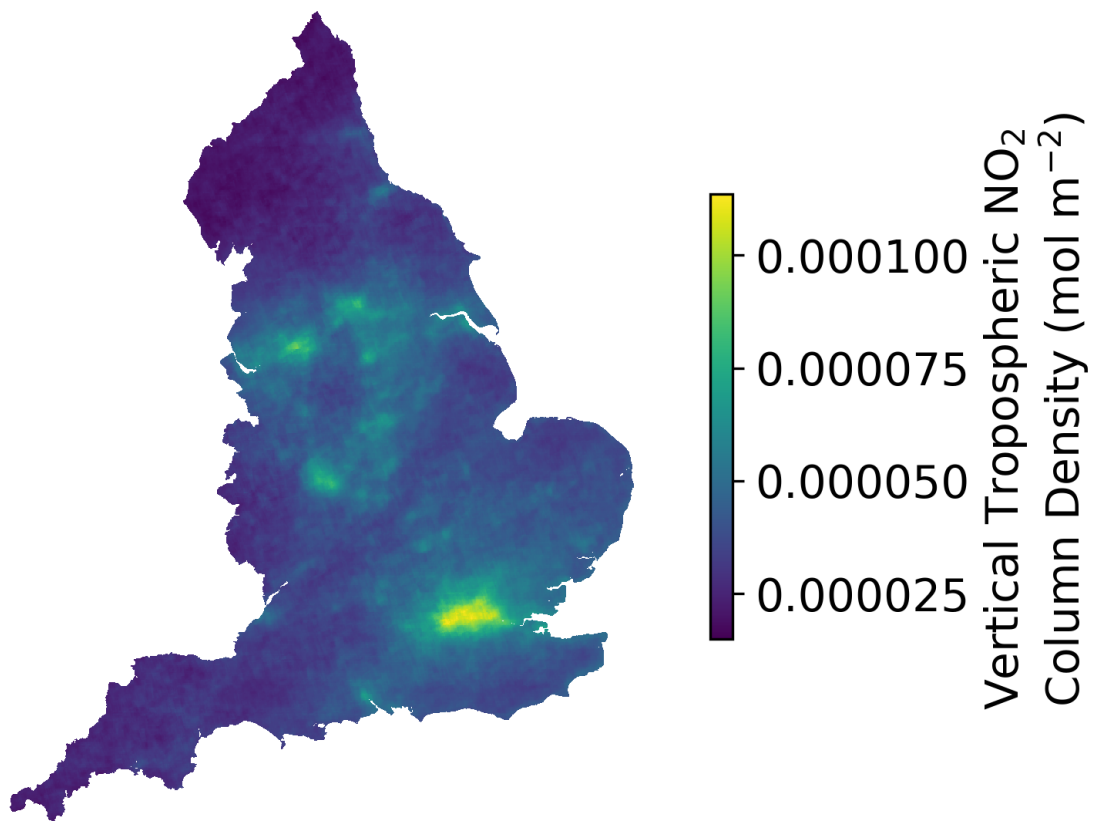
(d) CO

Month	2019	2020	2021	2022	Monthly Median Overall	Monthly Median Overall Interpolated	Month	2019	2020	2021	2022	Monthly Median Overall	Monthly Median Overall Interpolated
1.00	-	0.16	1.24	12.62	13.52	100.00	1.00	-	100.00	100.00	100.00	100.00	100.00
2.00	77.07	46.45	63.81	-	82.09	100.00	2.00	100.00	100.00	100.00	-	100.00	100.00
3.00	37.21	47.66	56.04	-	76.85	100.00	3.00	100.00	100.00	100.00	-	100.00	100.00
4.00	63.74	72.79	83.10	-	86.00	100.00	4.00	100.00	100.00	100.00	-	100.00	100.00
5.00	22.90	69.36	60.84	-	80.16	100.00	5.00	100.00	100.00	100.00	-	100.00	100.00
6.00	49.87	55.91	60.14	-	77.18	100.00	6.00	100.00	100.00	100.00	-	100.00	100.00
7.00	23.54	32.61	78.60	-	82.90	100.00	7.00	100.00	100.00	100.00	-	100.00	100.00
8.00	23.21	47.09	16.11	-	64.44	100.00	8.00	100.00	100.00	100.00	-	100.00	100.00
9.00	53.45	81.42	79.16	-	87.13	100.00	9.00	100.00	100.00	100.00	-	100.00	100.00
10.00	39.47	3.46	49.58	-	64.93	100.00	10.00	100.00	100.00	100.00	-	100.00	100.00
11.00	3.69	31.50	16.63	-	38.55	100.00	11.00	100.00	100.00	100.00	-	100.00	100.00
							12.00	100.00	100.00	100.00	-	100.00	100.00

(e) CH₄

(f) Absorbing Aerosol Index

Supplementary Table S6: **Missing Data for each of the months for each of the variables considered in the study.** All of the variables considered other than CH₄ had a spatially complete dataset at the monthly aggregate level and, as such, were included in the study as shown in Figure S15.



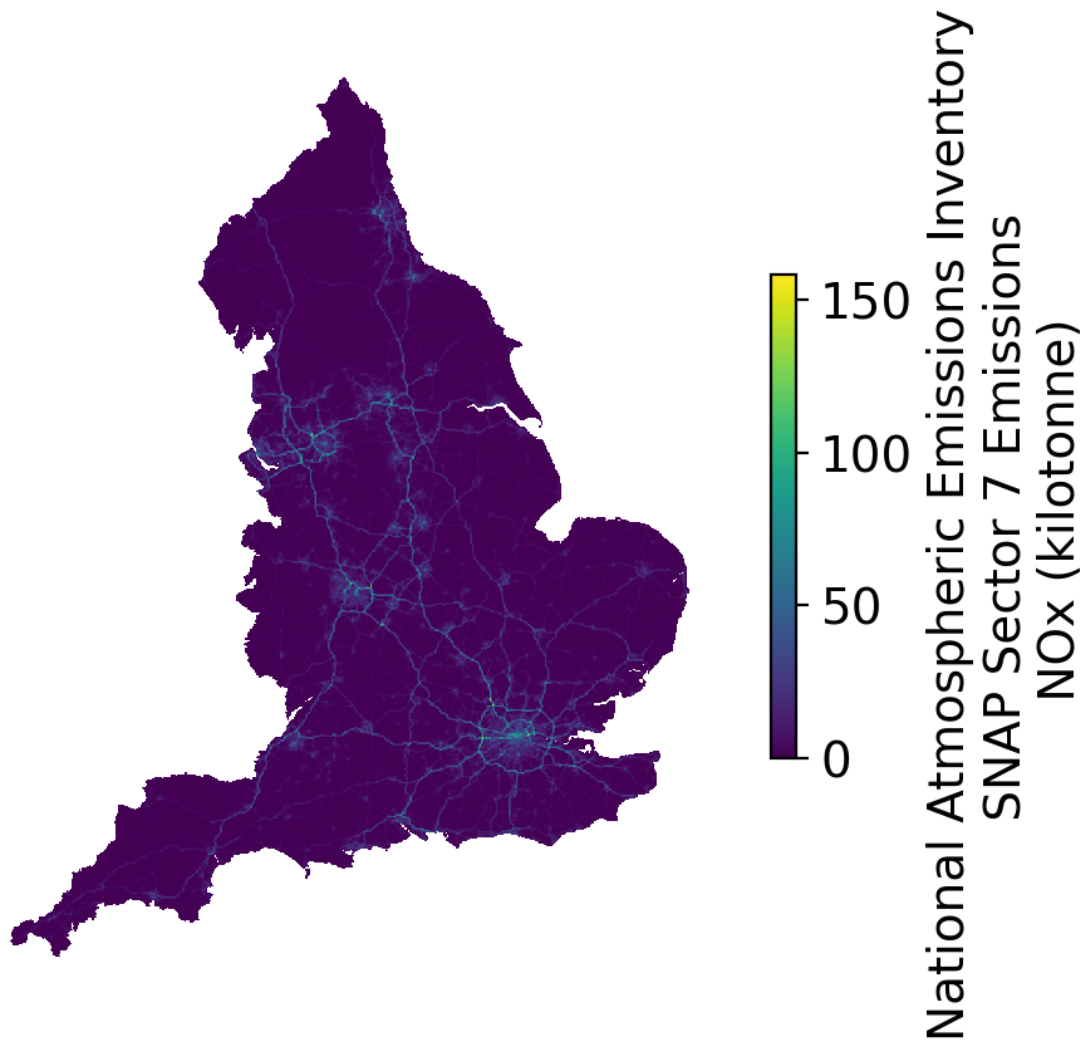
Supplementary Figure S15: **Example complete England remote sensing dataset from Sentinel 5P Google Earth Engine for NO₂.**

S1.7 Emissions

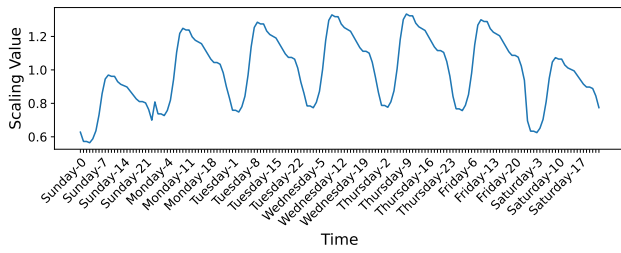
Emissions data is gathered from the UK National Atmospheric Emissions Inventory (NAEI) [13]. A set of seven air pollutants are included: $PM_{2.5}$, PM_{10} , (Non-methane volatile organic compounds (NMVOC), NH_3 , SO_x , CO, NO_x in the study. The emissions are classified into one of 11 sectors to denote the emission source, based on Selected Nomenclature for Air Pollutants (SNAP) sectors [14]:

- SNAP Sector 1 (Combustion Energy Production and Transformation)
- SNAP Sector 2 (Combustion in Commercial, Institutional, Residential and Agriculture)
- SNAP Sector 3 (Combustion in Industry)
- SNAP Sector 4 (Production Processes)
- SNAP Sector 5 (Extraction and Distribution of Fossil Fuels)
- SNAP Sector 6 (Solvent Use)
- SNAP Sector 7 (Road Transport)
- SNAP Sector 8 (Other Transport and Mobile Machinery)
- SNAP Sector 9 (Waste Treatment and Disposal)
- SNAP Sector 10 (Agriculture, Forestry and Land Use Change)
- SNAP Sector 11 (Nature)

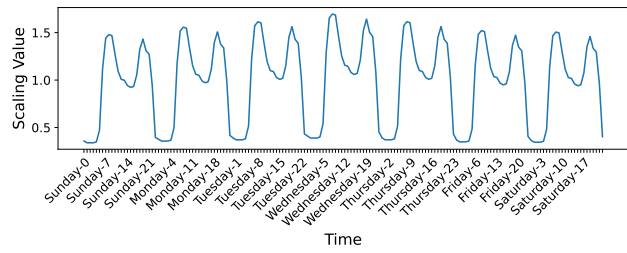
We created the emissions feature vector by summing the point and area emissions data [15] from the NAEI for each year per SNAP sector per species to map the emissions across the study area. We then subsequently scaled the emissions map depending on the timestamp of interest, applying a scaling for the hour and day of the week and month of interest [16]. Figure S16 gives an example of the emission feature vector for NO_x SNAP Sector 7 (Road) emissions across the study area.



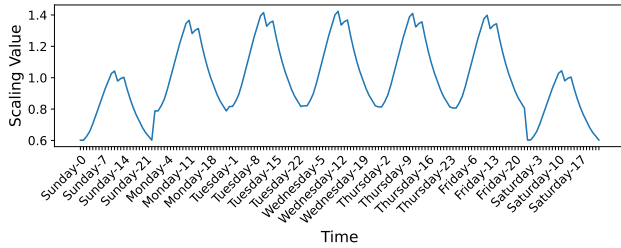
Supplementary Figure S16: **Example complete England emission dataset for SNAP Sector 7 (Road Emissions) for NO_x on 1st June 2018 at 0800AM.**



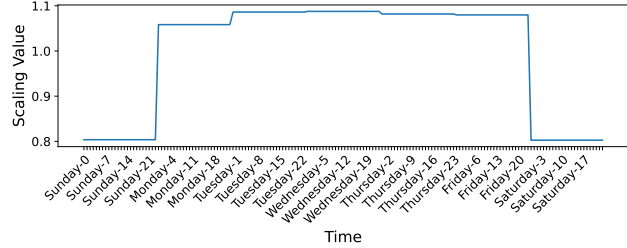
(a) SNAP Sector 1



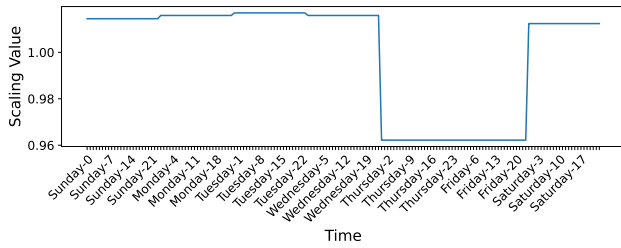
(b) SNAP Sector 2



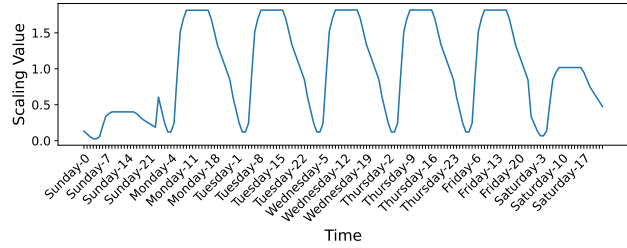
(c) SNAP Sector 3



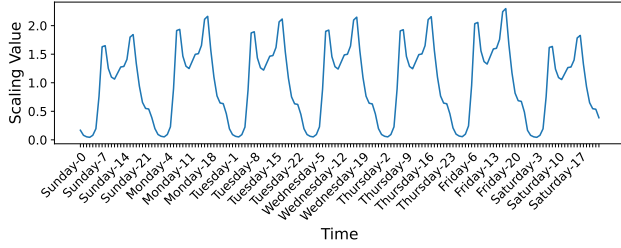
(d) SNAP Sector 4



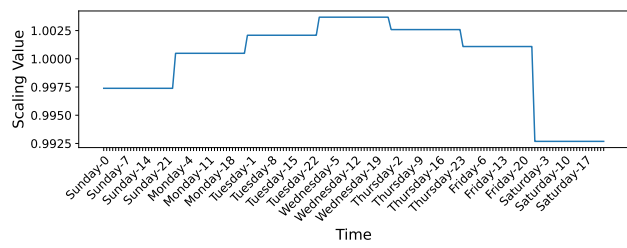
(e) SNAP Sector 5



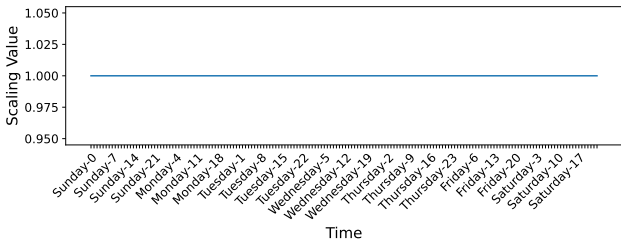
(f) SNAP Sector 6



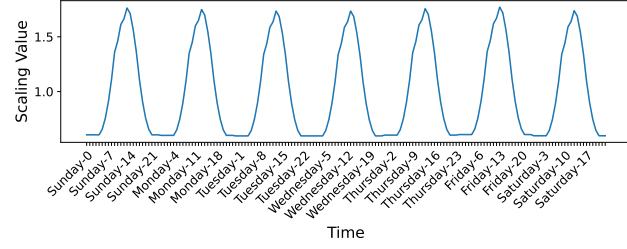
(g) SNAP Sector 7



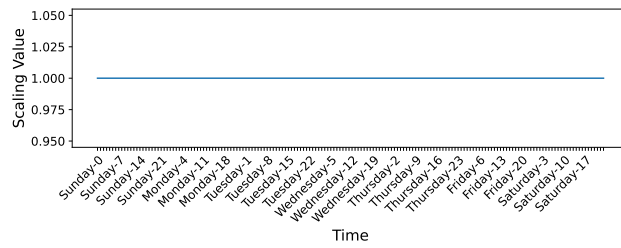
(h) SNAP Sector 8



(i) SNAP Sector 9

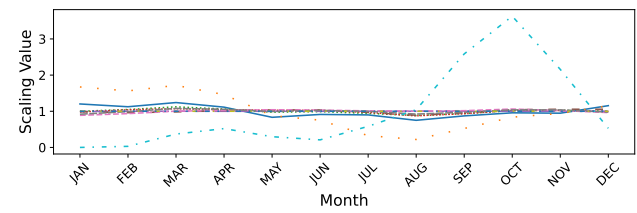


(j) SNAP Sector 10

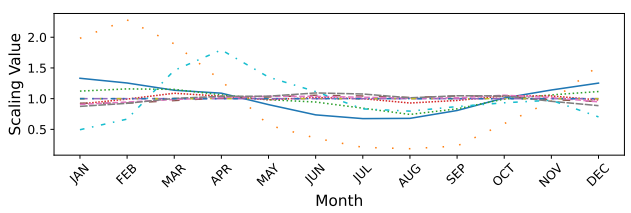


(k) SNAP Sector 11

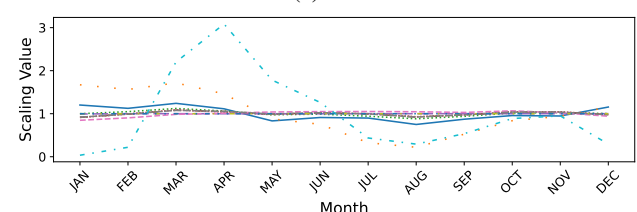
Supplementary Figure S17: Hourly and daily emissions scaling per SNAP sector.



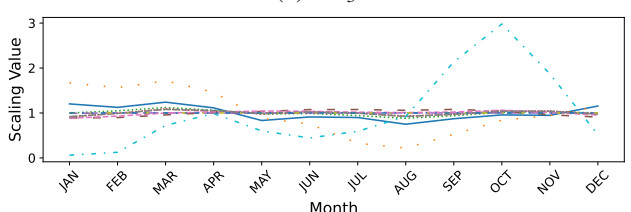
(a) CO



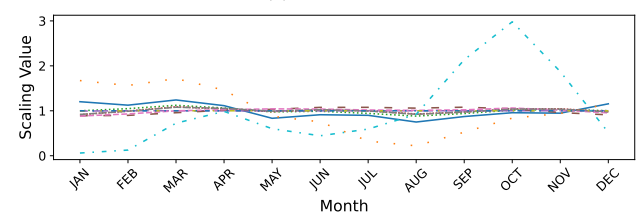
(b) NH₃



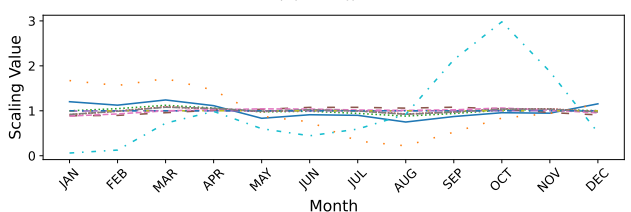
(c) NMVOC



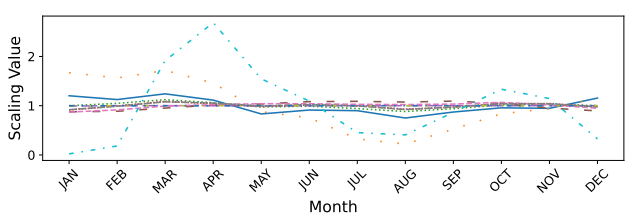
(d) NO_x



(e) PM₁₀



(f) PM_{2.5}



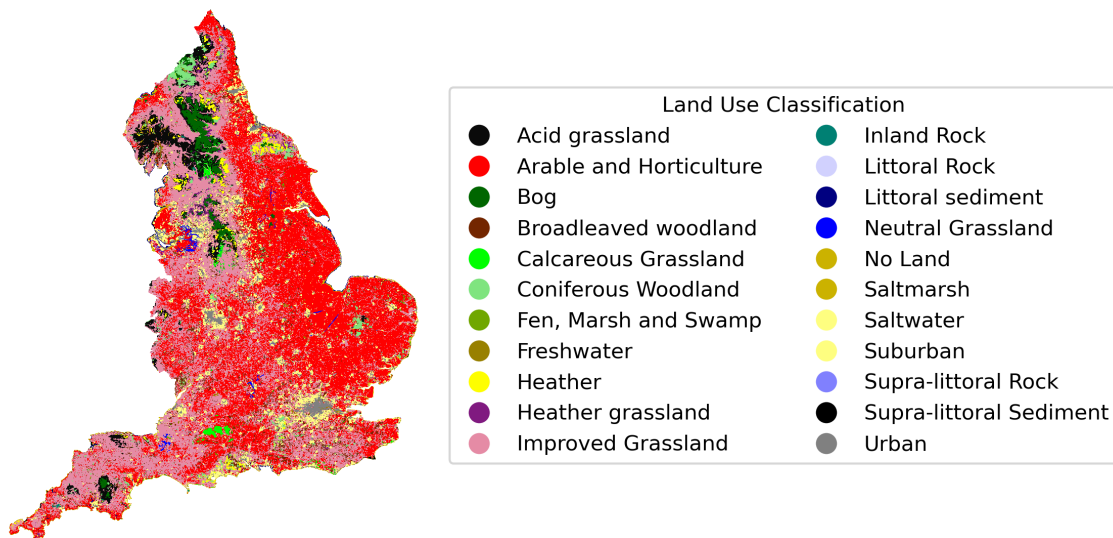
(g) SO_x



Supplementary Figure S18: Emissions scaling for each emissions species by SNAP sector across the months.

S1.8 Land Use

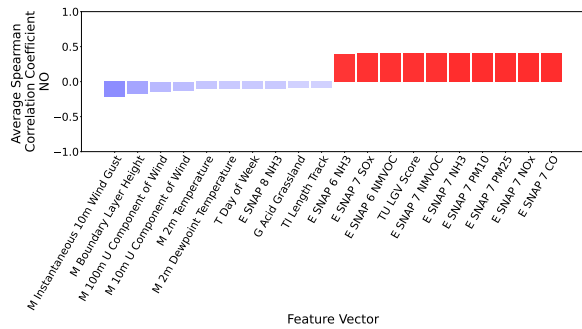
We created a geographic profile based on land use for each grid within the study. The 25m UKCEH Land Cover Maps [17] were used to profile each grid's land use composition across 22 possible land use classifications. The feature vector elements represent the number of pixels with a given land cover classification in the raster. Figure S19 shows the majority classification for each grid within the study.



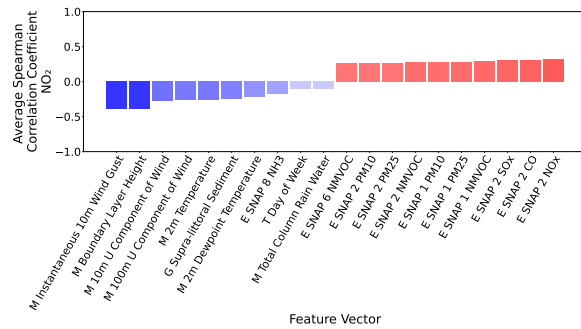
Supplementary Figure S19: **Land use majority classification per grid.**

S2 Feature Selection

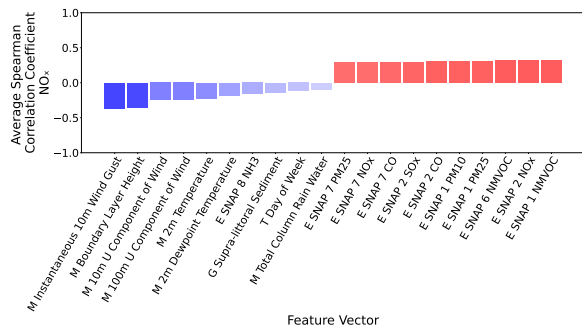
S2.1 Air Pollutants and Feature Vector



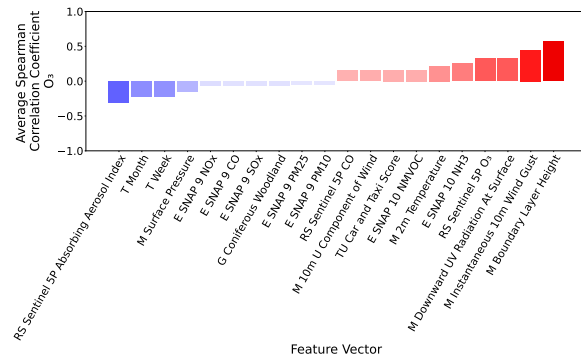
(a) NO



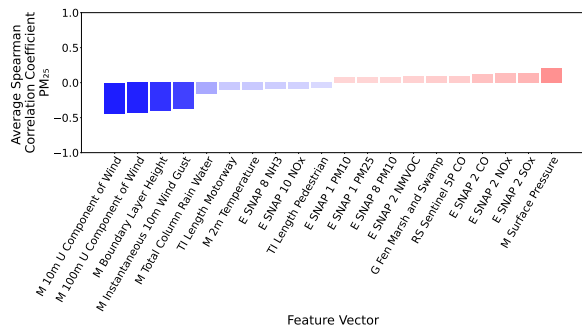
(b) NO₂



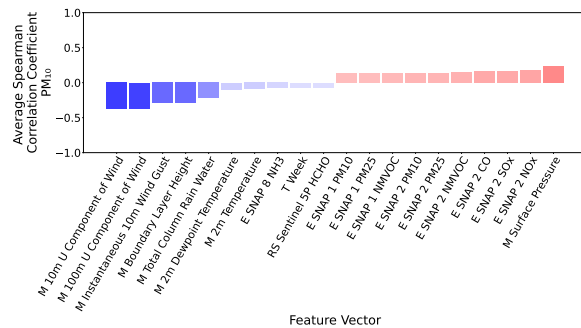
(c) NO_x



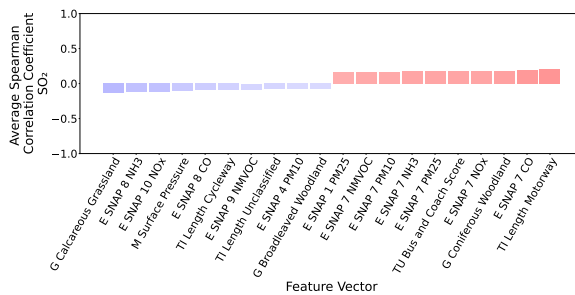
(d) O₃



(e) PM_{2.5}



(f) PM₁₀



(g) SO₂

Supplementary Figure S20: **Spearman correlation coefficients overall mean for all pollutants.** Of note is that the remote sensing dataset family does not have the highest correlation with the air pollutant that it measures directly, such as NO₂. The reason for this is the difference in temporal period, with the dataset being a monthly aggregate rather than the higher temporal resolution datasets included, such as the emissions datasets.

S2.2 Inter Feature Vectors

Linkage Distance	Number of Clusters
-1.00	139.00
0.05	112.00
0.10	103.00
0.25	83.00
0.50	62.00
0.75	51.00
1.00	29.00
1.25	15.00
1.50	11.00
1.75	8.00
2.00	6.00
2.50	4.00
3.00	1.00

Supplementary Table S7: **Linkage distance for hierarchial clustering of the feature vectors.** The linkage distance column provides a set of thresholds and the associated number of clusters grouped when all features under the threshold are put into a cluster. The smaller the linkage, the more similar the feature vectors are—the -1.00 threshold indicates that all feature vectors should be individual clusters, resulting in 139 clusters, with 4 missing due to land use and 9 emissions feature vectors not being present in a location with a monitoring station; providing the 152 feature vectors elements considered in the study.

S3 Modelling

S3.1 Data Subsetting - Temporal

Pollutant Name	Dataset Train Score	Dataset Validation Score	Dataset Test Score	Pollutant Name	Dataset Train Score	Dataset Validation Score	Dataset Test Score
NO ₂	-0.0	0.03	0.02	NO ₂	0.14	0.16	0.14
NO _x	-0.02	-0.01	0.01	NO _x	0.09	0.1	0.09
NO	-0.06	-0.06	-0.05	NO	0.03	0.02	0.01
O ₃	0.12	0.04	0.0	O ₃	0.43	0.41	0.34
SO ₂	-0.06	0.0	0.0	SO ₂	-0.02	0.04	0.03
PM ₁₀	-0.01	-0.01	-0.05	PM ₁₀	0.2	0.23	0.18
PM ₂₅	-0.05	-0.03	-0.08	PM ₂₅	0.25	0.26	0.24

(a) Temporal

(b) Meteorology

Pollutant Name	Dataset Train Score	Dataset Validation Score	Dataset Test Score	Pollutant Name	Dataset Train Score	Dataset Validation Score	Dataset Test Score
NO ₂	0.32	0.29	0.31	NO ₂	0.36	0.23	0.16
NO _x	0.26	0.25	0.27	NO _x	0.28	0.18	0.14
NO	0.19	0.18	0.2	NO	0.21	0.12	0.08
O ₃	-0.02	-0.04	-0.15	O ₃	0.09	0.02	-0.09
SO ₂	0.16	0.26	0.12	SO ₂	0.19	0.24	0.12
PM ₁₀	-0.01	0.02	-0.04	PM ₁₀	0.02	0.03	-0.06
PM ₂₅	-0.07	-0.02	-0.1	PM ₂₅	-0.07	-0.03	-0.08

(c) Transport Infrastructure

(d) Transport Use

Pollutant Name	Dataset Train Score	Dataset Validation Score	Dataset Test Score	Pollutant Name	Dataset Train Score	Dataset Validation Score	Dataset Test Score
NO ₂	0.35	0.31	0.36	NO ₂	0.31	0.23	0.29
NO _x	0.28	0.25	0.32	NO _x	0.25	0.2	0.26
NO	0.2	0.18	0.24	NO	0.18	0.12	0.2
O ₃	0.14	0.11	0.05	O ₃	-0.04	-0.1	-0.2
SO ₂	0.18	0.26	0.13	SO ₂	0.17	0.23	0.13
PM ₁₀	0.01	0.01	-0.01	PM ₁₀	-0.01	0.02	-0.07
PM ₂₅	-0.05	-0.03	-0.05	PM ₂₅	-0.08	-0.03	-0.11

(e) Remote Sensing

(f) Geographic

Pollutant Name	Dataset Train Score	Dataset Validation Score	Dataset Test Score
NO ₂	0.47	0.42	0.43
NO _x	0.39	0.34	0.39
NO	0.32	0.28	0.28
O ₃	0.1	-0.02	-0.01
SO ₂	0.23	0.29	0.13
PM ₁₀	0.05	0.06	-0.02
PM ₂₅	-0.02	-0.0	-0.08

(g) Emissions

Supplementary Table S8: **Temporal experiment results for different subsets of dataset families.** All dataset families provide some information about at least one of the air pollutants within the study. Still, none provide the complete picture of air pollution concentrations in the study, aligning with the scientific literature concerning air pollution sources and sinks with various phenomena from meteorological conditions, such as wind, and emissions sources, such as transportation and industry impacting seen air pollution concentrations. As such, it is clear that all of the datasets outlined are needed to predict air pollution concentrations in the future at an adequate level and no single dataset.

S3.2 Data Subsetting - Spatial

Pollutant Name	Estimation LOOV Max	Estimation LOOV Min	Estimation LOOV Mean	Estimation LOOV Median	Pollutant Name	Estimation LOOV Max	Estimation LOOV Min	Estimation LOOV Mean	Estimation LOOV Median
NO	0.11	-110.87	-2.16	-0.06	NO	0.35	-441.56	-5.97	0.08
NO ₂	0.29	-13.84	-0.63	-0.06	NO ₂	0.46	-14.89	-0.52	0.14
NO _x	0.22	-30.30	-1.09	-0.04	NO _x	0.44	-61.68	-1.49	0.13
O ₃	0.37	-2.44	-0.11	0.11	O ₃	0.70	-2.96	0.25	0.47
PM ₁₀	0.05	-0.60	-0.06	0.01	PM ₁₀	0.40	-0.34	0.20	0.24
PM ₂₅	0.08	-0.60	-0.06	-0.06	PM ₂₅	0.38	-0.20	0.25	0.27
SO ₂	0.01	-1.97	-0.28	-0.07	SO ₂	0.08	-3.15	-0.30	-0.03

(a) Temporal

Pollutant Name	Estimation LOOV Max	Estimation LOOV Min	Estimation LOOV Mean	Estimation LOOV Median
NO	0.00	-1.33	-0.20	-0.07
NO ₂	0.00	-3.02	-0.41	-0.23
NO _x	0.00	-3.35	-0.31	-0.11
O ₃	0.00	-1.39	-0.33	-0.20
PM ₁₀	-0.00	-0.79	-0.15	-0.12
PM ₂₅	0.00	-0.52	-0.11	-0.09
SO ₂	0.00	-1.86	-0.22	-0.07

(b) Meteorology

Pollutant Name	Estimation LOOV Max	Estimation LOOV Min	Estimation LOOV Mean	Estimation LOOV Median
NO	0.03	-18.60	-0.59	-0.14
NO ₂	0.01	-5.36	-0.46	-0.27
NO _x	0.03	-11.08	-0.50	-0.18
O ₃	0.04	-3.08	-0.30	-0.22
PM ₁₀	-0.01	-0.58	-0.14	-0.09
PM ₂₅	-0.01	-0.42	-0.12	-0.12
SO ₂	-0.01	-1.73	-0.26	-0.11

(c) Transport Infrastructure

Pollutant Name	Estimation LOOV Max	Estimation LOOV Min	Estimation LOOV Mean	Estimation LOOV Median
NO	0.01	-35.53	-0.80	-0.10
NO ₂	0.05	-2.41	-0.38	-0.21
NO _x	0.03	-6.96	-0.44	-0.21
O ₃	0.20	-1.54	-0.16	-0.10
PM ₁₀	0.03	-0.62	-0.10	-0.07
PM ₂₅	0.02	-0.50	-0.10	-0.09
SO ₂	-0.04	-1.79	-0.41	-0.21

(d) Transport Use

Pollutant Name	Estimation LOOV Max	Estimation LOOV Min	Estimation LOOV Mean	Estimation LOOV Median
NO	0.00	-3.53	-0.31	-0.15
NO ₂	0.04	-3.82	-0.46	-0.25
NO _x	0.00	-4.98	-0.41	-0.22
O ₃	-0.00	-1.28	-0.36	-0.23
PM ₁₀	-0.00	-0.72	-0.13	-0.08
PM ₂₅	-0.00	-0.53	-0.14	-0.11
SO ₂	-0.00	-2.36	-0.28	-0.08

(e) Remote Sensing

Pollutant Name	Estimation LOOV Max	Estimation LOOV Min	Estimation LOOV Mean	Estimation LOOV Median
NO	0.13	-3.30	-0.23	-0.10
NO ₂	0.25	-2.45	-0.23	-0.10
NO _x	0.17	-3.29	-0.25	-0.11
O ₃	0.15	-2.34	-0.26	-0.19
PM ₁₀	0.04	-0.73	-0.10	-0.05
PM ₂₅	0.02	-0.57	-0.09	-0.06
SO ₂	0.02	-2.13	-0.31	-0.18

(f) Geographic

(g) Emissions

Supplementary Table S9: **Summary statistics for individual monitoring station leave-one-out-validation (LOOV) for the spatial experiment with different subsets of dataset families.** The spatial LOOV experiments echo the results seen in Table S8 to a more extreme degree, where the median for the majority of the LOOV is negative when only a single dataset family is included, highlighting that the prediction of the concentrations performs worse than simply predicting the average for the station's measurements, highlighting the importance of including a range of phenomena data to be able to accurately predict the air pollution concentrations of a monitoring stations concentration measurements.

S3.3 Data Subsetting - Forecasting and Global Framework

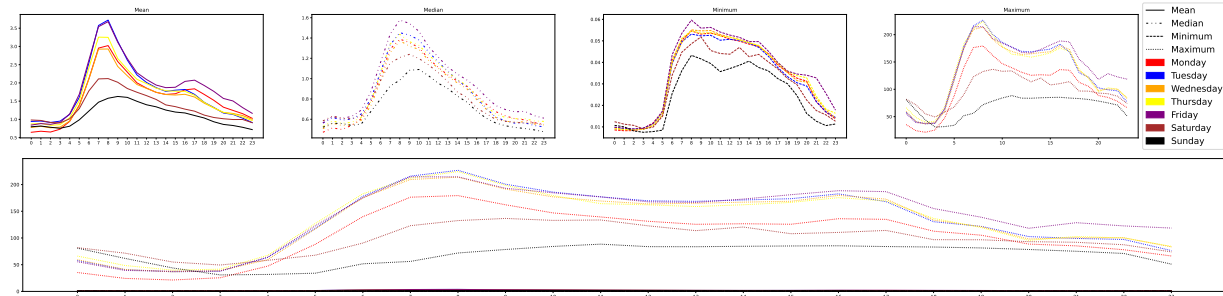
Pollutant Name	Dataset Train Score	Dataset Validation Score	Dataset Test Score	Mean LOOV
NO ₂	0.76	0.68	0.70	-0.09
NO _x	0.73	0.65	0.68	-0.69
NO	0.46	0.43	0.40	-1.87
O ₃	0.77	0.66	0.62	0.48
SO ₂	0.28	0.37	0.25	-0.47
PM ₁₀	0.49	0.35	0.31	0.38
PM ₂₅	0.53	0.35	0.30	0.46

Supplementary Table S10: **Overview of forecasting (test score) and filling missing data spatial (LOOV) performance for a model trained with data that is only available globally.** When using the dataset families available globally, it can be seen that the model’s performance in a forecasting situation is good. However, the LOOV is weaker, with some air pollutants having a negative performance overall, highlighting that the data that is available globally would be suitable for forecasting into the future in locations where monitoring stations are, but not when used to fill in missing monitoring station locations, without further improvements to the model or data used. The global datasets are the temporal, meteorological and remote sensing dataset families in this context.

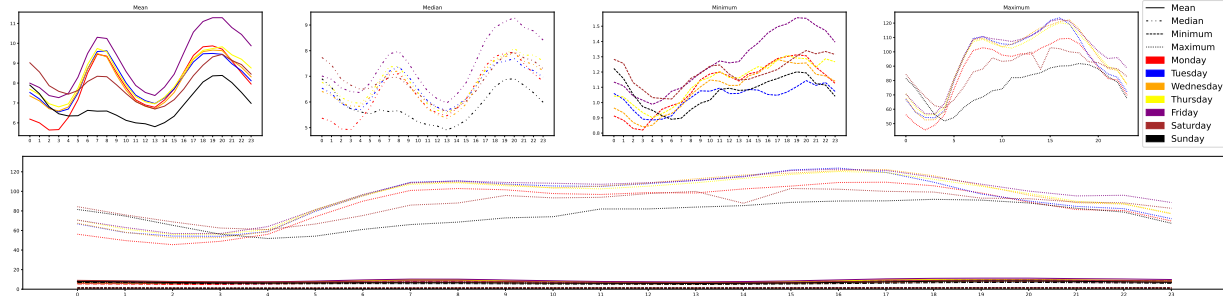
Pollutant Name	Dataset Train Score	Dataset Validation Score	Dataset Test Score	Mean LOOV
NO ₂	0.83	0.77	0.76	0.11
NO _x	0.80	0.74	0.73	0.03
NO	0.69	0.63	0.59	-0.05
O ₃	0.79	0.69	0.66	0.39
SO ₂	0.37	0.38	0.25	-0.11
PM ₁₀	0.51	0.38	0.33	0.32
PM ₂₅	0.52	0.35	0.31	0.42

Supplementary Table S11: **Overview of forecasting (test score) and filling missing data spatial (LOOV) performance for a model trained with data that is only available ahead of time (e.g. forecasting ahead of the current date).** When using the dataset families available ahead of time that could be used in a true forecasting mode, e.g. predict ahead of the current date, it can be seen that the model’s performance in a forecasting situation is similar to the global model seen in Table S10, showing good performance. However, the LOOV is considerably better, with most of the air pollutants having a strong LOOV performance, with only NO and SO₂ having negative performance, driven by a small number of bad predictions for particular stations. In this context, the forecasting datasets are road infrastructure, geographic, meteorological and temporal dataset families. The difference between the performance of the forecasting datasets and the global datasets models shows the importance of some datasets to the model’s overall performance, such as the road infrastructure is critical for NO_x and NO₂ where its inclusion improves performance considerably, particularly for the LOOV results.

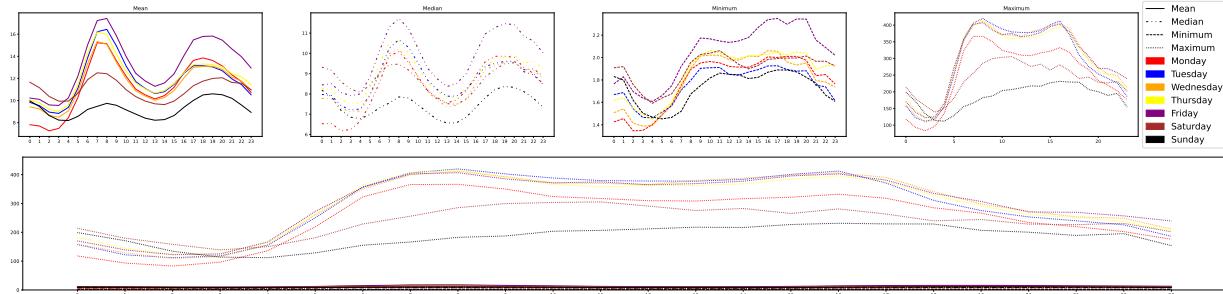
S4 Research Data Output Summary Statistics



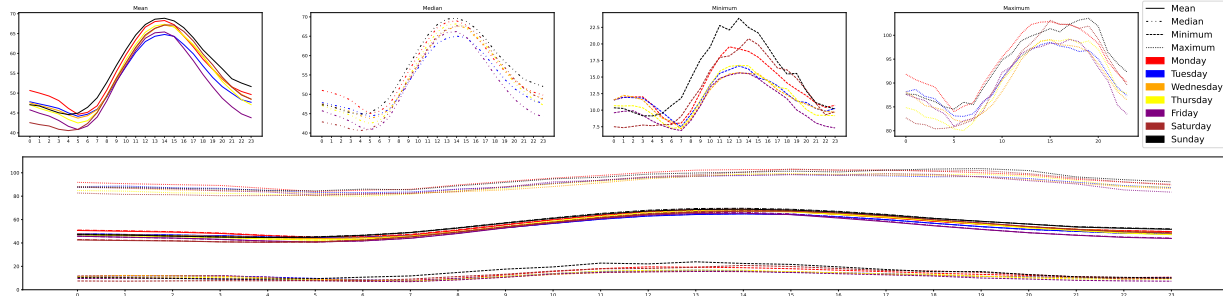
(a) NO



(b) NO₂

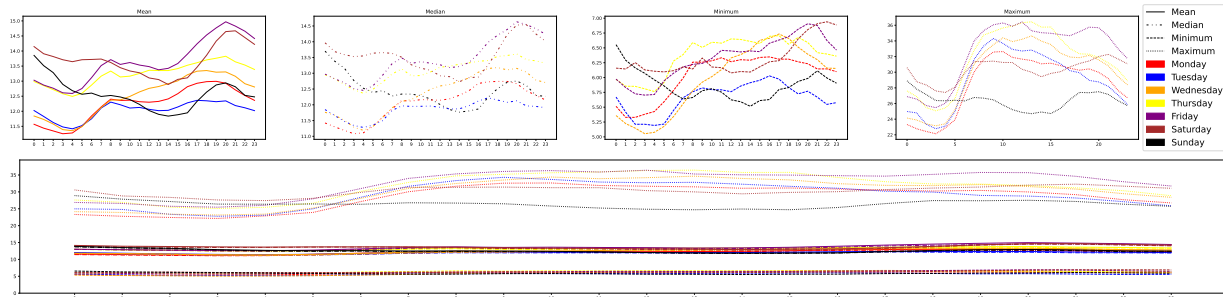


(c) NO_x

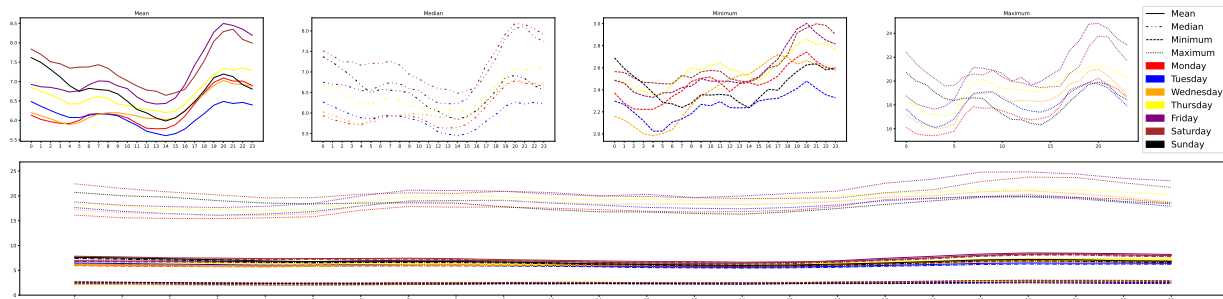


(d) O₃

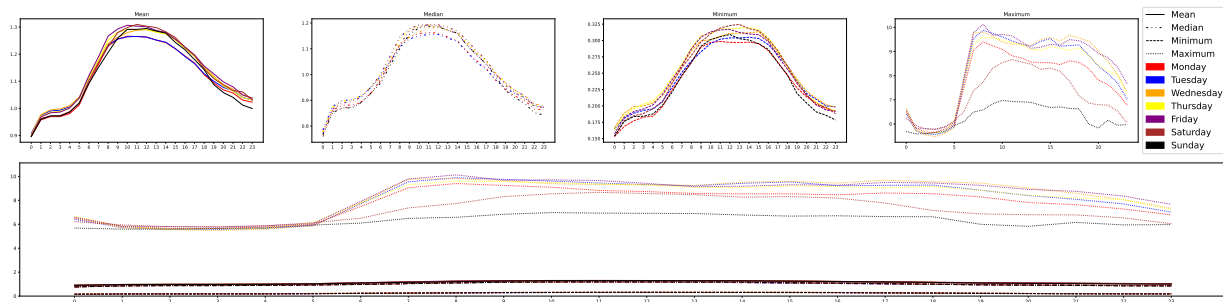
Supplementary Figure S21: Summary of the complete air pollution concentration dataset, spatially and temporal for England at the 1km² spatial resolution for the air pollutants NO, NO₂, NO_x, O₃, PM₁₀, PM_{2.5} and SO₂ at the hourly temporal level for 2018.



(e) PM₁₀



(f) PM_{2.5}



(g) SO₂

Supplementary Figure S21: **Summary of the complete air pollution concentration dataset, spatially and temporal for England at the 1km² spatial resolution for the air pollutants NO, NO₂, NO_x, O₃, PM₁₀, PM_{2.5} and SO₂ at the hourly temporal level for 2018. (cont.)** Summarised in the figures is the dataset made possible by the model developed and presented by this work. The mean, median, minimum and maximum at each hour of the day for each day of the week are shown for each air pollutant, highlighting their overall trends across England.

References

- [1] Daewon W. Byun, Avraham Lacser, Robert Yamartino, and Paolo Zannetti, “Chapter 10 eulerian dispersion models,” 2003.
- [2] D. W. Wong, “The modifiable areal unit problem (maup),” in *WorldMinds: geographical perspectives on 100 problems: commemorating the 100th anniversary of the association of American geographers 1904–2004*. Springer, 2004, pp. 571–575.
- [3] [Online]. Available: <https://uk-air.defra.gov.uk/data/pcm-data>
- [4] Department of Transport, UK Government. (2023) Road Traffic Stations - About. Accessed on: 29/11/2023. [Online]. Available: <https://roadtraffic.dft.gov.uk/about>
- [5] ——. (2023) Road Traffic Statistics - Meta Data. Accessed on: 29/11/2023. [Online]. Available: <https://storage.googleapis.com/dft-statistics/road-traffic/all-traffic-data-metadata.pdf>
- [6] J. Gershuny, “United kingdom time use survey, 2014-2015,” 2017.
- [7] O. for National Statistics, “2011 census aggregate data,” 2017. [Online]. Available: <https://www.ons.gov.uk/census/2011census>
- [8] R. Lovelace and M. Dumont, *Spatial microsimulation with R*. Chapman and Hall/CRC, 2017.
- [9] R. L. Dumont and Morgane, “Spatial microsimulation with r,” May 2018. [Online]. Available: <https://spatial-microsim-book.robinlovelace.net/svalidation#Internal>
- [10] H. Hersbach, “The era5 atmospheric reanalysis.” in *AGU fall meeting abstracts*, vol. 2016, 2016, pp. NG33D–01.
- [11] N. Gorelick, “Google earth engine,” in *EGU general assembly conference abstracts*, vol. 15. American Geophysical Union Vienna, Austria, 2013, p. 11997.
- [12] J. P. Veefkind, I. Aben, K. McMullan, H. Förster, J. De Vries, G. Otter, J. Claas, H. Eskes, J. De Haan, Q. Kleipool *et al.*, “Tropomi on the esa sentinel-5 precursor: A gmes mission for global observations of the atmospheric composition for climate, air quality and ozone layer applications,” *Remote sensing of environment*, vol. 120, pp. 70–83, 2012.
- [13] UK National Atmospheric Emissions Inventory (NAEI). (2023) NAEI - Data. Accessed on: 29/11/2023. [Online]. Available: <https://naei.beis.gov.uk/data/>
- [14] ——. (2023) UN/ECE Classification of Emission Sources. Accessed on: 29/11/2023. [Online]. Available: <https://uk-air.defra.gov.uk/assets/documents/reports/empire/naei/annreport/annrep98/naeiapp4.html>
- [15] ——. (2023) Emissions from NAEI large point sources. Accessed on: 29/11/2023. [Online]. Available: <https://naei.beis.gov.uk/data/map-large-source>
- [16] H. Denier van der Gon, C. Hendriks, J. Kuenen, A. Segers, and A. Visschedijk, “Description of current temporal emission patterns and sensitivity of predicted aq for temporal emission patterns,” *EU FP7 MACC deliverable report D_D-EMIS_1*, vol. 3, pp. 2019–07, 2011.
- [17] C. Rowland, R. Morton, L. Carrasco, G. McShane, A. O’neil, and C. Wood, “Land cover map 2015 (vector, gb),” *NERC Environmental Information Data Centre*, vol. 10, 2017.